

Technical optimization of a laser marking process of banana fruits and poinsettia bracts

Indera Sakti Nasution

Citation:

Nasution, I. S. (2018). Technical optimization of a laser marking process of banana fruits and poinsettia bracts. PhD Thesis, Dissertation Faculty of Natural Sciences, Leibniz Universität Hannover. Biosystems Engineering Report 20182. Biosystems Engineering Laboratory, Osnabrück University of Applied Sciences, Germany. <http://dx.doi.org/10.15488/4309>

Biosystems Engineering Report 20182

Indera Sakti Nasution

**Technical optimization of a
laser marking process of
banana fruits and poinsettia
bracts**

Biosystems Engineering Laboratory (BLab), Hochschule Osnabrück, University of Applied Sciences, Germany

Technical optimization of a laser marking process of banana fruits and poinsettia bracts

Von der Naturwissenschaftlichen Fakultät der
Gottfried Wilhelm Leibniz Universität Hannover

zur Erlangung des Grades

Doktor der Gartenbauwissenschaften (Dr. rer. hort.)

genehmigte Dissertation

von

Indera Sakti Nasution, M. Sc.

2018

Referent: Prof. Dr. rer. hort. habil. Thomas Rath

Korreferent: Prof. Dr. agr. Moritz Knoche

Tag der Promotion: 22.11.2018

ABSTRACT

The ability to place, mark and evaluate a product in production lines is critical for the laser marking of horticultural plants. This study was divided into two objectives. Firstly, the investigation aimed to find the optimal position for marking horticultural products. The study developed and examined algorithms for determining the optimal marking position of poinsettia leaves and banana hands. Two methods of segmentation were performed: distance transform-watershed segmentation and main leaf skeleton segmentation. Secondly, laser marking parameters were evaluated in order to optimize the marking process without destroying the horticultural products (i.e. poinsettia leaves and bananas) and to ensure readable text, patterns or codes. Methods of image processing were employed to develop a laser positioning system and to read and assess the quality of the pattern or codes.

According to the results, distance transform-watershed segmentation is effective in segmenting occluded plant leaves which show significant differences in depth. Using this method with Kinect V1 leads to a low identification rate. However, the precision of depth measurement can be enhanced by implementing Kinect V2, which yields a 92.5% classification rate, whereas the main leaf skeleton method yields a lower classification rate (80%). Moreover, the proposed algorithms are successful in placing a 2D code on banana hands effectively. Positioning of 2D codes on the ventral banana side is a suggested application.

It is possible to use laser marking on poinsettia leaves and bananas without damaging the product. Laser marking of 0.5 W [0.55 J per character] proved to be the lowest energy that can produce a high contrast, and also produces no apparent heat affected zone that is visually detectable on the poinsettia leaves. In terms of laser marking on bananas, readability results are achieved by applying low power and a longer marking time, whereby an 80-100% readability of data matrix codes after storage was obtained.

Keywords: laser marking, bananas, poinsettia, 2D codes, segmentation

ZUSAMMENFASSUNG

Für die Laserbeschriftung von Zier- und Nutzpflanzen während der Produktion ist es sehr wichtig, die Markierung genau zu platzieren, so dass die Beschriftung gut lesbar ist. Diese Studie diente zwei Zwecken: Erstens sollte die optimale Positionierung des Aufdruckes an Zier- und Nutzpflanzen ermittelt werden. Hierzu entwickelten und testeten wir Algorithmen fuer Weihnachsternblätter (Poinsettia) und Bananen. Zur Segmentierung verwendeten wir zwei Methoden: "distance transform watershed segmentation" und "main leaf skeleton segmentation". Zweitens wurden die Markierungsparameter evaluiert, um den optimalen Markierungsprozess zu bestimmen, der einerseits die Produkte nicht zerstört, aber gleichzeitig sicherstellt, dass Text, Muster oder Kodierungen gelesen werden können.

Methoden zur Bildaufbereitung wurden verwendet, um ein Laserpositionssystem zu entwickeln und die Qualität der Muster und Kodierungen zu bestimmen. Nach den Ergebnissen zeigte sich, dass die "distance transform-watershed segmentation" effektiv für überlappend Blätter ist, deren Dicke significant variiert. Die Verwendung von Kinect V1 führt zu einer geringen Identifizierung. bei Verwendung von Kinect V2 kann die Genauigkeit der Dickenmessung verbessert werden, was zu einer Klassifizierungsrate von 92.5% führte. Dagegen zeigte die Verwendung der "leaf skeleton segmentation" mit 80% eine niedrigere Klassifizierungsrate. Ausserdem liessen sich die vorgeschlagenen Algorithmen erfolgreich bei der Platzierung von 2D Kodierungen auf Bananen anwenden. Die Positionierung von 2D Kodierungen auf der ventralen Bananenseite wird empfohlen.

Es ist möglich, Lasermarkierungen auf Weihnachtssternblättern und Bananen zu verwenden, ohne das Produkt zu beschädigen. Lasermarkierungen mit 0.5 W (0.55 J/Character) wurde als niedrigste Energierate für Weihnachtssternblätter bestimmt, mit der ein hoher Kontrast ohne sichtbare Hitzeschaedigung erkennbar waren. Bei Bananen lieferte die Lasermarkierung gute Lesbarkeit bei Anwendung von geringerer Energie aber längerer Expositionszeit. Nach Lagerung dieser Proben, wurde eine 80 - 100%ige Lesbarkeit von Kodierungen festgestellt.

Schlagwörter: Lasermarkierung, Bananen, Poinsettia, 2D Kodierung, Segmentation

SYMBOLS AND ABBREVIATIONS

a. Symbols

<u>Symbols</u>	<u>Description [units]</u>
h_1	gray level histogram [-]
\cap	intersection [-]
Δm	change in mass [g]
ΔT	change in temperature [K]
σ	the standard deviation of the Gaussian distribution [-]
σ_w^2	within-class variance [-]
σ_1^2	variance of the pixels in the background (below threshold) [-]
σ_2^2	variance of the pixels in the foreground (above threshold) [-]
μ	mean value [-]
π	phi
A	major radius [pixels]
B	minor radius [pixels]
B_1 and B_2	minimum gray values of two neighboring basins [pixels]
C_B	class background [-]
C_F	class foreground [-]
CB	catchment basin [-]
C_p	specific heat [$J\ kg^{-1}\ K^{-1}$]
Dpi	dot per inch [-]
Gt	pixel at time t [pixels]
Gx	gradients in the x-directions [-]
Gy	gradients in the y-directions [-]
h	horizontal scan direction [-]
H_v	heat of vaporization for water [$J\ g^{-1}$]
HomMat2D	homogeneous 2D transformation matrix [-]
I_c	corrected image [-]
I_d	dark image recorded by closing the camera lens completely [-]
I_h	acquired hyperspectral image [-]
I_w	white reference image with 99% reflectance [-]
k	number of decoded codes [-]
L	gray levels of gray image [-]

M^2	beam quality factor [-]
m	mass of substance [kg]
N	sample size [-]
n	number of pixels [-]
p	laser power [W]
P	pixels of contour [pixels]
Φ	rotation angle [-]
p	probability [%]
Q_{total}	heat energy total [J]
Q_{water}	heat energy of water [J]
Q_{glass}	heat energy of glass [J]
$Q_{\text{water vaporization}}$	heat energy of vaporization [J]
r	readability [%]
RH	relative humidity [%]
SF	shape factor ratio [-]
SL	successful main leaf detected [%]
S_x	scale factor along x-axis [-]
S_y	scale factor along y-axis [-]
t	marking time [s per module]
th	threshold value [-]
T	temperature [°C]
T_x	translation along x-axis [-]
T_y	translation along y-axis [-]
T_{high}	upper threshold [-]
T_{low}	lower threshold [-]
v	vertical scan direction [-]
w_B	weight of the background [-]
w_F	weight of the foreground [-]
W	minimum gray value of the watershed that splits the two basins [pixels]
X_w, Y_w, Z_w	tristimulus of CIE-XYZ values with reference to the white spot [-]
x	the distance from the origin in the horizontal axis [-]
y	the distance from the origin in the vertical axis [-]
(x', y')	the neighbors of (x, y) along the direction to an edge [-]

b. Abbreviations

<u>Abbreviations</u>	<u>Description</u>
1D	one-dimensional
2D	two-dimensional
3D	three-dimensional
A	ampere
AIAG	automotive industry action group
AIDC	automatic identification and data capture
AIM	association for automatic identification and mobility
ANU	axial non-uniformity
ASCII	American standard code for information interchange
ATA	air transportation association
B/W	black and white
°C	degree of Celsius
CCD	charge-coupled device
CIE	French commission internationale de l'éclairage
CMOS	complementary metal–oxide–semiconductor
CO ₂	carbon dioxide
CW	continuous wave
dpi	dot per inch
DM code	data matrix code
4-DoF	four degrees of freedom
ECC200	error correction code 200
EIA	electronics industry association
EU	European Union
FPD	fixed pattern damage
Fps	frame per second
GNU	grid non-uniformity
GPM	gallon per minute
GPS	global positioning system
h	hour
HAZ	heat affected zone
HomMat2D	Homogeneous 2D transformation matrix
HSV	hue, saturation, value
IEC	international electro technical commission

IR	infrared
ISO	international organization for standardization
L	liter
LASER	light amplification by stimulated emission of radiation
MOD	modulation
mRad	micro radiance
mW	microwatt
mm	millimeter
μm	micrometer
μl	microliter
μsec	microsecond
Nd:YAG	neodymium-doped yttrium aluminum garnet
nm	nanometer
OCR	optical character recognition
PDF 417	portable data file 417
Phi	rotation angle
PLU	price look-up
PWM	pulse width modulation
QR code	quick response code
RAM	random access memory
RFID	radio frequency identification
RGB	red, green, blue
RGB-D	red, green, blue, depth
RH	relative humidity
SC	symbol contrast
SEMI	semiconductor equipment and materials international
SDK	software development kit
SF	shape factor ratio
SL	successful main leaf detected
Sx	scale factor along x-axis
Sy	scale factor along y-axis
SVM	support vector machine
TEM	transvers electromagnetic mode
ToF camera	time-of-flight camera
Tx	translation along x-axis

Ty	translation along y-axis
UEC	unused error correction
USA	united states of America
USB	universal serial bus
UV	ultraviolet
VDC	volt direct current
V1	version 1
V2	version 2
W	watt
WPF	windows presentation foundation
YAG	yttrium aluminum garnet
ZXing	zebra crossing

TABLE OF CONTENTS

Abstract.....	i
Zusammenfassung.....	ii
Symbols and Abbreviations	iii
Table of Contents	viii
1. Introduction	1
2. State of the art of laser marking on horticultural products.....	3
2.1. Effects, scopes and applications	3
2.1.1. Technical aspects of laser marking	3
2.1.2. Effects of laser radiation on surfaces.....	5
2.1.3. Laser marking applications on horticultural products	6
2.2. Challenges in laser marking on horticultural products	8
2.2.1. Positioning of the laser	8
2.2.1.1. General aspects.....	8
2.2.1.2. Image processing as a tool for positioning in complex plant situations	9
2.2.1.2.1. Positioning and localization on leaves	9
2.2.1.2.2. Positioning and localization on fruits and stems.....	12
2.2.1.3. Tasks (first).....	13
2.2.2. Laser and marking parameters.....	14
2.2.2.1. General aspects.....	14
2.2.2.2. Parameters for laser application on leaves	15
2.2.2.3. Parameters for utilizing lasers on fruits and stems.....	17
2.2.2.4. Tasks (second)	17
2.2.3. Detection and quality assessment of marking patterns.....	19
2.2.3.1. General aspects of marking codes.....	19
2.2.3.2. Detection of 2D codes.....	19

5.2.1. Evaluation of energy output	81
5.2.2. Laser parameter optimization for poinsettia	82
5.2.3. Laser parameter optimization for bananas	87
5.2.3.1. Spectral reflectance of marked bananas	87
5.2.3.2. Quality of codes	87
5.2.3.2.1. Decode	87
5.2.3.2.2. Contrast values	89
5.2.3.2.3. Axial non-uniformity (ANU)	90
5.2.3.2.4. Grid non-uniformity (GNU)	91
5.2.3.2.5. Unused error correction (UEC)	92
5.2.3.2.6. Damages to the codes during storage time	93
5.2.3.3. Readability of the codes	94
6. Discussion	98
6.1. Discussion of the results relating to the positioning problems	98
6.1.1 Procedures for poinsettia	98
6.1.1.1. Color segmentation based depth image	98
6.1.1.2. Depth image segmentation based on a distance transform- watershed method	98
6.1.1.3. Main leaf skeleton	99
6.1.2. Procedures for bananas	101
6.1.2.1. Evaluation for banana fingers	101
6.1.2.2. Evaluation of banana hands	102
6.2. Discussion of the results relating to the optimization of laser parameters	104
6.2.1. Application for poinsettia	104
6.2.1.1. Laser-poinsettia leaves interactions	104
6.2.1.2. Technical aspects	105
6.2.2. Application for bananas	105
6.2.2.1. Spectral reflectance of marked bananas	105
6.3.2.2. Quality of the codes	106

6.3.2.3. Readability of the codes.....	107
6.3. Possible application relating to the results	108
6.3.1. Application for poinsettia and bananas	108
6.3.2. Application for other products (for example: petunia stems)	109
6.4 Future work	111
7. Conclusions.....	112
7.1. Optimization of laser positioning for poinsettia leaves	112
7.2. Optimization of laser positioning for bananas.....	112
7.3. Optimization of laser parameters for marking poinsettia leaves	112
7.4. Optimization of laser parameter for marking bananas	113
References.....	114
List of Figures.....	131
List of Tables.....	135
Publications.....	136
Curriculum Vitae.....	138

1. INTRODUCTION

A number of policies and standards regarding food safety issues and quality management have been established for the food industry (Aung and Chang, 2014). A key tool to fulfill legislative requirements and meet food quality and safety standards is traceability. According to Trienekens et al. (2014), traceability is the capability to describe the ongoing location of products and to trace products based on their origins of production. Achieving a transparent production circle by improving the availability of consumer data is expected to improve knowledge-based consumer trust towards the food sector.

Consumers need valid information of traceability with regard to safety protection against fraud. Traceability has become a process of providing safer food in the food supply chain (Aung and Chang, 2014). It contributes to increased consumer trust and plays an essential role in establishing the authenticity of the food (van Rijswijk et al., 2008; Verbeke et al., 2007) and connecting producers to consumers (Regattieri et al., 2007).

Furthermore, traceability is a necessary practice which gives information about the origin, handling, retailing, and final destination of foodstuffs (Bertolini et al., 2006; Peres, et al. 2007). According to Armenta and Guardia (2016), a product traceability system needs to identify all of the physical entities involved in the product's manufacture: the locations of processing, packaging, and storage, as well as every agent in the supply chain. One of the technologies of a traceability system is Automatic Identification and Data Capture (AIDC) technology. According to Scholten et al. (2016), AIDC consists of some methods such as: automatically identifying objects, collecting data, and entering data into personal computer. Components of AIDC technologies include barcodes, optical character recognition (OCR), radio frequency identification (RFID), smart cards, voice recognition, and so on.

The labeling of horticultural products has the potential to provide product traceability, thereby strengthening food safety systems against foodborne outbreaks. Currently, horticultural products entering into conventional retail sales chains are marked with paper stickers. However, paper stickers have some disadvantages: they can easily become detached, lost, exchanged, and can be quite expensive (Drouillard and Kanner, 1999; Edxeberria et al., 2006a; Marx et al., 2013). Applying laser labeling instead of traditional labels is a promising alternative and can aid in the avoidance of

counterfeiting. Laser marking involves marking a permanent, higher quality mark, with a greater marking speed and higher reproducibility.

2. STATE OF THE ART OF LASER MARKING ON HORTICULTURAL PRODUCTS

2.1. Effects, scopes and applications

2.1.1. Technical aspects of laser marking

Laser marking has three basic procedures that have been extensively used in laser marking: dot marking (Ion, 2005), synchronized image scanning (Golnabi, 1999) and galvanometric scanning marking (Chen, et al. 2008). Dot marking systems produce characters by creating small dots in given patterns to generate the required characters. The beam is scanned and pulses when a dot is required. A rotating polygon mirror, acoustic-optical device, or piezoelectric scanning can be used to generate the pulse (Ion, 2005). The disadvantage of this method is its lower resolution in bitmap mode processing. The synchronized image scanning process involves a laser source, a laser beam expander, a mask, and a focusing lens (Golnabi, 1999). Laser beams pass through the expander and project the patterns on the mask (a kind of printed negative), created in advance, and then mark images on the workpiece. The images marked on the workpiece are the same as those on the mask of patterns. The advantages of this method are its high marking speed and high repetition rate. According to Allota, et al. (2016), galvanometric scanning involves deflection through two mirrors and a lens before the object can be marked. Moreover, the galvanometric method is flexible and able to transmit a higher density mark than dot marking and synchronized image scanning (Chen, et al. 2008).

In general, according to Chen, et al. (2008) laser marking systems are comprised of a laser source, a power supply, delivery optics, a control system, and a cooling system. According to Dongyun and Xinpiao (2014), the control system delivers characters, which are converted into data describing a scanner's voltage position. Either pulse width modulation (PWM) or continuous commands that control a CO₂ laser in pulse mode or continuous mode, coupled with voltage position commands, guide the dual-mirror scanner to a certain angle and position simultaneously. In order to deliver optics, the laser beam output reaches the galvanometer-based scanning system via a pinhole and an expander. Then the beam direction is changed direction by the dual mirrors. Finally, it focused by a flat-field lens at the surface of the workpiece to engrave the mark (Wang, et al. 2015).

Some laser sources used for marking applications are CO₂, Nd:YAG, and excimer lasers (Ion, 2005). CO₂ lasers utilize a gas mixture of helium, nitrogen, and carbon dioxide as a lasing medium, which is generally excited by an electrical gas

discharge. Whereas, an excimer laser is operated in the ultraviolet (UV) spectral range and generates nanosecond pulses. Nd:YAG (neodymium-doped yttrium aluminum garnet; $\text{Nd:Y}_3\text{Al}_5\text{O}_{12}$) refers to a crystal used as an active medium for solid-state lasers. Qi, et al. (2003) studied a Q-switched Nd:YAG laser marking process on stainless steel material. Q-switching refers to a technique that enables the generation of a short optical pulse by a sudden switching of the cavity Q factor (a measure of the damping of resonator modes). Haferkamp, et al. (2002) used an Nd:YAG laser and infrared technology to respond to increasing product imitations and requests for protection against plagiarism. Infrared reflection technique in conjunction with a focal plane array detector was used for the detection of invisible laser markings on products shielded by a painting layer. Chen, et al. (2009) proposed a CO_2 laser marking system to code on eggshells. Parker (2004) suggested a technique for marking an egg with a freshness date and an advertisement. CO_2 lasers have good marking results especially on materials such as glass, plastic, paper, wooden products, and coated materials (Deprez et al. 2012; Chitu, et al. 2003; Kubovsky and Kacik, 2014). According to Ueda, et al. (1990), CO_2 laser marking is faster and cheaper than YAG laser marking. However, the visibility of CO_2 laser markings is inferior to that of YAG laser markings, except when viewed using optimum observation directions. In industrial operations, CO_2 lasers, which have a wavelength of $10.6 \mu\text{m}$, can be emitted either pulsed or in a continuous wave (CW). Continuous waves are delivered continuously over a given time as opposed to a pulsed operation, in which power is delivered in pulses of a chosen duration over a given time. Some industrial laser applications are shown in Table 2.1.1.

Table 2.1.1. Some common applications of industrial lasers (Wangui, et al. 2012)

Type	Operating mode	Power range (Watts)	Applications
CO_2	Pulsed	5 – 3000	Cutting, welding, drilling, marking
CO_2	Super pulsed	1000 – 5000	Cutting
CO_2	Continuous	100 – 25,000	Cutting, welding, surface treatment
CO_2	Continuous	3 – 100	Drilling, marking
Nd:YAG	Pulsed	10 – 2000	Cutting, welding, surface treatment, drilling, marking, micro-machining
Nd:YAG	Continuous	500 – 3000	Cutting, welding, surface treatment
Nd:YAG	Q-Switched	5 – 150	Drilling, marking, micro-machining

The laser-material interaction has been investigated by varying laser parameters and analyzing the effects on either a single or multiple substrates (Carpene, et al. 2010). According to (Lazov, et al. 2015), laser parameters are divided into two groups, depending on the type of laser used:

a. Continuous wave lasers

The basic parameters are: wavelength, output laser power, scanning speed, beam quality factors, and Q-switch mode (minimum pulse duration, maximum pulse repetition rate, laser peak power).

b. Pulsed lasers

The parameters include: wavelength, average power of the laser, maximum peak power, pulse repetition rate, pulse duration, maximum energy per pulse, frequency stability, quality of the beam.

2.1.2. Effects of laser radiation on surfaces

The laser (Light Amplification by Stimulated Emission of Radiation) was discovered by Theodore H. Maiman, who used a flash lamp pumped through ruby crystal as the medium (Maiman, 1960). In recent years, the laser has been utilized for marking. Laser marking is the technique of marking or labeling materials using a laser machine. Product marking can be carried out for various purposes, included product identification and traceability. Laser marking is rapid, permanent, non-contact, and produces high-resolution images on surfaces (Ion, 2005). Laser marking commonly involves inducing a visible color or texture change on a surface. According to (Buchfink, 2007; Lazov, et al., 2015) laser marking uses various marking processes, such as: 1) Engraving: the process of removing material due to melting and evaporation by a laser beam. 2) Etching or ablation: the laser beam removes a coating layer from the underlying base material. 3) Annealing and color change processes: the laser heats the workpiece, altering the color but allowing the surface to remain smooth. 4) Foaming: the laser beam melts a material, creating gas bubbles that reflect the light diffusely. 5) Carbonizing: a process that produces strong contrasts on surfaces, and is usually used on polymers or bio-polymers such as leather, paper, and wood.

Laser marking systems use various lasers and optical delivery systems to mark products such as metals, glass, ceramics, plastics, wood, leather, and horticultural products. Laser marking generally prints alphanumeric characters, logos, barcodes, and data matrix codes on the surface of a product to specify the date of manufacture, best-before date, serial number, and so on (Jangsombatsiri and Porter, 2007). According to

Markov, et al. (2015), the general advantages of laser marking techniques are: permanence, high speed, high economic effectiveness, high contrast inscriptions, ease of automation, and high reproducibility.

Various types of lasers are necessary because of the varied parameters of energy absorption for different materials. Based on Fig. 2.1.1, ferrous and non-ferrous materials have magnificent absorption at 1064 nm, while precious metals exhibit good absorption at 355 and 532 nm. Plastics also absorb higher wavelengths of laser output. A higher absorptivity value means that more laser radiation is required for processing (Sobotova, 2014). According to Sobotova (2015), there are many aspects to consider when selecting a laser marking system for a particular application:

- a. Power density
- b. Thermal aspects: thermal conductivity, heat capacity, melting point and heat of vaporization
- c. Reflectivity: material, wavelength, and temperature

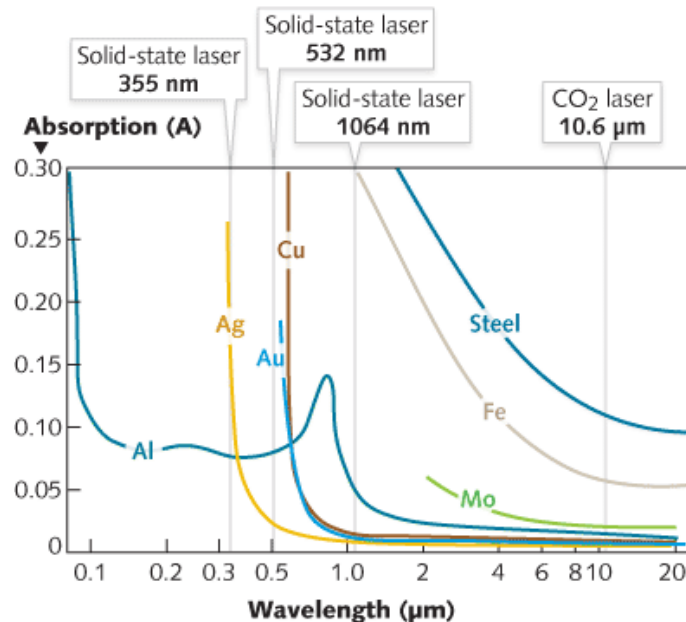


Fig. 2.1.1. The absorption of materials vs wavelengths (Kaminski, 2011)

2.1.3. Laser marking applications on horticultural products

Laser marking of horticultural products was approved in the USA by the Food and Drug Administration and is generally used for labelling citrus fruits (Etxeberria, et al. 2006b; Sood, et al. 2008). Laser marking technology was also approved in 2013 by the European Union (EU) in regulation 510/2013 (Commission Regulation EU, 2013). Longobardi (2007) integrated sorting machine and laser marking of apples and melons

fruits using a CO₂ laser beam. The technology was suggested for composing 1D barcodes. Heck, et al. (2007) studied the use of an additive on products' surfaces that implemented a color change. Another method of laser marking was implemented by Marx, et al. (2013), who marked 2D patterns or barcodes onto the surface of apples and rhododendron cuttings with various laser systems.

A number of applications of marking have been developed for fruit and ornamental plants. Commonly, price look-up (PLU) stickers are adhered to fruits in packing lines, typically after pre-processing or before the final packaging. PLU stickers are currently used to each piece of fresh produce, and comprise a four-number code to allow food business operators to identify the product in order to facilitate checkout and inventory control. Floral industries have also utilized marking to mark potted and cut flowers. Sometimes the markings include various greetings (i.e. a small card) when delivering flowers for special occasions. However, paper labels or stickers on fresh fruits and ornamental plants have several drawbacks, such as that labels can easily be detached, lost or exchanged (Drouillard and Kanner, 1999; Edxerberria, et al. 2006a; Marx, et al. 2013). Recently, a number of researchers have utilized laser marking on horticultural products, as shown in Table 2.1.2.

Table 2.1.2. Various examples of laser marking on horticultural products

References	Products	Laser sources
Drouillard and Kanner (1999)	Oranges, tangerines, grapefruits, apples, pears, plums, nectarines, pears, kiwi	CO ₂
Edxerberria, et al. (2006b)	Oranges, avocados, tomatoes, potatoes, peppers, cucumbers	CO ₂
Sood, et al. (2008)	Tangerines	CO ₂
Sood, et al. (2009)	Grapefruits	CO ₂
Edxerberria, et al. (2009)	Citrus fruits	CO ₂
Danyluk, et al. (2013)	Citrus fruits	CO ₂
Marx, et al. (2013)	Apple fruits and rhododendron cuttings	CO ₂ , Excimer, Nd:YAG, Diode, Fiber laser
Edxerberria and Gonzalez (2014)	Citrus leaves	CO ₂
Zigelboim (2015)	Coconut	CO ₂
Edxerberria, et al. (2016)	Citrus leaves	CO ₂
Hoult (2017)	Apple fruits and bananas	Fiber laser

2.2. Challenges in laser marking on horticultural products

2.2.1. Positioning of the laser

2.2.1.1. General aspects

The conventional laser marking process can be enhanced by modern machine vision. Moreover, the combination of laser systems and machine vision, which is able to identify the position and orientation of an object, could increase cost effectiveness and efficiency in manufacturing processes across a wide range of industries. Another benefit is its flexibility, which allows the implementation of the laser process on objects with various 3D surfaces (Diaci, et al. 2011), such as objects with tilted or curved surfaces (Chen, et al. 2009). The camera is integrated onto the laser by two different methods (Lehmann, 2017): 1) on-axis machine vision control: laser deflection unit is combined with a camera coupled to the path of the laser beam; 2) off-axis machine vision control: One or more cameras (usually not more than four cameras) are installed outside of the deflection unit. With this function, the user can see a live image preview on a screen, which helps to easily position text, barcodes, or numbers directly onto the workpiece (Scanlab, 2017).

A number of studies using this positioning system have been conducted. Diaci, et al. (2011) utilized a structured-light 3D sensor to determine the 3D surface of a marking object. Qi, et al. (2015) proposed a stereo-vision laser galvanometric scanning system for irregularly shaped objects. Beck, et al. (2016) applied an on-axis CCD camera for inspection and monitoring of the subtractive laser of a short-pulse fiber laser. Audouard, et al. (2017) implemented an off-axis CCD camera to accurately set the focusing position of ultrafast lasers. Due to the enhanced precision, efficiency and flexibility, the assistance of a camera in precise laser marking has been proven to have high potential as a prominent laser machining device with many applications (Qi, et al. 2015).

Some studies have implemented combined systems (laser systems and vision systems) for use with agricultural products. A design of mechanical arms for laser-guided weeding has been implemented by Ge, et al. (2013). Marx (2014) investigated the effects of different laser wavelengths, as well as a CCD camera, in capturing plant images and locating plants for weed control. The system developed achieved a mean positioning accuracy of about less than 2 mm. The positioning of the system for meristem detection by laser beam was limited by problems of overlapping, which occurred whenever random placement of weeds led to occluded leaves. Shah and Lee (2015) studied a laser weeding system for elimination of in-row weeds. The system consisted of a four-wheeled robot cart, a laser, a simple plug-and-play USB camera to

detect the plants, an encoder, a GPS, and halogen lamps. A range of HSV color space of the green plants was used to threshold the image between plants and soil. The system achieved an accuracy of 63.6% in eliminating weeds. The study could possibly be improved by using a lower resolution encoder and by increasing weed detection using shape and texture features. Xuelei, et al. (2016) studied the kinematics and statics analysis of a novel 4-DoF parallel device for use by a laser weeding robot. Xiong, et al. (2017) proposed a prototype laser weeding robot which was comprised of three subsystems: a robotic platform, machine vision, and a laser pointing system. In order to detect the weeds, three segmentations were applied: differences in area, erosion and dilation operations, and two shape features (solidity and compactness). However, the machine vision system could not distinguish plants with similar parts if they were overlapping. Separation of a specified object among similar objects is the most important task in the positioning process. This process becomes difficult when objects occlude each other.

2.2.1.2. Image processing as a tool for positioning in complex plant situations

2.2.1.2.1. Positioning and localization on leaves

Segmentation is a challenging task because of the uncertainties about the background and overlapping of horticultural objects. This means that there are cases when the objects are not recognized because there is missing visual information. Recently, numerous methods for use in overlapping conditions have been proposed. Pastrana and Rath, (2013) proposed a model involving ellipse approximation and active shape to solve the problem of overlapping leaves. Wang, et al. (2013) described an adaptive thresholding algorithm using Otsu and Canny operators to segment a single leaf. Cerutti, et al. (2013) proposed a two-step active contour segmentation algorithm by a polygonal leaf model. This model involved analyzing the image to retrieve the contours of the leaf from a complex background. A study of different segmentation approaches to the extraction of tree leaves from natural images is given in the study of Grand-Brochier, et al. (2015). Chopin, et al. (2016) studied basic a-priori information about shape of plant leaves local image orientations to fit active contour model. Zhang, et al. (2016) studied a segmentation algorithm based on leaves' similar tangential directions in order to identify individual leaves automatically. Wang, et al. (2017a) proposed image segmentation by solving overlapping leaves based on a Chan-Vese model and Sobel operator.

Other researchers have used shape features for pattern recognition in addition to colors and textures (Table 2.2.1). However, all the studies reviewed in Table 2.2.1 so far only apply to the detection of one leaf. According to Lee and Chen (2006), processes involving shape features can be classified into two main categories: a) processes that use the contour of a shape to extract information and b) region-based approaches that use a whole object region to obtain information.

Table 2.2.1. Examples features used in leaves detection

Features	References
Shape	Amin and Khan, 2013; Lakshmi and Mohan, 2017
Shape, color	Satti, et al. 2013; Laresse et al. 2014; Munisami, et al. 2015
Shape, contours	Wang, et al. 2014; Diaz, 2017
Shape, texture	Chaki, et al. 2015; Kan, et al, 2017

Some studies have used different cameras to exploit plants' shapes in order to constrain the plants-finding problem, as shown in Table 2.2.2. Regular 2D cameras are commonly used to assess plant parameters with high speed and robustness. Nevertheless, some systems fail to exploit plants' full shapes due to occlusion on complex leaf structures in a 2D image plane.

Table 2.2.2. Different cameras used in plants detection

Sensors	Methods	Limitations	References
RGB camera	Plant identification based on dendrological determinations	Only consider single leaf identification	Rath, 1997
	Ellipse approximation and active shape model for solving overlapping leaves	Increasing area of overlapping (>32%) leads to decreasing identification effectiveness	Pastrana and Rath, (2013)
	Using Otsu and Canny operators to extract the area of the target leaf	Background overlapped	Wang, et al. 2013
	Using active polygons for leaf segmentation and shape estimation	Not enough representation of the diversity of colors in a single leaf	Cerruti, et al. 2013
Scanner	Solving overlapping leaves based on Chan–Vese model and Sobel operator	Varying lighting conditions	Wang, et al. 2017
	Identification of disease	Objects analyzed by	Matsunaga, et

	symptoms on living plant leaves using HSB color space	scanners are required to be flat	al. 2017
Spectral camera	Leaf extraction and segmentation based on edge-subtraction	Not able to reconstruct occluded or partial leaves	Noble and Brown, 2008
Stereo vision and infrared	Leaf segmentation and classification of leaves using 3D information	Requires manual adjustments of thresholding angle	Aksoy, et al. 2015; Guo and Xu, 2017
3D Lidar	Plant detection and mapping	The sensors have a low resolution	Sanz-Cortiella, et al. 2011; Weiss and Biber, 2011
ToF camera	Characterization system for indoor and outdoor depth imaging of leaves' 3D morphological traits	Low resolution and expensive camera	Kazmi, et al. 2014 Li and Tang, 2017
Kinect camera	Segmentation of individual leaves and plant phenotyping	Kinect v1 did not exactly measure smaller objects, and the lowest distance between the object and the Kinect is 50 cm	Paulus, et al. 2014; Wang and Li, 2014; Xia, et al, 2015; Andujar, et al. 2016

Commercial 3D laser scanning systems could be used as a method of recording 3D reconstructions and acquisition of entire plants (Yan, et al. 2009). However, 3D acquisition can be time-consuming, expensive, and requires a huge amount of data when applied to large areas of plants. Moreover, a full reconstruction of all plants may not be necessary for the characterization of specific features of their morphologies.

RGB-depth (RGB-D) imaging systems have been progressively studied and applied to agricultural products. A RGB-D camera can capture depth and color images of the scene simultaneously and automatically map the RGB-D data, resulting in a colored point cloud in a 3D spatial domain. RGB-D cameras are a low-cost (about 150 U.S. dollars) cheaper than conventional laser scanners (approximately ten thousands of U.S. dollars). RGB-D cameras have been rapidly adapted to use in several areas, particularly robotics, mapping, forensics, and 3D modeling (Henry, et al., 2010; Canessa, et al., 2013). The opportunity of using consumer-grade RGB-D cameras for phenotyping trees was introduced by Chéné, et al. (2012). A size estimation of sweet onions was demonstrated by Wang and Li (2014), and the use of depth cameras to assess the growth state and yield of cauliflower crops was described by Andujar, et al. (2016).

2.2.1.2.2. Positioning and localization on fruits and stems

Some studies locating fruit under natural conditions have been conducted. A binocular stereovision system was utilized to locate tomatoes by Xiang, et al. (2010). Song, et al. (2012) proposed a convex hull method to locate occluded apples. A machine vision-based method to recognize and locate ripe tomatoes was studied by Arefi, et al. (2011). Tanigaki, et al. (2008) studied a cherry-harvesting robot. Xie, et al. (2012) suggested four key methods in fruit localization: least slope variance, least distance, three collinear points and second-order central moment methods. However, each of the four methods has its drawbacks, and the combination of the four methods was time consuming.

Numerous researchers have combined many features to increase the accuracy of fruit detection, as shown in Table 2.2.3. In general, the accuracy of machine vision systems in the recognition and localization of fruit can be affected by occlusions, variable lighting conditions, and variations in the color, shape, and size of the fruit.

Table 2.2.3. Some examples of multiple features used in fruits detection

Features	Limitations	References
Color and shape	Varying lighting condition	Zawbaa, et al. 2014
Combination of color, shape and texture	Overlapping objects	Yamamoto, et al. 2014; Hosen, et al., 2017
Combination of color and arc contours	Natural light might cause strong shading and saturation. Variable size, shape and overlap of fruits	Linker, et al., 2012

Furthermore, some studies have used thermal and hyperspectral sensors for fruit detection, as shown in Table 2.2.4 and Table 2.2.5, respectively. These cameras typically provide better results in fruit detection than color cameras. This is because objects with similar colors may show different reflectances in non-visible areas.

Table 2.2.4. Some applications of thermal cameras for fruits detection

Applications	Thermal camera brand	Wavelength range	References
Estimation of number and diameter of apple fruits in an orchard during the growing season	Thermal camera AGEMA 570 (Flir Systems Inc, MA, USA)	7.5 – 13 μ m	Stajnko, et al. 2003
Temporal variation in citrus canopy for citrus detection	ThermaCAM P65HS (Flir Systems Inc, MA, USA)	7.5 – 13 μ m	Bulanon, et al. 2008
Image fusion of visible and thermal images for oranges detection	ThermaCAM P65HS (Flir Systems Inc, MA, USA)	7.5 – 13 μ m	Bulanon, et al. 2009

Table 2.2.5. Some applications of hyperspectral cameras for fruits

Applications	Wavelength range	References
Green citrus detection	369 – 1042 nm	Okamoto and Lee, 2009
Measuring color of vine tomatoes	325 – 985 nm	van Roy, et al. 2017
Detection of defect on green-peel citrus	523 nm, 587 nm, 700 nm and 768 nm	Chun-wang, et al. 2013

2.2.1.3. Tasks (first)

Positioning image processing systems on complex leaves, fruits and stems is challenging. Implementing positioning systems for use with horticultural products is not an easy task (Zhao, et al. 2016). There are many different variables and segmentation approaches that could be optimized for a desired laser marking position. Integrating positioning systems with lasers is a way to increase accuracy and drive efficiency in horticultural uses.

2.2.2. Laser and marking parameters

2.2.2.1. General aspects

In automotive and electronics industries, some important laser parameters that are often investigated are: laser power, scanning speed, and frequency (Ng and Yeo, 2001; Jangsombatsiri, 2006; Kasman 2013; Amara, et al. 2015; Brihmat-Hamadi, et al. 2017). Other parameters, such as material properties, also affect the marking line width (Ng and Yeo, 2001). The depth of marking is influenced by various parameters, particularly: energy density, type of material, and interaction times between beam and material (Chen, et al. 2009). The sharpness of the marked edges influences the marking contrast. According to Han and Gubencu (2008), this parameter is particularly essential in marking barcodes, as poor edge sharpness may fail to decode a barcode. Jiang, et al. (2017) studied high contrast patterning on glass substrates with a 1064 nm pulse laser. The method consists of heating graphite plate with a laser. Higher peak laser power or power density will provide a better edge resolution. Mark width refers to the width of the line segments that form a character. Mark width in characters is basically determined by the geometry of the mask and the imaging quality of the lens (Chen, et al. 2009). The quality of laser marking is measured based on grade visibilities (Ueda, et al., 1990), mark contrast (Wang, et al. 2003), and mark width and depth (Chen, et al. 2009). These features are usually evaluated using several techniques such as image processing, contrast evaluation, optical microscopy, electron microscopy, and surface roughness measurement devices. Acceptable levels of each of these features usually depend on the materials used. Marking contrast is the visual difference between the apparent brightness of the marked surface and the apparent brightness of the unmarked surface of a workpiece (Wang, et al. 2003).

In biomedical studies, Farkas, et al. (2013) described five laser parameters that were applied for use with patients, namely, laser power, wavelength, spot size, pulse width, and cooling. A low laser power (0.001 – 0.1 Watts) has been used as a method to reduce pain, inflammation, and edema; to promote wound, deep tissue, and nerves healing; and to prevent tissue damage (Farivar, et al. 2014). Dawood and Salman (2013) studied the utilization of a pulse diode laser (5 mW) with a low power level to enhance and accelerate wound healing. Illescas-Montes, et al. (2017) investigated the effects of a 940 nm diode laser on cultured human fibroblasts using different irradiation levels. They used a 940 nm diode laser at different doses of energy (0.2–1 W and 1–7 J cm⁻²) using continuous and pulsed mode. The best results were observed with a power of 0.2 or 0.5 W and an energy density between 1 and 4 J cm⁻². No difference was detected between

continuous and pulsed modes. Chaves, et al (2014) investigated the effects of low-power light therapy on wound healing using lasers and light emitting diodes. The biological effects were dependent on the irradiation parameters, mainly wavelength and dose. Generally, in the ultraviolet (UV) to the near infrared (IR) spectrum, shorter wavelengths have a more superficial penetration because of their absorption pattern, and longer absorption wavelengths (650-1200 nm) have a deeper penetration in the tissue (see Fig. 2.2.2). The least penetrating wavelengths appear in the far UV (excimer) and far IR (CO₂) spectrum because of their high affinity for water (Farkas, et al. 2013).

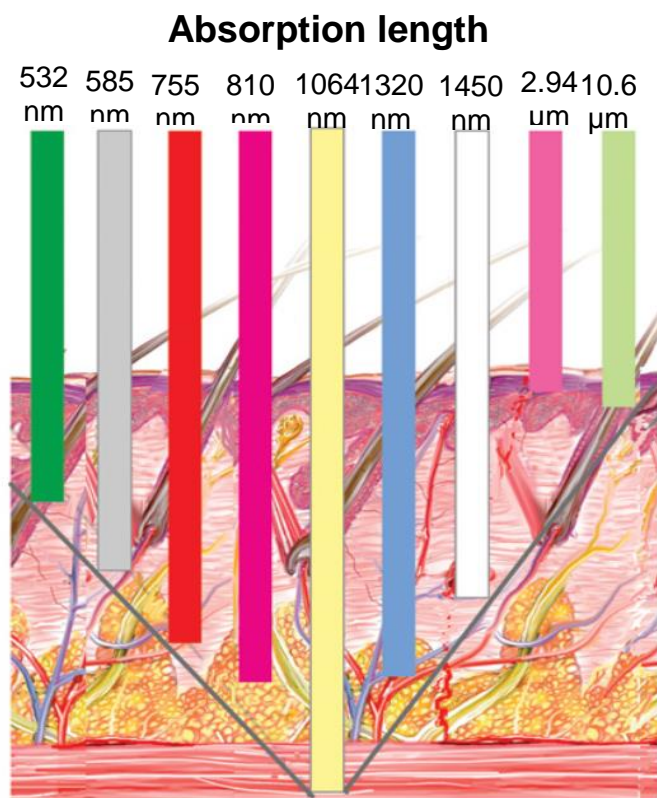


Fig. 2.2.2. Illustration of the penetration depth on tissue of various common wavelengths (Farkas, et al. 2013)

2.2.2.2. Parameters for laser application on leaves

The interaction of a laser beam with any material depends on the laser's wavelength. According to Csele (2011), due to their relatively long infrared wavelength, CO₂ lasers are well-absorbed by some materials, such as: plastics, glass, water molecules and many common materials. However, when it comes to metals, shorter wavelengths (i.e. Nd:YAG laser, 1.06 μm) are absorbed to a higher degree. The low

absorption of CO₂ lasers by metal is due to high density energy beams, which create small changes in surface temperature that tend to increase the beam coupling coefficient (Robert and Erik, 1997). Wöltjen, et al. (2008) studied the absorption spectra of *Nicotiana tabacum* (Solanaceae) and *Echinochloa crus-galli* (Poaceae). The results showed that absorption of spectral values above 2500 nm was close to 95%. The absorption of laser radiation in plant tissue is dependent on the wavelength of the laser used. Fig. 2.2.3 shows the absorption spectrum of a leaf in a fresh and dry state.

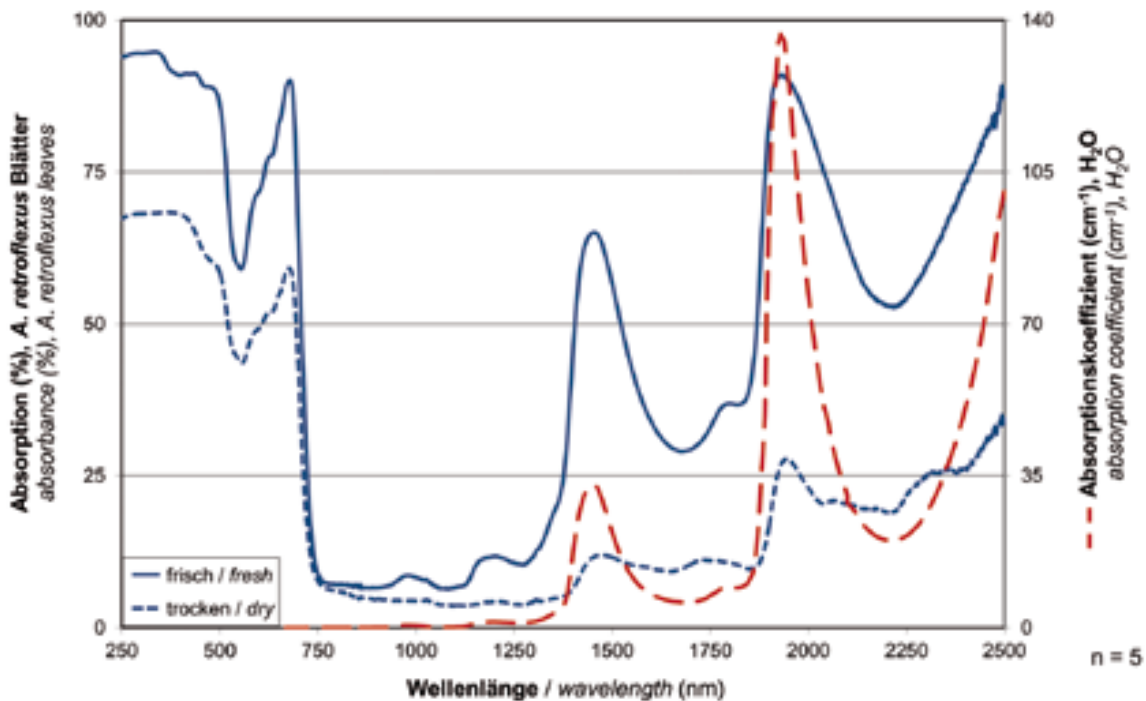


Fig. 2.2.3. Absorption spectra of fresh and dried leaves (*A. retroflexus*) depend on the laser wavelength (Marx, et al. 2012)

Due to the high water content of leaves, the absorption of spectral values in plant tissue was mainly affected by the water composition of the leaves. Langner, et al. (2006) determined that plant material rich in water absorbs CO₂ radiation very well and can be heated faster. Griepentrog, et al. (2006) also found that a wavelength of 10.6 μm is strongly absorbed by intra-cellular and extra-cellular water, leading to a temperature rise in tissue water. Thus, this wavelength has a low penetration depth in plant tissue.

2.2.2.3. Parameters for utilizing lasers on fruits and stems

A laser marking device has been designed for labeling citrus fruit surfaces with a low-energy carbon dioxide laser beam (Drouillard & Rowland, 1997). Etxeberria, et al. (2006a) found that the diameter and depth of penetration depressions due to laser marking were fairly similar on the surfaces of avocados and tomatoes, averaging 200 μm and 25 μm , respectively, and affecting only the outermost 2-5 epidermal cells. The formation of pinhole depressions caused disruptions to the cuticular barrier of citrus' surfaces, which could allow for the penetration of pathogenic microorganisms (Etxeberria, et al., 2006b). Studies of the susceptibility of laser marked tangerines (Sood, et al. 2008) and grapefruits (Sood, et al. 2009) to *Penicillium digitatum* spoilage unsuccessful to show the ability of decay microorganisms to colonize the marked surfaces of fruits. According to Bain (1957), this is due to the unique anatomical organization of citrus peels, which contain numerous oil glands and a loosely packed thick mesoderm. Sood, et al. (2008) reported that laser marking tangerines (*Citrus reticulata*) using a laser energy of 0.38 J mm^{-2} resulted in a heat-affected zone of 50 μm . Sood, et al. (2009) found that there was no infection risk to grapefruits after laser marking at 0.5 J per pattern and storage for 5 weeks at 10 °C and a relative humidity of 65% or 95%. Danyluk, et al. (2010), studied laser labeling of mature green tomatoes using a CO₂ laser with a maximum energy of 0.578 W per character. The results demonstrate that laser labeling does not support the growth of decay or pathogenic organisms at that energy level, even in the presence of soft-rot organisms. The same results were reported by Yuk, et al. (2007) on mature red tomato fruits. Danyluk, et al. (2013) reported that laser marking on citrus peels (0.578 W per character), combined in any order with waxing, does not influence the fate of Salmonella populations on citrus fruits. Marx, et al. (2013) studied laser marking 2D codes on apples and rhododendron cuttings at a low laser power (5-10 W) using a CO₂ laser. Barcikowski, et al. (2006) found that applying 2.15 J mm^{-2} of laser energy to pine wood resulted in a heat-affected zone of about 70 μm .

2.2.2.4. Tasks (second)

Optimal laser marking parameters should be determined to avoid destroying markings on horticultural products. Physical interactions between the laser beam and the horticultural products during the marking process play an essential role in the production of laser marks on different types of products. In addition, the type of marks and the assessment of the quality of the marks depend on the purposes of the application.

2. State of the art of laser marking on horticultural products

These significant issues, including the effects of laser parameters on the quality of marks produced and the mark's readability, should be understood in order to obtain the optimal results.

2.2.3. Detection and quality assessment of marking patterns

2.2.3.1. General aspects of marking codes

Barcodes are an important technology for use in data identification and data capture. Barcodes are divided into two categories: one-dimensional (1D) barcodes and two-dimensional (2D) barcodes. 1D barcodes typically contain parallel lines of varying widths and spacing. 2D barcodes are graphical images that store data vertically and horizontally. Based on GS1 (2018), barcodes are generally used to encode information or data such as serial numbers, product numbers, and batch numbers. Barcodes are necessary for use in product supply chains, which enable parties like manufacturers, retailers, transportation providers to identify and track their products. Barcodes can be scanned electronically using laser and camera based systems. According to Microscan (2018), laser scans are a better option if barcodes are extremely damaged or if high is projected in different symbol orientations.

According to Aung and Chang (2014), 1D barcodes are simple to use and economic; however, they exhibit high data integrity corruption and poor performance. 1D Barcodes are easily read by scanning the code's lines and spaces. 1D codes represent short tags, however, and adding more string characters results in unbearably long and inefficient symbols. According to Rinkalkumar, et al. (2014), 1D barcodes must be scanned in one direction; if the angle of a scan line is not within a specific range, the information in the barcode will not be encoded correctly. However, 2D barcodes have wide ranges of angles for scanning. Moreover, 2D barcodes have advantages in terms of their ability to store large amounts of data, as well as their robust error correction capabilities.

2.2.3.2. Detection of 2D codes

A two-dimensional barcode has a high readability, even with distorted codes and a small symbol size (GS1, 2018). In general, 2D barcodes are classified in two groups: stacked 2D barcodes (code 49 and PDF 417) and matrix 2D barcodes (data matrix codes and QR codes). Data matrix (DM) codes are very effective 2D barcodes that use a small area of square modules, which include both error detection and correction (GS1, 2018). Numbers and characters are determined in terms of bits, represented by dark or light modules of an identical size. The larger the amount of bits required, the larger the symbol will be, increasing the density of modules in the code. A dark module and a white module represent binary 1 and binary 0, respectively. They are bordered by an "L finder

pattern”, which is enclosed by a quiet zone area on all four sides of the symbol (Figure 2.2.4).

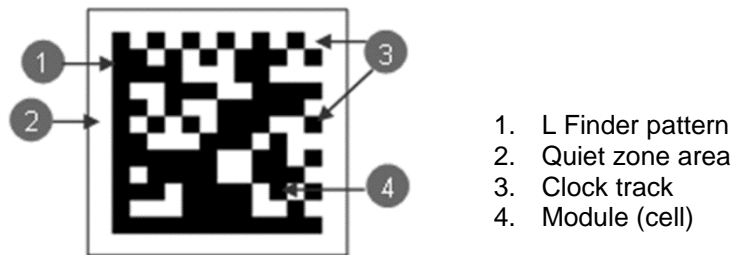


Fig. 2.2.4. Data matrix structure

Two adjacent sides are solid dark lines mainly used to define orientation, physical size, and code distortion. Two opposite sides known as “clock tracks” comprise alternating dark and white modules. These are primarily used not only to define cell structure, but also to determine the code’s physical size and distortion. The latest form of the DM method is known as ECC200, which uses Reed-Solomon error correction. Besides being advantageous in terms of readability, the ECC200 Reed-Solomon error correction algorithm allows the detection of partially damaged DM codes (Reed and Solomon, 1960), whereas traditional barcodes have no error correction capability (GS1, 2018).

Data matrix codes are graphical patterns. They are divided into three components: 1) a finder pattern, which is needed to find the symbol and its orientation in an image, 2) data patterns, which consist of binary modules grouped relative to the finder pattern, and 3) a quiet zone. In order to decode the barcode, the regions of the barcode are segmented by locating the finder pattern. The finder pattern can be detected by an edge detector based on a Hough transform (ISO/IEC 16022, 2006), which consists of advanced edge reconstruction methods (Chen et al. 2012). Following this, the barcode image quality is enhanced and returned to the original form in black and white. The binary values in the code are read out and error correction is generated to produce the decoded data. Commonly, the data matrix code is decoded using the ISO/IEC 16022 standard algorithm. In addition, ZXing (zebra crossing) open source algorithm decoder (Owen and Switkin, 2015) can also be used to read the code.

2.2.3.3. Quality standards and assessment of 2D code

Laser marking barcodes by a process that produces reliably readable, permanent marks that are unaffected to harsh operational situations directly on parts has produced much interest in industries in recent years. Several industry associations have adopted direct-part marking as a technique for implementing permanent marks for identification purposes (Cherniavsky, 1999), as follows: The International Organization for Standardization (ISO), Semiconductor Equipment and Materials International (SEMI), Association for Automatic Identification and Mobility (AIM), Automotive Industry Action Group (AIAG), the Air Transportation Association (ATA), and Electronics Industry Association (EIA). The data matrix, a 2D matrix symbol, has been approved by many organizations as a standard for direct-part marking identification. According to International Organization for Standardization/International Electro technical Commission ISO/IEC 15415 standards, the quality of a Data Matrix can be determined by assessing the following performance measures: decoding, symbol contrast, axial non-uniformity, grid non-uniformity and unused error correction.

2.2.3.4. Effects of laser marking on 2D codes

2.2.3.4.1. Effects on industrial materials

Detection of codes after laser marking is necessary for determining the potential for using the codes to label certain materials. Different laser parameters and types of material create different appearances (NASA, 2002). Therefore, it is necessary to determine the best parameters and find out a relationship between critical laser parameters and the quality of the symbol (code). Several researchers have investigated the relationships between specific sets of laser parameters and their effects on different substrates and quality of codes. Jangsombatsiri and Porter (2007) studied different parameters in laser marking data matrix symbols onto carbon steel materials. They found that contrast and print growth factors were critical factors for the laser mark to achieve a higher grade. Qiu, et al. (2011) utilized an Nd:YAG laser (1064 nm) to produce data matrix symbols on aluminum alloys. The quality of the laser marked data matrix symbol was assessed based on the ISO/IEC standards. The study focused on the following parameters: vector step, inter-step time, laser Q-frequency and laser Q-release time. Lazov and Angelov (2012) described the relationship between the contrast of the marks on the surface of carbon tool steel and operating parameters (such as power density and speed). Li, et al. (2016a) studied the influence of laser parameters (fill

spacing, current intensity, laser scanning speed, and pulse frequency) on the barcodes quality laser marked onto aluminum alloys using a Q-switched lamp-pumped Nd:YAG laser. Li, et al. (2016b) applied direct laser marking to aluminum alloys by rasterizing miniature data matrix codes. According to their study, the average laser power and the Q-frequency have important effects on the contrast and print growth of miniature data matrix codes. The qualities of the code were evaluated in terms of surface roughness and code quality based on ISO/IEC 16022, respectively. Li and Lu (2017) investigated the effect of laser parameters on the symbol contrast and surface roughness of data matrix codes. They established a non-linear regression model in order to forecast the quality of the data matrix codes and the surface roughness.

2.2.3.4.2. Effects on biological/horticultural products

Currently, little information is available in detecting laser marked 2D codes on horticultural products. Marx, et al. (2013) evaluated laser marking data matrix codes on apples and rhododendron cuttings. The quality of the codes was measured according to the minimum spaces between the laser-affected areas and the infection intensities around the laser marked area. The parameters of the laser marking process (laser power, laser energy, laser wavelength, code size) considerably influence the representation accuracy of the code patterns used. In their study, at higher laser powers, the readability decreases rapidly due to damage in the heat-affected zone. Therefore, they recommended the use of a lower laser power (less than 5 W) with a CO₂ laser in future studies in order to find the optimal energy for laser marking. Moreover, the study performed laser marking with a small code edge length, 3 x 3 mm²; however, no information was provided regarding the stability of the code's readability during storage.

2.2.3.5. Tasks (third)

Maintaining the stability of readable 2D laser mark-codes on horticultural products during storage is challenging and requires more research. Distortions in the surface of the code, uneven and complex color backgrounds of horticultural products, and uneven lighting all impose problems on the detection of 2D codes.

3. RESEARCH OBJECTIVES

Laser marking applications have been developed for horticultural products (Edxeberria, et al. 2006; Marx, et al. 2013; Zighelboim, 2015; Hoult, 2017). The ability to find, mark and evaluate products in production lines is critical for the laser marking of horticultural products. Positioning systems are necessary in order to increase accuracy and drive efficiency for the laser marking of horticultural products. Laser positioning systems for marking horticultural products are rare and must perform challenging tasks due to overlapping products and complex shapes in natural conditions. Because of these challenges, positioning systems must detect the characteristic properties of the objects, and automatically position the laser for an exact marking process without destroying other unmarked plants, leaves, fruits or stems.

Optimal parameters for marking horticultural products are necessary in order to produce excellent marking quality, including the ability to mark text and pattern or codes. The effects of laser marking parameters on the quality of marks produced and mark assessment should be determined. The type and quality of the marks depend on the materials used. Therefore, proper understanding of the optimal laser marking conditions of certain materials is critical. This process lacks a standard protocol due to its status as a relatively new application.

Moreover, laser marking of 2D codes on horticultural products is challenging due to various factors, such as: errors in marking codes due to damage on the products, variable lighting conditions, and low contrast. The stability of the 2D codes during storage is a critical issue and needs more investigation. Previously, there has been little discussion about the usage of laser marking of 2D codes in horticultural products. Hence, this study applies image processing as a tool to assess codes correctly.

In order to achieve these goals, the objectives of this study are as follows:

- 1) Finding optimum positions for laser marking of horticultural products
- 2) Optimization of laser marking parameters of horticultural products to achieve an optimal marking result

In order to solve the problem, it is necessary to select examples of horticultural products. Horticultural products include ornamental leaves, ornamental stems, fruits, and vegetables. In this study, poinsettia plants (*Euphorbia pulcherrima* Willd. ex Klotzsch) and bananas (*Musa spp.*) are selected as possible representatives for other products.

In addition to their popularity, poinsettia plants were chosen due to their complex leaf structures. The plant has similar leaf color and overlapping leaves. The extraction of the complex poinsettia leaf images are critical aspects in the segmentation processes. Additionally, the red bracts of the poinsettia are susceptible to bract brushing and abrasion. Since the plants have white bract latex in their cells, the interaction between laser beams and the latex is an additional benefit for this study.

Banana hands were selected as samples due to their complex shapes compared to other fruits. The effect of dynamic changes of bananas' colors during storage, from green unripe bananas to yellow mature bananas, is necessary feature when laser marking. Moreover, bananas' peels are non-edible parts that allow for the application of optimization parameters of laser beams to it. To date, there are few available studies that deal with the laser marking of bananas.

4. MATERIALS AND METHODS

4.1. Materials

4.1.1. Poinsettia plants

Poinsettia plants (*Euphorbia pulcherrima* Willd. ex Klotzsch) 'Prestige Early Red' were grown in a research greenhouse at the University of Applied Science, Osnabrueck. The temperature in the greenhouse was set at 20°C, and the plants were covered with blackout cloth from 19:00 to 09:00 h. The plants were analyzed after 8 weeks of treatment. The samples were distributed into three parts (see Table 4.1.1).

Table 4.1.1. Data sets for parameter estimation and testing

Experiments	Number of plants	
	Parameter estimation/modelling	Parameter testing/evaluation
Optimization laser parameters	240	-
Optimization laser positioning	80	80

The overall samples used were 400 plants. In which only 240 of the plants were used for parameter optimization and no parameter testing. For the laser positioning, 80 plants were used to create parameter estimation, and for testing used 80 other plants.

4.1.1.1. Optimum laser positioning

Plants were captured with Kinect cameras (see Fig. 4.1.1). Afterward, the images were analyzed via image processing by comparing two different cameras (Kinect V1 and Kinect V2) in order to find the right leaves for laser marking. The Kinect V1 and Kinect V2 cameras, which are RGB-D cameras, consist of one color and one depth camera. The experiment was conducted with fluorescent lamps in the laboratory. Direct sunlight, which disrupts correct measurement, was avoided. The background was set to white.

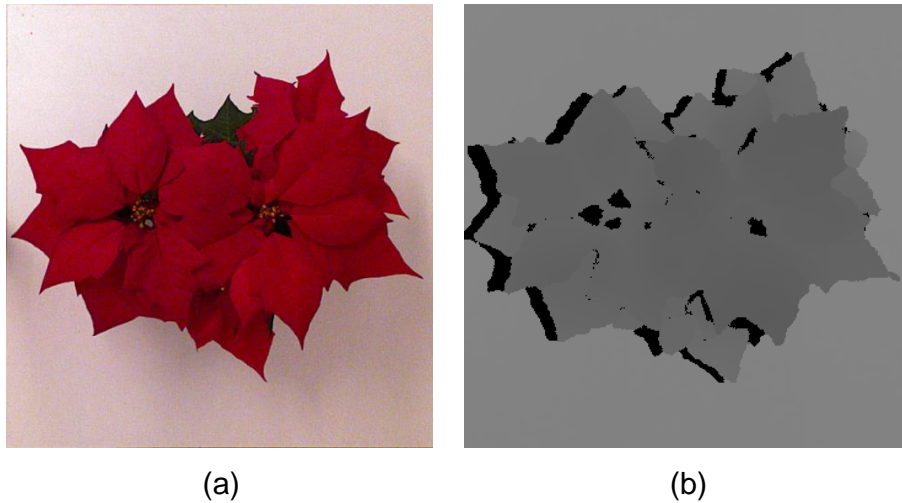


Fig. 4.1.1. Capturing poinsettia plant using Kinect camera from top view, (a) RGB image; (b) Depth image

4.1.1.2. Optimum laser parameters

The plants were marked with a CO₂ laser (continuous wave) using 48 different parameters (see Table 4.7.1). Then, the plants were stored in the greenhouse (temperature at 20°C) and the characters marked on the leaf were captured by using an ASUS T00G camera (2304 * 4096 pixels color images). Damage on red leaves during storage was observed every day for 14 days of storage.



Fig. 4.1.2. Poinsettia plants after laser marking in greenhouse

4.1.2. Bananas

4.1.2.1. Optimum laser positioning

Green mature banana hands (*Musa spp.*, Cavendish subgroup) were collected from Dole® Fresh Fruit Company (Stelle, Germany). Images of banana hands were captured with a CCD camera (DBK41BU02.H, The Imaging Source Europe GmbH, Bremen-Germany) equipped with a 4.5-12.5 mm lens (Computar H3Z4512CS-IR 1/2" varifocal day/night lens). The resolution of each image was 1280 * 960 pixels. All measurements were performed from the same distance and with controlled light conditions. The auto exposure was adjusted; camera gain and gamma value was set 675 and 100, respectively. Additionally, white balance for red and blue was set to 32, respectively; while white balance for green was set to 0. The background was set to be the color red (see Fig. 4.1.3). A total of 140 green mature banana hands and 60 green mature banana fingers were used.



Fig. 4.1.3. Example of banana hands image using CCD camera (top view)

4.1.2.2. Optimal laser parameters

A number of 400 green individual bananas or banana fingers (*Musa spp.*, Cavendish subgroup) were collected from Dole® Fresh Fruit Company (Stelle, Germany). Banana fingers that were separated from the banana hands were selected and then marked using a continuous wave CO₂ laser (wavelength: 10,6 μm, type 48-5, Synrad Inc., USA). In order to initiate ripening, the samples were subjected to ethylene treatment at 1000 μl/L for 24 h. Afterward, the samples were stored in a ripening chamber at 16.6°C (RH 80%) for five days in order to become a yellow color. Then, the samples were stored in a room with a temperature of 20°C for 4 days to simulate conditions of the banana supply chain from the ripening room to the market. The

ripening room temperatures were set on a five-day schedule to achieve a ripening index number of 6 (Table 4.1.2).

Table 4.1.2. Banana ripening stages based on a five-day schedule

Day	Ripening index	Ripening stage	T (°C)
1	2	Green, trace of yellow	16.6
2	3	More green than yellow	16.6
3	4	More yellow than green (fruit is almost ripe)	16.6
4	5	Green tip (green at the end of the banana)	16.6
5	6	All yellow	15.5
6	6	All yellow	20
7	6	All yellow	20
8	6	All yellow	20
9	7	Yellow (flecked with brown)	20

Images of the codes on the bananas were acquired with a CCD camera (DBK41BU02.H, The Imaging Source Europe GmbH, Bremen-Germany) equipped with a 4.5-12.5 mm lens (Computar H3Z4512CS-IR 1/2" varifocal day/night lens). The setup of the camera and the background of the objects were based on the sub-section of 4.1.2.1. The distance between the camera and bananas was set to 5 cm.

4.2. Laser systems

4.2.1. Technical data

A CO₂ laser (Synrad Inc., USA), which is a continuous wave laser, was used to generate data matrix codes and characters on horticultural plants. Table 4.2.1 shows general technical information of the laser. The laser beam was focused and positioned using a marking head (Marking head SH3-200C, galvanometer-operated mirrors, Synrad Inc., USA). WinMark pro software (Synrad Inc., USA) was used in order to create files containing a variety of objects including text and 2D barcodes. The software is capable of controlling every feature of the laser marking process, including altering laser parameters. The specifications of the marking head are shown in Table 4.2.2.

Table 4.2.1 Specifications of the CO₂ laser

	Information
Model	48-5 (S)W
Output power	50 W
Wavelength	10.57 – 10.63 μm
Mode quality	TEM ₀₀ , 95% purity; M ² <1.2
Rise time	< 150 μsec
Beam diameter	3.5 mm
Beam divergence (full angle)	4 mR
Power stability, from cold to start (guaranteed)	$\pm 5\%$
Polarization	Random
Cooling	Water
Heat load (max)	800 W
Flow rate, water (18-22°C)	1.5 GPM
Input voltage / Current	30 VDC / 28 A
Dimensions (mm)	886 x 135 x 114
Weight	20 kg

Table 4.2.2. Specifications of SH series marking head

	Information
Model number	SH3-200C
Field size (mm)	110 x 110
Spot size at 50% (μm)	176
Spot size at 1/e ² (μm)	250
Scan angle (degrees)	48, diagonal
Beam angle to surface normal, max (degrees)	14
Effective focal length (mm)	200
Scanning aperture (mm)	15
Input beam diameter at 1/e ² (mm)	3-4
Continuous input power (W)	65
Input power	28-30 VDC at 3 A maximum
Size (mm)	140 x 250 x 250
Weight (kg)	5

4.2.2. Implementation of the laser process

A computer was connected to the laser in order to control the power, velocity and direction of the laser beam. The distance from the laser scanning system to the object's surface was set to 246 mm (flat-field lens). Manual positioning of the lifting table was used in order to ensure a similar working distance between the laser

scanner and the poinsettia leaves (Fig. 4.2.1). In order to continuously ensure a similar distance from the bananas' surfaces to the laser scanner focus system, an automatic lifting machine was developed (Fig. 4.2.2). The machine includes a stepper motor, three laser diodes and three photodiode sensors. The diode system was used to steer the lifting machine to the exact right object-laser distance by sending a signal to the stepper motor to move up and down.

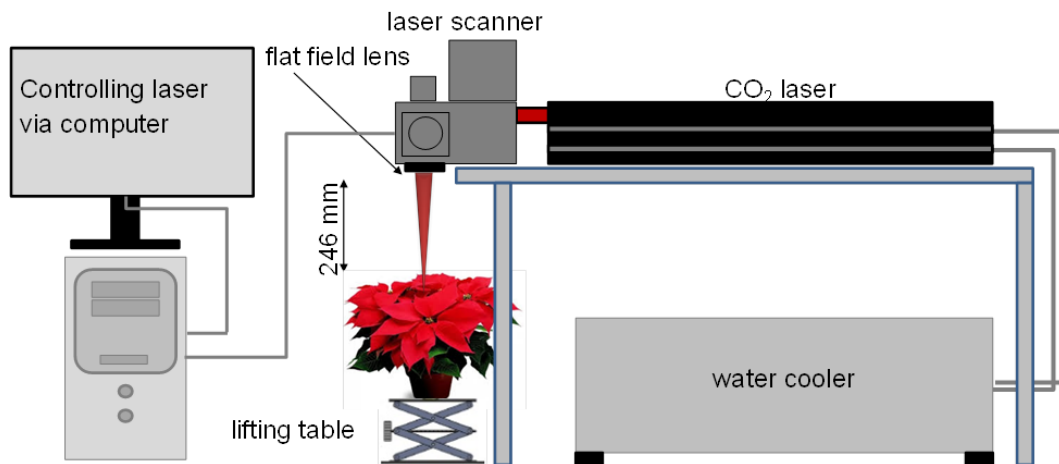


Fig. 4.2.1. Laser marking setup on poinsettia plants: CO₂ laser, laser scanner, manual lifting table and computer-based control

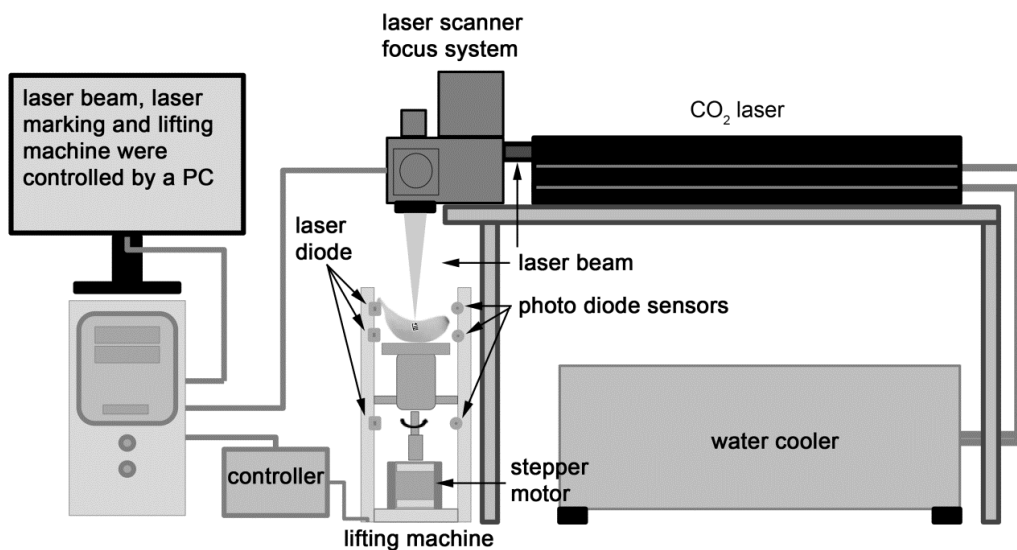


Fig. 4.2.2. Laser marking setup on bananas: CO₂ laser, laser scanner and focus system, lifting machine and computer-based control

4.2.3. Calculation of the laser output

The laser power output (W) was checked by developing a water calorimeter chamber (Fig. 4.2.3) and by comparing the result to a CO₂ laser power meter (Fig. 4.2.4). The CO₂ laser power meter is a calorimeter-type power meter which measures laser power by means of its time exposure.

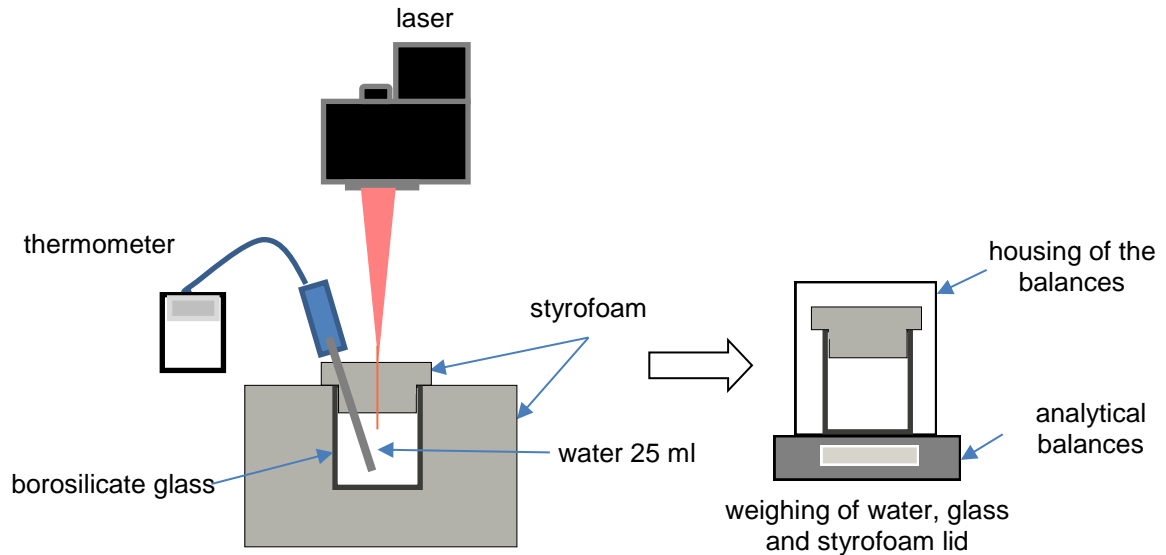


Fig. 4.2.3. Water calorimeter systems

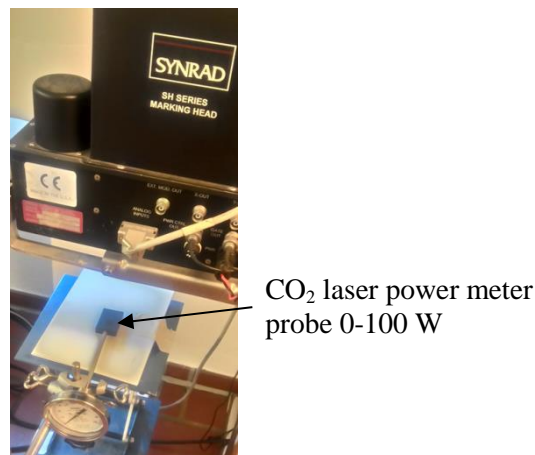


Fig. 4.2.4. The use of a CO₂ laser power meter (Mahoney, USA)

Water in a calorimeter chamber was placed in the path of the unfocused laser beam (see Fig. 4.2.3). The laser machine was turned on for 180 seconds. After the laser was turned off, the digital thermometer values (GMH 3710, Greisinger Germany) continued to change. At the point when the thermometer values stopped changing, the

maximum temperature was noted. Directly following this, the amount of water in the glass was weighed using analytical balances (Cubis® analytical balance, Sartorius). The change in mass of the water before and after lasering indicates water loss due to laser heating effects. The total heat energy (Q_{total}) was calculated by using the following equations:

$$Q_{total} = Q_{water} + Q_{glass} + Q_{water\ vaporization} \quad (4.1)$$

The amount of heat required to rise temperature can be expressed as:

$$Q_{water} = m * cp_{water} * \Delta T \quad (4.2)$$

$$Q_{glass} = m * cp_{glass} * \Delta T \quad (4.3)$$

$$Q_{water\ vaporization} = H_v * \Delta m \quad (4.4)$$

Where:

Q is heat energy (J), m is mass of substance (kg), C_p is specific heat ($J\ kg^{-1}\ K^{-1}$), ΔT is the change in temperature (K), H_v is the heat of vaporization to convert 1 g of water at 100°C to 1 g of steam at 100°C ($J\ g^{-1}$) and Δm is the change in mass (g).

4.3. Cameras and image acquisition tools

4.3.1. RGB image acquisition

Marked bananas images were captured with a CCD camera (DBK41BU02.H, The Imaging Source Europe GmbH, Bremen-Germany) equipped with a 4.5-12.5 mm lens (Computar H3Z4512CS-IR 1/2" varifocal day/night lens). All samples were measured from the same distance and with controlled light conditions (Fig. 4.2.5). The image acquisition was performed with the IC Capture ver. 2.0 TIS software (The Imaging Source Europe GmbH, Bremen-Germany).

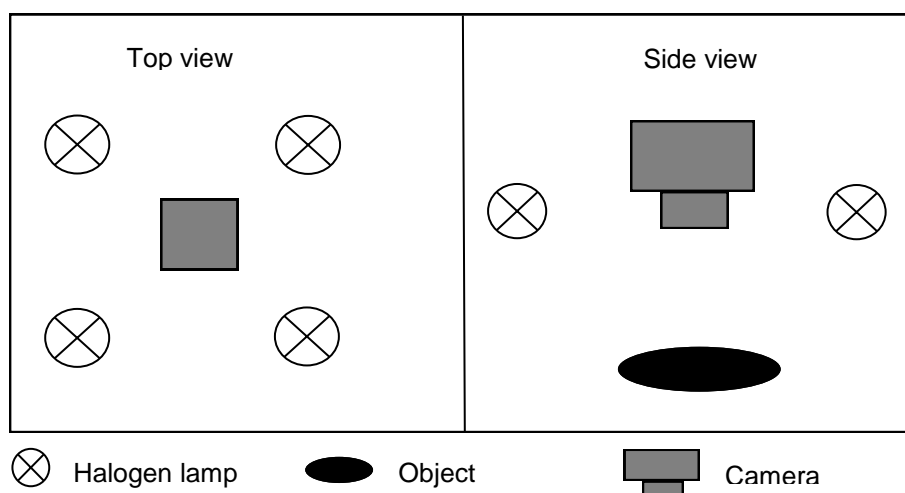


Fig. 4.2.5. Lighting setup

4.3.2. Hyperspectral image acquisition

Images were acquired using a hyperspectral imaging camera (Helios, EVK DI Kerschhaggl GmbH Austria). The camera has 240 * 240 pixels with a spectral resolution of 2 nm and a spectral range from 1,100 nm to 1,700 nm. The acquired images were corrected with a white and dark reference. The corrected image (I_c) is calculated as follows:

$$I_c = \frac{I_h - I_d}{I_w - I_d} \quad (4.5)$$

where I_h is the acquired hyperspectral image, I_d is the dark image recorded by closing the camera lens completely and I_w is the white reference image with 99% reflectance using a teflon white board.

4.3.3. 3D image acquisition

According to Andujar, et al. (2016), the Kinect V1 camera is a RGB camera with a depth camera containing a structured-light device integrated, an infrared emitter, and an infrared depth sensor. The infrared camera is equipped with an 850 – 1100 nm bandpass filter, which captures the depth of the image. The monochrome depth-sensing video stream has an 11-bit depth, which provides 2,048 levels of sensitivity. The RGB camera has a 400 – 800 nm bandpass filter. The Kinect can be switched to near mode, which provides a range of 0.5 – 3 m. In normal mode the camera has a minimum limit of 0.8 m and a maximum limit of 4 m needed to work. The depth accuracy error resolution is typically 10 mm (Ch  n   et al. 2012).

The Kinect V2 camera is based on the time-of-flight (ToF) principle, whereas the previous Kinect V1 device uses structured light to reconstruct the third dimension. The Kinect v2 has a depth resolution of 13-bit depth, which provides 8,192 levels of sensitivity. The camera is able to acquire at a maximum frequency of 30 Hz. The operating field is defined by a depth range of 0.5 – 4.5 m and a 70° horizontal and 60° vertical view angle. The average depth accuracy error resolution is from 2 mm to more than 4 mm (Yang, et al. 2015), depending on the distance and tilt angle. A larger tilt angle and greater distance lead to a lower depth resolution (Yang, et al. 2015).



Fig. 4.3.1. Kinect V1 (left) and Kinect V2 (right)

4.4. Image processing tools

4.4.1. Image processing software tools

Image analysis was carried out with the software package Halcon 12 (MVTec GmbH, Munich). In order to acquire real-time images from the Kinect V1 and Kinect V2, a custom image acquisition application was developed by capturing the RGB and Depth images (Fig. 4.4.1 and Fig. 4.4.2). Algorithms were written in C# and WPF (Windows Presentation Foundation). A Software Development Kit (SDK), provided by Microsoft®, provides the possibility of writing algorithms to control the Kinect; in particular, to acquire and save the depth stream and the color stream via a USB adapter.

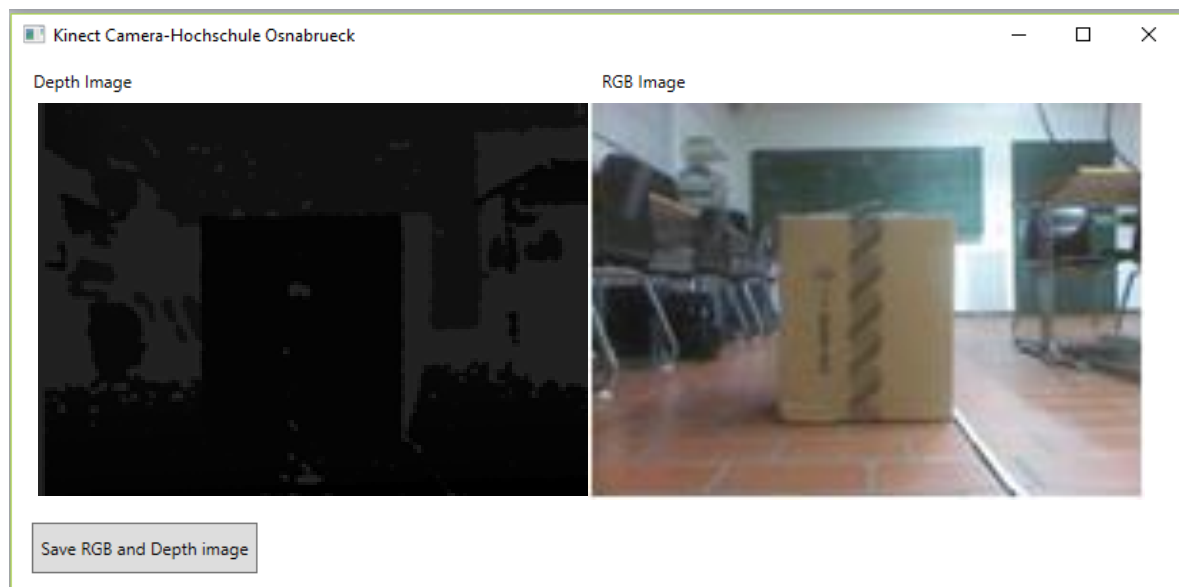


Fig. 4.4.1. Image acquisition application for Kinect V1 camera

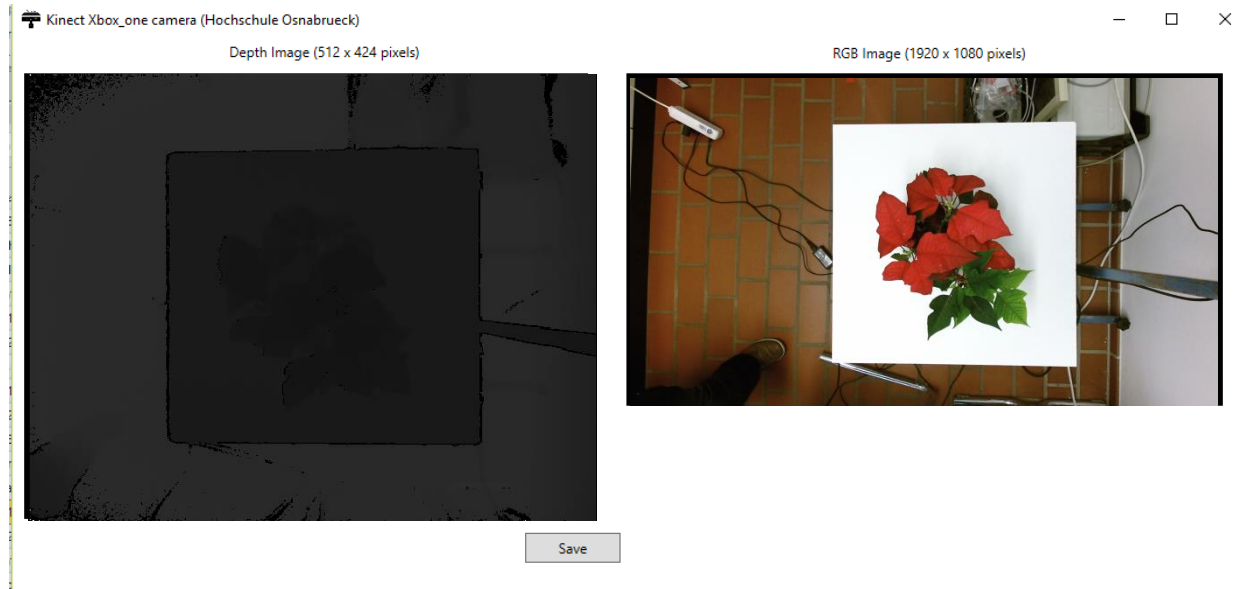


Fig. 4.4.2. Image acquisition application for Kinect V2 camera

The Kinect V2 adopts 'Time of Flight' method instead of 'light coding' method of the Kinect V1 for the depth measurements. The image acquisition application for Kinect V2 uses a different sensing method for depth measurement and provides higher image resolutions. Details comparison between Kinect V1 and Kinect V2 are shown in Table 4.2.3 below.

Table 4.2.3. Specifications of Kinect V1 and Kinect V2

	Kinect V1	Kinect V2
Resolution of color image (pixels)	640 * 480	1920 * 1080
Resolution of depth image (pixels)	640 * 480	512 * 424
Field of view of color image (°)	62 * 48.6	84.1 * 53.8
Field of view of depth image (°)	57.5 * 43.5	70.6 * 60
Method of depth measurement	Light coding	Time of Flight
Working range (m)	0.5 ~ 4	0.5 ~ 4.5

4.4.2. Halcon operators used

The Halcon image processing software was utilized to develop the algorithms in this study. Some Halcon operators are shown in Table 4.4.1.

Table 4.4.1 Halcon operators used (Halcon MVTec, 2014)

Operators	Function
<code>affine_trans_region</code>	Applying an arbitrary affine 2D transformation to regions
<code>area_center</code>	Calculating the area and the center of the input regions
<code>binary_threshold</code>	Segmenting an image using binary thresholding (Otsu method)
<code>connection</code>	Determining the connected components of the input regions given in region
<code>create_data_code_2d_model</code>	Creating a model of a 2D data code class
<code>decompose3</code>	Converting a 3-channel image into three one-channel images with the same definition domain
<code>diameter_region</code>	The operator maximal distance derived between two boundary points of a region
<code>distance_transform</code>	Computing the distance transformation of a region
<code>eccentricity</code>	The operator shape features derived from the ellipse parameters
<code>edges_sub_pix</code>	Extracting sub-pixel precise edges using Deriche, Lanser, Shen, or Canny filters
<code>elliptic_axis</code>	Calculating the parameters of the equivalent ellipse
<code>fill_up</code>	Filling up holes in regions
<code>find_data_code_2d</code>	Detecting and read 2D data code symbols in an image or train the 2D data code model
<code>gen_ellipse</code>	Creating an ellipse
<code>gen_polygons_xld</code>	Approximating XLD contours by polygons
<code>gen_rectangle2</code>	Creating a rectangle of any orientation
<code>get_data_code_2d_objects</code>	Accessing iconic objects that were created during the search for 2D data code
<code>get_data_code_2d_results</code>	Getting the alphanumerical results that were accumulated during the search for 2D data code
<code>get_data_code_2d_results</code>	Getting the alphanumerical results that were accumulated during the search for 2D data code
<code>get_lines_xld</code>	Returning an XLD polygon's data (as lines).
<code>hom_mat2d_identity</code>	Generating the homogeneous transformation matrix of the identical 2D transformation
<code>hom_mat2d_scale</code>	Adding a scaling to a homogeneous 2D transformation matrix
<code>hom_mat2d_translate</code>	Adding a translation to a homogeneous 2D transformation matrix
<code>intersection</code>	Calculating the intersection between two regions

4. Materials and methods

<code>line_position</code>	Calculating the center of gravity, length, and orientation of a line
<code>min_max_gray</code>	Determining the minimum and maximum gray values within regions
<code>move_region</code>	Translating the input regions by the vector given by (row, column)
<code>reduce_domain</code>	Reducing the definition domain of the given image to the indicated region
<code>select_lines_longest</code>	Selecting the longest input lines
<code>select_shape</code>	The operator chooses regions based on shape
<code>set_data_code_2d_param</code>	Selecting parameters of the 2D data code model
<code>set_tposition</code>	Setting the position of the text cursor
<code>smallest_rectangle2</code>	Calculating as smallest surrounding rectangle with any orientation
<code>trans_from_rgb</code>	Transforming an image from the RGB color space to an arbitrary color space
<code>tuple_max</code>	Returning the maximal element of a tuple
<code>tuple_real</code>	Converting the input tuple into a tuple of floating point numbers
<code>watersheds_threshold</code>	Extracting watershed basins from an image using a threshold
<code>write_string</code>	Printing text in a window

4.5. Statistics and hardware data processing

The collected data were analyzed using software Sigma Plot (ver. 11.0, Systat software, San Jose, CA, USA). A bar chart, linear regression and sigmoid regression analysis were used to analyse the main variables. Image analysis was carried out using a laptop with Intel® Core™ i7-4510U processor, 2.6 GHz, 12.0 GB RAM, 64-bit operating system.

4.6. Implementation of the investigation for optimum laser positioning

4.6.1. Experiment and quality assessment for poinsettia

4.6.1.1. Combined RGB-Depth

4.6.1.1.1. Color segmentation based depth image

Since laser marking only considers the colored part of poinsettias from a top view, called colored bracts (modified leaves), the green part was separated from the plants' depth image. For this purpose, RGB-depth image segmentation steps were applied (Fig. 4.6.1).

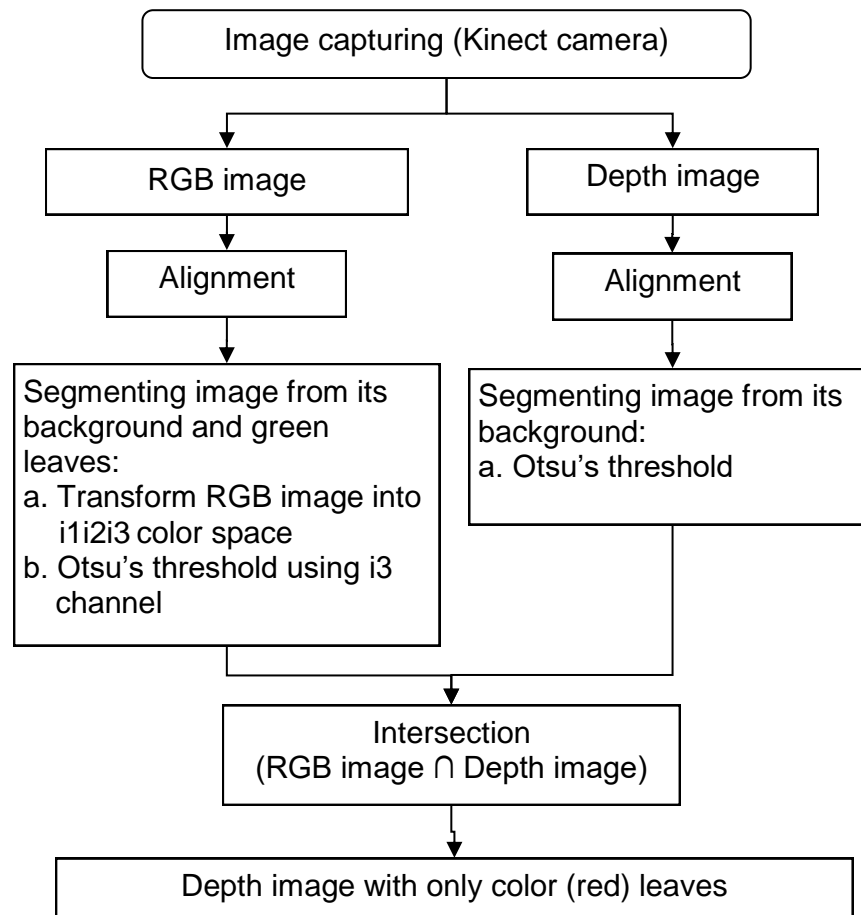


Fig. 4.6.1. Separation of green leaves the depth image of poinsettia leaves

The RGB image and depth image were aligned to compensate for differences in image size. The Kinect camera can capture color and depth images simultaneously. Although the resolutions are the same, in practice a raw match of the color and depth images is not aligned properly. There is a significant difference in size and some differences in position. Since the difference takes place in 2D image space, a rigid affine transformation from points and angles is appropriate between the two images.

This transformation consisted of a rotation matrix, a translation vector from a correspondence point and corresponding angles, and a scaling by scale factors along the x-axis and y-axis. The following formula shows the chain of transformation matrices (MVtec, 2014):

$$\text{HomMat2D} = \begin{bmatrix} \cos(\text{Phi}) & -\sin(\text{Phi}) & 0 \\ \sin(\text{Phi}) & \cos(\text{Phi}) & 0 \\ 0 & 0 & 1 \end{bmatrix} * \begin{bmatrix} 1 & 0 & \text{Tx} \\ 0 & 1 & \text{Ty} \\ 0 & 0 & 1 \end{bmatrix} * \begin{bmatrix} \text{Sx} & 0 & 0 \\ 0 & \text{Sy} & 0 \\ 0 & 0 & 1 \end{bmatrix} \quad (4.6)$$

Where:

HomMat2D = homogeneous 2D transformation matrix

Phi = rotation angle

Tx = translation along x-axis

Ty = translation along y-axis

Sx = scale factor along x-axis

Sy = scale factor along y-axis

At the same resolution, the depth image has a relatively bigger size than the color image. Hence, the depth image was transformed into the color image using Equation [4.6], whereas the color image was set as the fixed point of the transformation. This strategy was performed in order to avoid the deterioration of image quality due to 2D transformation, i.e., scaling. In order to find the scale factor ratio, the region of the color image was divided by the region of the depth image.

The pixels in RGB color space were transformed into the $i1i2i3$ color space. The $i3$ channel was chosen to allow easier segmentation between red leaves and green leaves. According to Meyer, et al. (1998), the $i3$ channel is usually referred as the “excess green index” and has been used for direct segmentation of plants. This transformation simplified the color segmentation and only the $i3$ channel was applied. The $i1i2i3$ color space was calculated from the RGB color space by the following equation (proposed by Ohta et al. 1980).

$$\begin{bmatrix} i1 \\ i2 \\ i3 \end{bmatrix} = \begin{bmatrix} 0.333 & 0.333 & 0.333 \\ 0.5 & 0.0 & -0.5 \\ -0.25 & 0.5 & -0.25 \end{bmatrix} * \begin{bmatrix} R \\ G \\ B \end{bmatrix} \quad (4.7)$$

Plant leaves and background objects (i.e. RGB image and depth image) were extracted according to Otsu's thresholding method (Otsu, 1979). Otsu thresholding is an optimal threshold for binarizing an image with a bimodal intensity histogram. Subsequently, the regions of both images were intersected. In order to determine the segmentation performance of the algorithm, 80 poinsettia plants were evaluated. The successful extraction of the green leaves from the depth images using the proposed algorithm was calculated in percentages.

4.6.1.1.2. Depth image segmentation based on distance transform watershed method

Segmentation of complex leaf images is not an easy task with standard RGB images, because the leaves are overlapped and poorly contrasted with each other (Chéné, et al. 2012). Depth images can be more easily segmented than RGB images and allow for recognizing objects in terms of similar color. The next step is to split the objects that are located at different depths. In this experiment, poinsettia plants were captured using Kinect V1 and Kinect V2, respectively. Microsoft Kinect® cameras were used to provide RGB-D information. The segmentation of the images was carried out by a distance transformation and watershed algorithm.

A distance transformation is defined as an operation that converts a binary image to an image where each element has a value that approximates the distance to the nearest feature element (Borgefors, 1984). Generally, distance metrics are used for different situations, such as city-block, chessboard and Euclidean distance. The Euclidean metric is one of the most appropriate metrics and is an adequate model for numerous geometrical facts and is used in many applications, since it is radially symmetric and virtually invariant to rotation (Wang and Tan, 2013). Therefore, a Euclidean metric parameter was selected for calculating the distances. The exact distance between two points with coordinates of (i_1, j_1) and (i_2, j_2) can be calculated from the Euclidean distance transformation formula below (Danielsson, 1980):

$$\text{Euclidean } (i, j) = \sqrt{(i_1 - i_2)^2 + (j_1 - j_2)^2} \quad (4.8)$$

Where, in Euclidean plane, if $i = (i_1, i_2)$ and $j = (j_1, j_2)$, then the distance between two pixel coordinates is denoted as $[i_1, j_1]$ and $[i_2, j_2]$. This formula is equivalent to the Pythagorean Theorem.

By convention, binary 0 is associated to black, and 1 to white. Hence, we have a foreground or object represented by all white pixels. The background is represented by black pixels. Figure 4.6.2 shows a numerical example of Euclidean distance with the straight-line distance between two pixels. The corresponding pixel in distance transformation shows the smallest distance between each pixel in the object to the nearest pixel in the background.

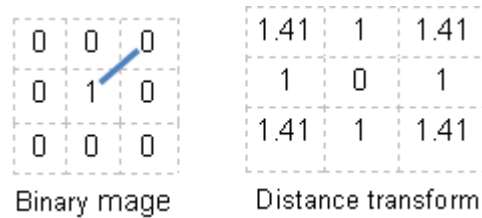


Fig. 4.6.2. Illustration of Euclidean distance transform

The term “watershed” indicates a ridge that is used to divide areas drained by different river systems. Therefore, the name of this technique is “watershed-based segmentation.” According to Roerdink and Meijster (2000), the watershed segmentations compute catchment basins and ridgelines which also known as watershed lines, where catchment basins correspond to image regions and watershed lines correspond to the region boundaries (Fig. 4.6.3).

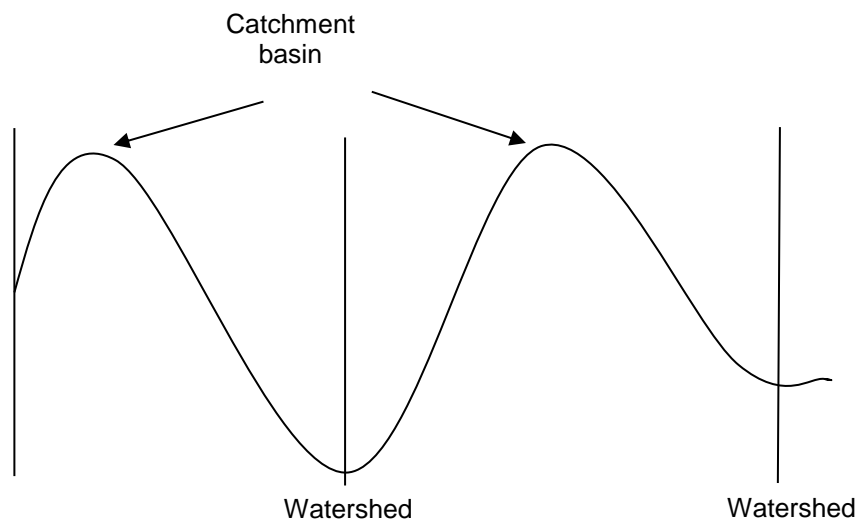


Fig. 4.6.3. Illustration of watershed segmentation, local minima of gray level yield catchment basins, and local maxima define the watershed lines

In order to detect the potential basins, an appropriate threshold for each object region should be defined. A Halcon image processing program was performed to compute the watershed segmentation. According to MVTec (2014), the watershed is eliminated and the two basins are merged if:

$$\max[W - B_1, W - B_2] < Threshold \quad (4.9)$$

Where, B_1 and B_2 are the minimum gray values of two neighboring basins. W is the minimum gray value of the watershed that splits the two basins depending on every image. The threshold value is set 20. It is calculated based on parameter estimation/modelling results.

The algorithm extracts watersheds and basins from an image. The watershed algorithms segment an image according to the topology of the gray values. Higher gray values correspond to “mountains,” whereas lower gray values correspond to “valleys.” A watershed is a single region per input image, while basins contain a separate region for each basin. The basins are successively combined if they are separated by a watershed that is lower than the threshold.

Finally, the corresponding basins were used to split the connected regions by intersecting the basins with the selected regions. A leaf was selected for the purpose of laser marking. Since poinsettia leaves is nearly elliptical leaves, two criteria for selecting the best leaf for marking are calculated: a) shape factor ratio (SF), and b) the maximum diameter of the leaf. The shape factor ratio is denoted by the following equation:

$$SF = \frac{\text{Leaf area}}{\text{Ellipse area}} \quad (4.10)$$

$$\text{Ellipse area} = \pi * A * B \quad (4.11)$$

Where, A and B is major radius and minor radius, respectively.

The maximum diameter is defined as the maximum distance between two boundary points of a leaf region (MVTec, 2014).

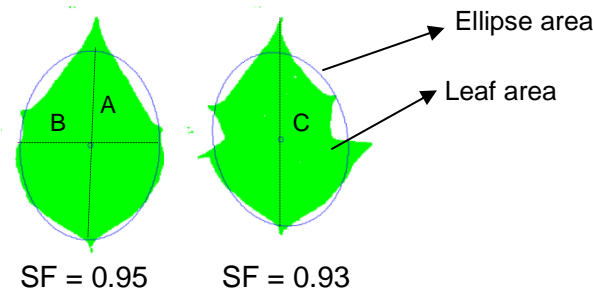


Fig. 4.6.4. Illustration of shape factor ratio (SF) of two different types of poinsettia leaves. (A) major radius of ellipse; (B) minor radius of ellipse; (C) maximum diameter of leaf region

Eighty successfully detected poinsettia leaves were analyzed according to the best leaf classification based on Fawcet (2006). The classification specified a classifier and the test set, a two-by-two confusion matrix (contingency table), which can be constructed representing the dispositions of the set of instances (see Fig. 4.6.5). There are four possible results:

- 1) If the instance is positive and it is classified as positive, it is calculated as a true positive
- 2) If the instance is positive and it is classified as negative, it is calculated as a false negative
- 3) If the instance is negative and it is counted as negative, it is counted as a true negative
- 4) If the instance is negative and it is classified as positive, it is calculated as a false positive

		True class	
		p	n
Hypothesized class	Y	True Positive	False Positive
	N	False Negative	True Negative
Column totals:		P	N

Fig. 4.6.5. Confusion matrix (Fawcet, 2006)

In this study, the detected of poinsettia leaves were grouped based on four possible results, as follows:

- I. True positive : a correctly identified leaf
- II. False positive : overlapping leaves detected as a leaf
- III. True negative : no leaf and no overlapping leaves detected as a leaf
- IV. False negative : a partial leaf is detected

4.6.1.2. The usage of main leaf skeleton

In this study, individual leaves were automatically identified from images of horticultural crops. This identification refers to the thickest and longest venation in a leaf as the main skeleton, as shown in Fig. 4.6.6.

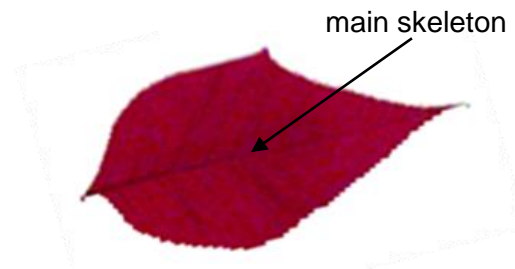


Fig. 4.6.6. Main skeleton and branches of poinsettia leaf

This identification system was comprised of several steps, as shown in Fig. 4.6.10. RGB images were captured and converted into L^*a^*b channels. The a^* channel was chosen and Otsu's method (see Eq. 4.5.7) was selected to segment the foreground and background automatically. Unwanted small objects (noise) were removed. The color image was intersected by the region of interest (called the reduced domain). The Red channel was used to extract edge contours. Canny edge detection (Canny, 1986) was chosen and hysteresis thresholding values were selected in order to have less detail in the edges. The general stages of the Canny edge detector are:

- a. Smoothing: blurring of the image to remove noise

The Gaussian smoothing filter was used to remove image noise. The filter is denoted as:

$$\exp(x, y) = \frac{1}{2\pi\sqrt{\sigma}} \exp\left(-\frac{x^2 + y^2}{2\sigma^2}\right) \quad (4.12)$$

Where,

x = the distance from the origin in the horizontal axis

y = the distance from the origin in the vertical axis

σ = the standard deviation of the Gaussian distribution

- b. Finding gradients (Canny edge detection): Finding the edge strength (magnitude) by computing the gradient of the image using a standard Sobel edge operator. The Sobel operator implements a 2D spatial gradient measurement on the image.

$$G_x = \begin{array}{|c|c|c|} \hline -1 & 0 & 1 \\ \hline -2 & 0 & 2 \\ \hline -1 & 0 & 1 \\ \hline \end{array} \quad G_y = \begin{array}{|c|c|c|} \hline 1 & 2 & 1 \\ \hline 0 & 0 & 0 \\ \hline -1 & -2 & -1 \\ \hline \end{array}$$

Fig. 4.6.7. Kernels used in Sobel operator

The operator uses a pair 3 * 3 kernel (see Fig. 4.6.7), G_x and G_y are gradients in the x - and y -directions, respectively. The magnitude and angle of the directional gradients calculated as follows:

$$\text{The magnitude of gradient: } |G| = \sqrt{G_x^2 + G_y^2} \quad (4.13)$$

$$\text{Approximate strength: } |G| = |G_x| + |G_y| \quad (4.14)$$

$$\text{The orientation of the edge: } \arctan\left(\frac{|G_y|}{|G_x|}\right) \quad (4.15)$$

- b.1. Non-maximum suppression: Only local maxima should be noticeable as edges

The image magnitude produced thick edges; therefore non-maximum suppression was performed to thin out the edges. Fundamentally, this was done by preserving all local maxima in the gradient image, and removing everything else. Fig. 4.6.8 shows points along the curve where the magnitude is biggest. This can be done by looking for a maximum along a slice to the curve.

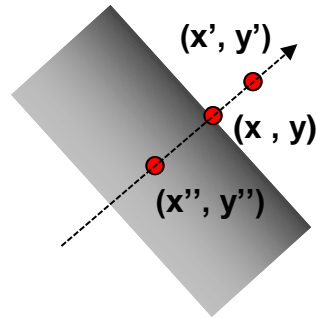


Fig. 4.6.8. Illustration of the non-maximum suppression

Where, (x'', y'') and (x', y') are the neighbors of (x, y) along the direction to an edge.

b.2. Double thresholding: potential edges are determined by hysteresis thresholding.

This technique applied dual thresholding followed by a connected component analysis to preserve weak foreground pixels (see Eq. 4.16).

$$G_t(x, y) = \begin{cases} \text{Foreground (strong)} & \text{if } G_t(x, y) > T_{high} \\ \text{Background} & \text{if } G_t(x, y) < T_{low} \\ \text{Candidate (weak)} & \text{otherwise} \end{cases} \quad (4.16)$$

Where, the image pixels were compared to two thresholds (i.e. T_{low} and T_{high}). T_{low} and T_{high} manually adjusted based on the modelling images data sets. The results for T_{low} and T_{high} are 1 and 5, respectively. Let $G_t(x, y)$ be the pixel at time t and location (x, y) .

Explanation of equation (4.16):

- 1) If the gradient at a pixel is above T_{high} , declare it an 'edge pixel'
Pixels above the upper threshold (T_{high}) are considered strong foreground.
- 2) If the gradient at a pixel is below T_{low} , declare it a 'non-edge-pixel'
Pixels below the lower threshold (T_{low}) are considered background and discarded.
- 3) If the gradient at a pixel is between T_{low} and T_{high} then declare it an 'edge pixel' if and only if it is connected to an 'edge pixel' directly.

Intermediate pixels were categorized as weak candidates or weak foreground pixels. If a weak pixel was connected directly or through a path to a foreground, it was preserved by changing it to a foreground pixel. Otherwise, it was made a background pixel and discarded.

b.3. Edge tracking: final edges are defined by suppressing all edges that are not connected to a very certain (strong) edge.

c. Ramer approximation method

The contour was represented as a polygon when it fit the edge points with a sequence of line segments. The Ramer approximation method (Ramer, 1972) was chosen to simplify a polygon by reducing the number of points by use of a threshold. The smaller the threshold, the closer the polygonal fit will be to the original data. However, in this study, more straight-line fit segments will be required. The Ramer method offered an iterative method which starts with an initial segmentation and splits the segment at the point which had the greatest distance from the corresponding segment, unless the approximation error was no more than the pre-specified threshold, as illustrated in Figure 4.6.9.

d. The longest line

The longest line was selected according to the longest input lines by subtracting coordinates between ending points and starting points. In order to place characters on a leaf during laser marking, a larger area of the leaf is required. Therefore, we assume that the longest main leaf skeleton represents a larger leaf.

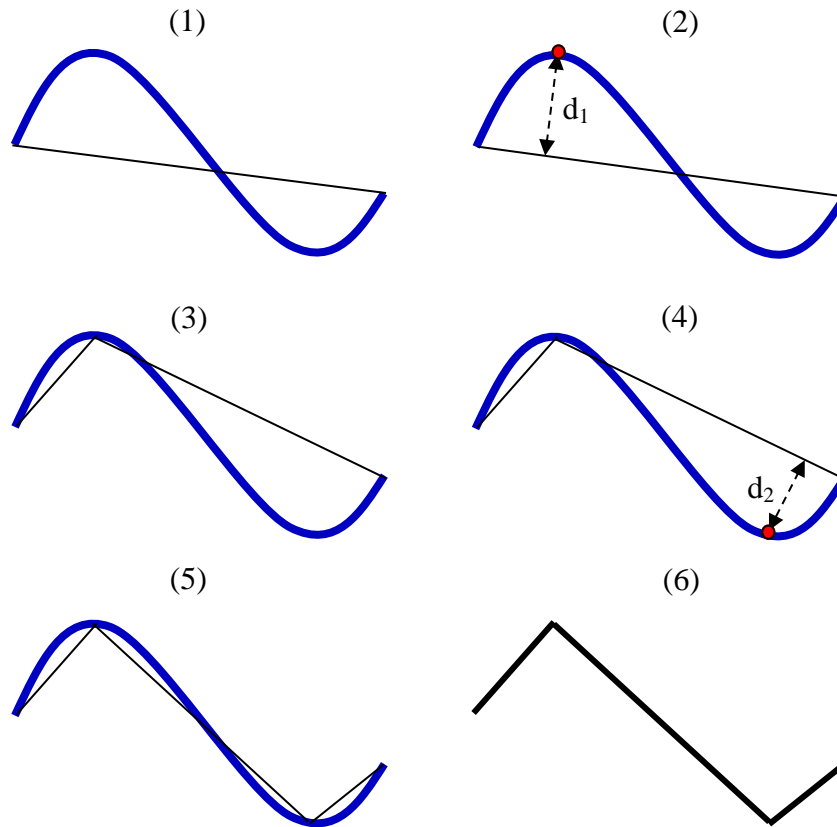


Fig. 4.6.9. Simplifying a curve using Ramer approximation. (1-6) A curve (blue line) together with the initial approximation (black line) is shown. First step: As the maximum distance d_1 between the curve and its approximation (marked red) is larger than threshold (t), the line is subdivided. Second step: The lower line is subdivided again ($d_2 > t$). For t , the standard Halcon (see MVTec, 2014) value was used. The final Ramer approximation is illustrated at number (6)

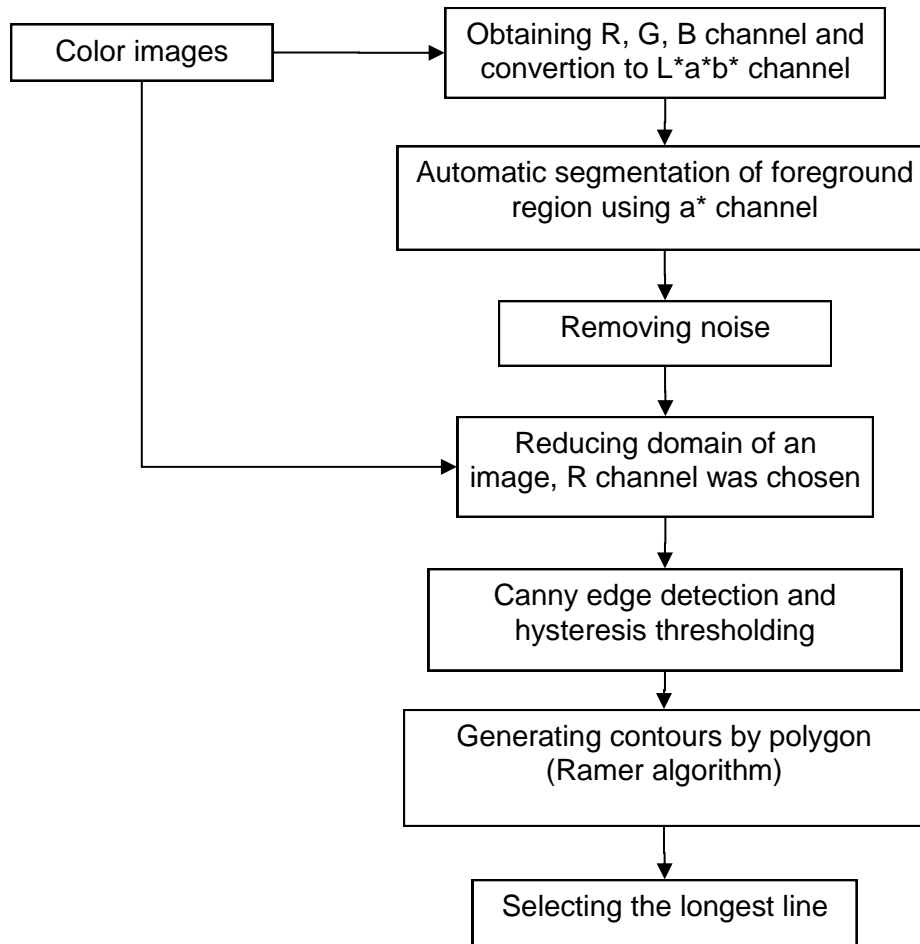


Fig. 4.6.10. Overview of leaf identification system

Poinsettia plants were captured by the camera. The camera could produce 1280*1024 pixel color images. The color images were analyzed using the proposed algorithms (see Fig. 4.5.18). Three analyses were performed to examine the successful identification of this system, as follows:

a) The longest five main leaf skeletons detected

The longest five main leaf skeletons detected were identified using the Halcon v12 image processing software. The successful results were measured as percentages based on Equation (4.17) as follows:

$$SL (\%) = \frac{\text{number of correct classification}}{\text{total number of test images}} * 100\% \quad (4.17)$$

Where SL is the percentage of main leaves detected successfully

b) The longest main leaf skeleton detected

The longest main leaf skeleton was detected using the Halcon image processing software. The classification of the detected leaf in the test set was performed using a confusion matrix (Fawcet, 2006), see Fig. 4.6.5. The detected leaves were grouped based on four possible results, as follows:

- i. True positive : main skeleton correctly identified
- ii. False positive : branches detected as main skeleton
- iii. True negative : no main skeleton and no branches detected as main skeleton
- iv. False negative : line detected is too short but it represents a larger leaf

c) Effect of different orientation

In order to understand the effect of different orientations on the detection of leaves, a reliable leaf identification system should take this issue into consideration. In this section, the camera was used to capture the first image (color image) and move the object sample to slightly different orientations (such as: 0°, 90°, 180° and 270°) to obtain the second, third and fourth images.

4.6.2. Experiment and quality assessment for bananas

4.6.2.1. Pre-processing and background removal

The steps in the algorithm for removing background are shown in Figure 4.6.11. An individual color image was captured by a CCD camera. The process of background removal was achieved by accessing R, G and B chromatic components from the color image. However, this color space has the disadvantage of being very sensitive to changes in lighting. Converting the RGB channels to CIE-Lab channels avoids the sensitivity by increasing the accuracy of color segmentation. The CIE-Lab (1976) color is organized as shown in Figure 4.6.12.

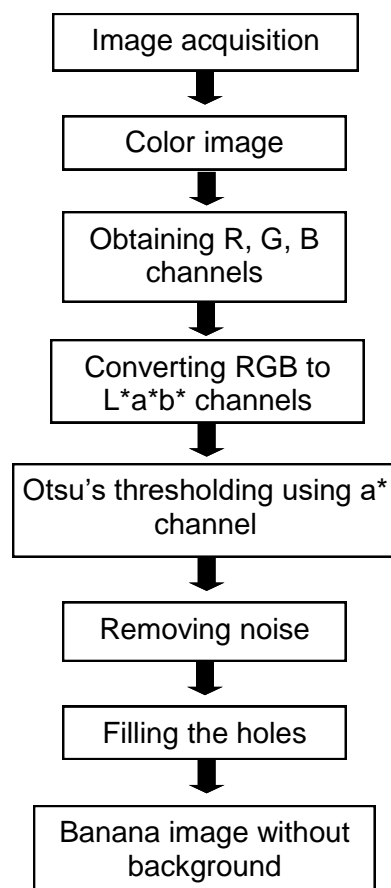


Fig. 4.6.11. The process of removing the background of single banana fruit

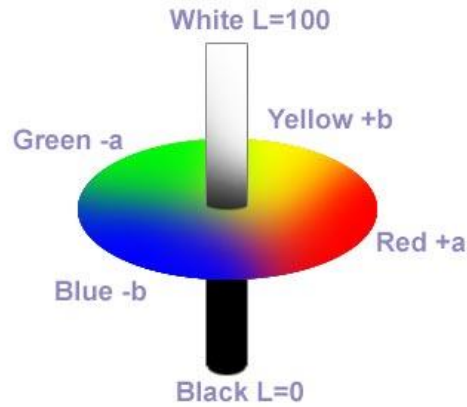


Fig. 4.6.12. CIE-Lab color space structure

The RGB color space was converted to $L^*a^*b^*$ color space by the following set of equations (MVtec, 2014):

$$\begin{pmatrix} X \\ Y \\ Z \end{pmatrix} = \begin{bmatrix} 0.412453 & 0.357580 & 0.180423 \\ 0.212671 & 0.715160 & 0.072169 \\ 0.019334 & 0.119193 & 0.950227 \end{bmatrix} \begin{bmatrix} R \\ G \\ B \end{bmatrix} \quad (4.18)$$

$$L^* = 116 \left[f\left(\frac{Y}{Y_w}\right) \right] - 16 \quad (4.19)$$

$$a^* = 500 \left[f\left(\frac{X}{X_w}\right) - f\left(\frac{Y}{Y_w}\right) \right] \quad (4.20)$$

$$b^* = 200 \left[f\left(\frac{Y}{Y_w}\right) - f\left(\frac{Z}{Z_w}\right) \right] \quad (4.21)$$

$$f(t) = \begin{cases} t^{\frac{1}{3}} & \text{if } t > \left(\frac{6}{29}\right)^3 \\ \frac{1}{3}\left(\frac{29}{6}\right)^2 t + \frac{4}{29} & \text{if } t \leq \left(\frac{6}{29}\right)^3 \end{cases} \quad (4.22)$$

Where, X_w, Y_w, Z_w are tristimulus of CIE-XYZ values with reference to the white spot.

$$\begin{pmatrix} X_w \\ Y_w \\ Z_w \end{pmatrix} = \begin{bmatrix} 0.9504 \\ 1.0000 \\ 1.0887 \end{bmatrix} \quad (4.23)$$

In order to find the optimal thresholding value between two peaks automatically, Otsu's method was selected (Otsu, 1979). The Otsu method is based on establishing the optimal threshold that minimizes within-class variance. The within-class variance is the sum of the object of interest and background variances multiplied by their associated weights, as follows:

$$\sigma_w^2(th) = w_B(th) \sigma_1^2(th) + w_F(th) \sigma_2^2(th) \quad (4.24)$$

Where:

σ_w^2 = within-class variance

σ_1^2 = the variance of the pixels in the background (below threshold)

w_B = the weight of the background

σ_2^2 = the variance of the pixels in the foreground (above threshold)

w_F = the weight of the foreground

th = threshold value (automatically calculated via Halcon (see MVTec, 2014))

The calculation for finding the background and the foreground variances for a single threshold (th) are shown below:

$$Weight (w_B) = \sum_{i=1}^{th} \frac{n_i}{N} \quad (4.25)$$

$$Weight (w_F) = \sum_{i=th+1}^L \frac{n_i}{N} \quad (4.26)$$

$$Mean (\mu_B) = \frac{\sum_{i=1}^{th} i * n_i}{\sum_{i=1}^{th} n_i} \quad (4.27)$$

$$Mean (\mu_F) = \frac{\sum_{i=th+1}^L i * n_i}{\sum_{i=1}^{th} n_i} \quad (4.28)$$

$$Variance (\sigma_B^2) = \frac{\sum_{i=1}^{th} (i - \mu_B)^2 * n_i}{\sum_{i=1}^{th} n_i} \quad (4.29)$$

$$Variance (\sigma_F^2) = \frac{\sum_{i=th+1}^L (i - \mu_B)^2 * n_i}{\sum_{i=1}^{th} n_i} \quad (4.30)$$

Where:

L is gray levels of gray image [1, 2, 3, ..., L]

The number of pixels at level i is expressed by n_i

N is the total number of pixels (equal to $n_1 + n_2 + n_3 + \dots + n_L$)

The pixels are divided into a background class (C_B) and a foreground class (C_F) by a threshold at level t

C_B denotes pixels with levels $[1, 2, 3, \dots, t]$

C_F denotes pixels with levels $[t+1, t+2, \dots, L]$

The final value is the 'within-class variance' (see Eq. 4.24) for the threshold value t . The similar calculation needs to be made iteratively for all the possible threshold values from 1 to L . Finally, threshold T , which has the lowest 'within-class variance,' was selected to be the final threshold. All pixels with a level less than T are background, while all those with a level greater than or equal to T are foreground or objects of interest.

4.6.2.2. Selecting the area of interest

This section was focused on locating a small rectangle as a data matrix code (2D code) on the banana's surface. Generally, a banana's greatest diameter is in its middle part. Therefore this area was recommended for placement of the code. However, since bananas have irregular shapes, applying a simple image processing method center of gravity of a region in a gray value image was not able to find the center point of a banana correctly. With the help of Fig. 4.6.13, the following steps demonstrate how to select and generate a small rectangle at the center point of a banana.

- 1) Region (a) was extracted based on the steps in Fig. 4.6.13.
- 2) Applying a smallest-area enclosed rectangle to the banana region with any orientation (region b). This step determined the smallest enclosed rectangle of a region (closed curve) based on Freeman and Shapira (1975), in the center of which the inclination and the two radii of the rectangle were calculated.

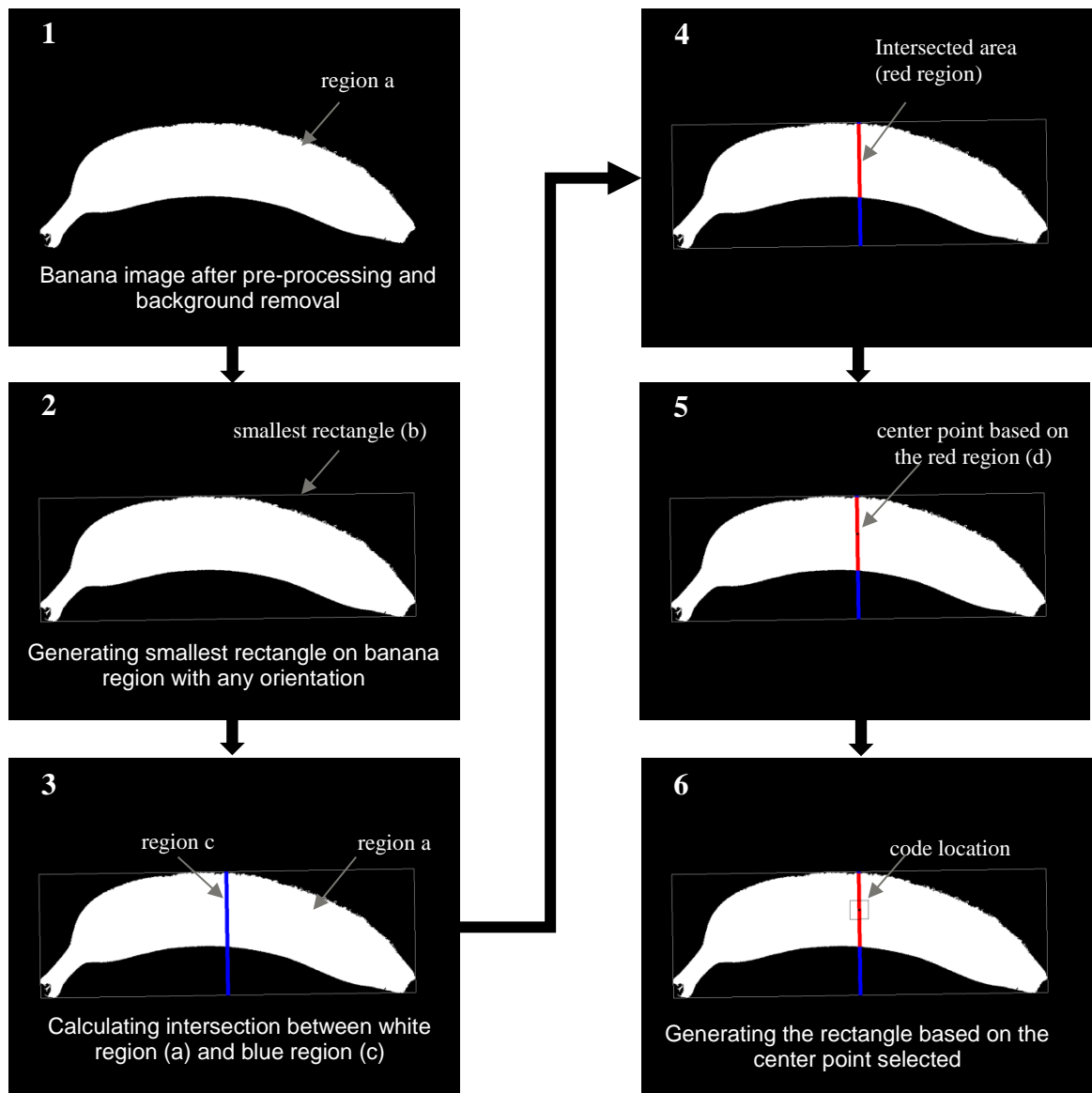


Fig. 4.6.13. Steps for positioning a code on banana

- 3) Generating the rectangle in the center of the banana as region (c). The width of the rectangle was set to about 5 pixels. Then, the intersection between region (a) and region (c) was calculated.
- 4) Computing the length of the intersected area of the banana as a diameter. This diameter was calculated based on pixels.
- 5) Calculating the middle point of the intersected area, meaning the center part of the banana (d).
- 6) Generating the rectangle based on the given middle point in Step 5 (Fig. 4.6.14). The inclination of the rectangle was measured based on the result

given by Step 2 (Fig. 4.6.13). In this 10 mm * 10 mm sample the edge length of the 2D code was generated.

In order to evaluate the successful localization of codes on the fruit, the following samples were examined. The success rate of the localization of the codes is defined as a percentage.

1. Implementation of the algorithms for banana fingers
 - a. A total of 30 green banana fingers with different shapes, from slightly curved to very curved, were randomly selected
 - b. A total of 30 green banana fingers were posed randomly at different orientations
2. Implementation of the algorithms for different fruits, such as avocados, apples, peppers, and cucumbers
3. Implementation of the algorithms for banana hands

Seventy green mature banana hands were used for the training set. Based on the training data set, the range of diameter values of each finger was added into the algorithm in order to increase the correct localization of the codes. The diameter values of the fingers depended on variety and quality standards of the bananas. In general, the diameter of green mature Cavendish bananas, from small-sized fruits to large-sized fruits, was set to around 31 – 39.5 mm (Mencarelli and Mejia, 2004). Another seventy green mature banana hands were used to measure the performance of the training set. The banana hands were examined by comparing the banana's ventral and dorsal sides to obtain the best format for each category (see Fig. 4.6.14). In the country of production, banana hands are commonly cut from the stalks of banana bunches and immediately deposited in a tank of cool water. Generally, the banana hands are separated into clusters of five to eight fingers. Afterwards the bananas are labeled with stickers while wet. Therefore, the algorithm has to be adapted to the wetness and irregular shapes of banana fingers.



Ventral side

Dorsal side

Fig. 4.6.14. Ventral side and dorsal side of banana hands

4.7. Implementation of the investigation for optimum laser parameters

4.7.1. Experiment and quality assessment for poinsettia

4.7.1.1. Laser marking parameters

WinMark pro software (Synrad Inc., USA) was used in order to control every aspect of the laser marking process, including changing the laser parameters. Four laser parameters (laser power, resolution, raster scan direction and storage time) with five repetitions were applied in the marking of poinsettia leaves (Table 4.7.1). The resolution was expressed as dot per inch (dpi). Dot per inch represents the intensity of laser spots in a given area.

Table 4.7.1. Different laser output power, resolution, and raster scan direction applied to poinsettia leaves

No.	Power (W), [resolution (dpi)]	Laser energy (J per character)	No.	Power (W), [resolution (dpi)]	Laser energy (J per character)
1	7.0 [200] v	3.90	25	0.71 [600] h	1.08
2	7.0 [200] h	1.73	26	0.71 [500] h	0.79
3	5.2 [200] v	2.92	27	0.71 [400] h	0.54
4	5.2 [200] h	1.29	28	0.71 [200] h	0.17
5	3.5 [200] v	1.93	29	0.50 [700] v	2.21
6	3.5 [200] h	0.85	30	0.50 [600] v	1.67
7	1.7 [200] v	0.95	31	0.50 [500] v	1.22
8	1.7 [200] h	0.42	32	0.50 [400] v	0.83
9	0.93 [700] v	4.08	33	0.50 [200] v	0.28
10	0.93 [600] v	3.09	34	0.50 [700] h	1.00
11	0.93 [500] v	2.26	35	0.50 [600] h	0.76
12	0.93 [400] v	1.54	36	0.50 [500] h	0.55
13	0.93 [200] v	0.51	37	0.50 [400] h	0.38
14	0.93 [700] h	1.86	38	0.50 [200] h	0.12
15	0.93 [600] h	1.40	39	0.43 [700] v	1.89
16	0.93 [500] h	1.02	40	0.43 [600] v	1.43
17	0.93 [400] h	0.69	41	0.43 [500] v	1.05
18	0.93 [200] h	0.22	42	0.43 [400] v	0.71
19	0.71 [700] v	3.14	43	0.43 [200] v	0.24
20	0.71 [600] v	2.39	44	0.43 [700] h	0.86
21	0.71 [500] v	1.74	45	0.43 [600] h	0.65
22	0.71 [400] v	1.19	46	0.43 [500] h	0.47
23	0.71 [200] v	0.39	47	0.43 [400] h	0.32
24	0.71 [700] h	1.43	48	0.43 [200] h	0.10

v: vertical scan direction, h: horizontal scan direction

The time required for a laser head to finish one complete marking operation is expressed as cycle time. The laser energy was calculated by multiplying output power by the cycle time. Raster marking was accomplished by switching the beam on and off as it moved across the image. Raster marking can create filled objects or text, or it can reproduce photographic images. The raster marking direction was divided into two different types, i.e. vertical scan direction and horizontal scan direction (see Fig. 4.7.1). Figure 4.7.1 shows an example of laser marking text formatted on a poinsettia leaf.

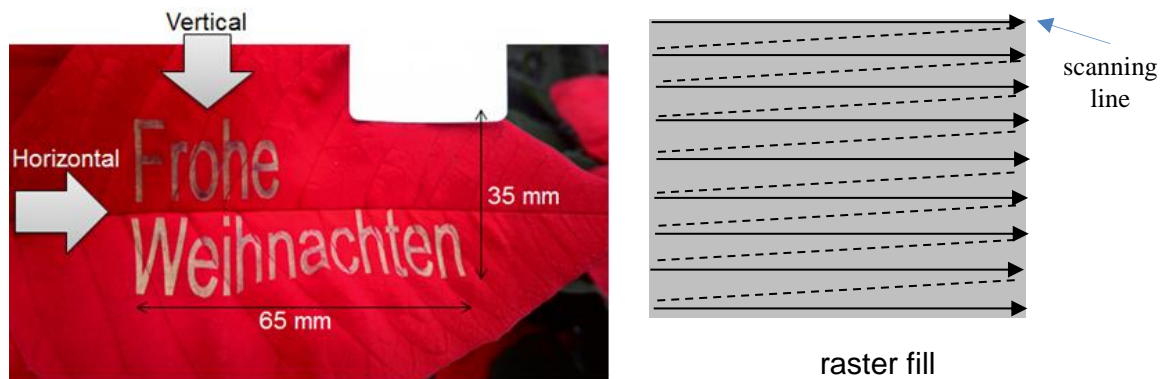


Fig. 4.7.1. Laser-marked poinsettia leaf and illustration of raster marking method

4.7.1.2. Assessment of marking

Each leaf was evaluated by assessing the heat affected zone (HAZ) and the unaffected zone. The marked area had the most energy and the highest temperature of the laser marking process. The heat affected zone had a temperature that rose less than in the mark area. The unaffected zone was relatively not influenced by the laser beams. The visual assessment was classified based on a 4-level scale:

- a. No apparent HAZ: corresponding to HAZ index 0
- b. Slight HAZ: total affected area 1%-25%, corresponding to HAZ index 1
- c. Moderate HAZ: total affected area: 26%-75%, corresponding to HAZ index 2
- d. Severe HAZ: total affected area 76%-100%, corresponding to HAZ index 3

A leaf affected zone index formula was developed and is presented in Equation [4.31]. During evaluation, each leaf was put into a category according to the severity of the damage in a 4-level scale with five repetitions. Each leaf was evaluated after three days of treatment.

$$\text{HAZ index} = \frac{\text{number of visual damage on each character}}{\text{total number of characters}} \times 100\% \quad (4.31)$$

4.7.2. Experiment and quality assessment for bananas

4.7.2.1. Spectral reflectance of marked bananas

Ripe bananas were marked at different laser powers (Fig. 4.7.2) with 10 repetitions. The laser marking speed was set to 400 mm s⁻¹. The images were captured using a hyperspectral imaging camera (Helios, EVK DI Kerschhaggl GmbH Austria). Significant differences in reflectance among treatments were calculated.

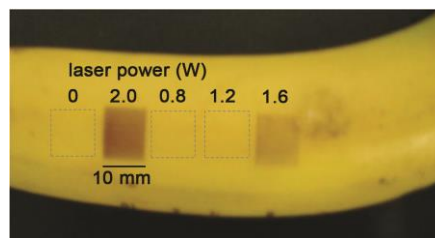


Fig. 4.7.2. Laser-marked areas on a banana created at different laser powers

4.7.2.2. Quality of the codes

The modules of the DM codes were created with the energy inputs, the laser powers, and the marking times shown in Table 4.7.2. The treatments were selected from four levels of low-power laser in order to cause minimum damage to the banana peels. Various levels of marking time corresponded to contrast values that could be stably decoded. Overall, 16 different treatments with five repetitions were conducted.

Table 4.7.2. Laser energy applied to the bananas depending on the laser power (p) and the marking time (t)

Laser power (W)		Laser energy (Joule per module)			
(p1) 2.2	p1t1 (0.206)	p1t2 (0.159)	p1t3 (0.118)	p1t4 (0.084)	
(p2) 2.0	p2t1 (0.187)	p2t2 (0.145)	p2t3 (0.107)	p2t4 (0.076)	
(p3) 1.8	p3t1 (0.169)	p3t2 (0.130)	p3t3 (0.097)	p3t4 (0.068)	
(p4) 1.6	p4t1 (0.150)	p4t2 (0.116)	p4t3 (0.086)	p4t4 (0.061)	

t1 = 0.0937 s per module; t2 = 0.0724 s per module; t3 = 0.0537 s per module; t4 = 0.0381 s per module

The DM code images were assessed based upon ISO/IEC 15415 standards (2011). In order to decode and assess a DM code in an image, some general image processing steps in the Halcon software (MVTec Software GmbH, Munich, Germany) were used (see Fig. 4.6.2). All treatments were evaluated every day with five repetitions for nine days of storage. Table 4.7.3 provides information concerning how the parameters in step 6 in Fig. 4.7.3 have to be used in the ISO/IEC 15415 (2011) to grade DM codes.

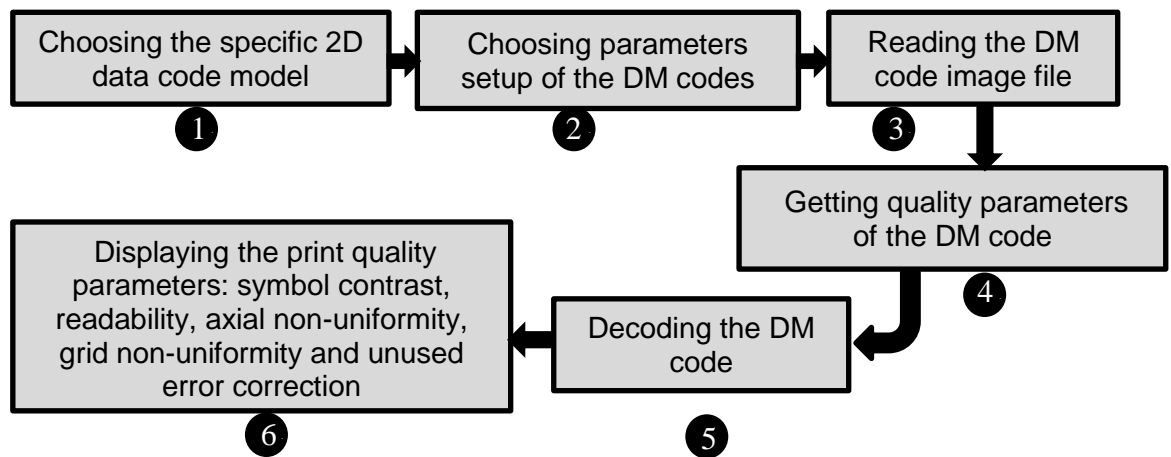


Fig. 4.7.3. Image analysis steps to evaluate data matrix codes using the Halcon software

Table 4.7.3. Data matrix code print quality (ISO/IEC 15415, 2011)

Parameter Grade	Decode	Symbol Contrast (SC)	Axial Non-Uniformity (ANU)	Grid Non-Uniformity (GNU)	Unused Error Corection (UEC)
4 (A)	Passes	≥0.70	≤ 0.06	≤ 0.38	≥0.62
3 (B)	Passes	≥0.55	≤ 0.08	≤ 0.50	≥0.50
2 (C)	Passes	≥0.40	≤ 0.10	≤ 0.63	≥0.37
1 (D)	Passes	≥0.20	≤ 0.12	≤ 0.75	≥0.25
0 (F)	Fails	<0.20	> 0.12	> 0.75	<0.25

Explanations:

- a. Contrast: difference between minimal and maximal pixel intensity in the data code domain
- b. Decoding or readability: determining whether the symbol (DM code) can be decoded or not. The percentage of readability (r) is calculated as follows: $r = (k/100)/N$, where k represents the number of read codes and N stands for the sample size

- c. Axial non-uniformity: the squareness of the symbol (distance between modules center position is the same in horizontal and vertical directions)
- d. Grid non-uniformity: the deviation of the modules from their ideal grid
- e. Unused error correction: the amount of error-correcting capacities not already used by the present data code symbol

4.7.2.3. Readability of the codes

4.7.2.3.1. Encoding data matrix code

Different levels of data matrix sizes were chosen based on Table 4.7.4. Table 4.7.4 demonstrates the percentage of space for error correction and the number of *codewords* (data bytes). There are three steps required to encode a data matrix code: data encoding, error correction and matrix building (GS1, 2018). As an example, if 24 numeric digits have to be encoded, the matrix size is containing of 16 rows and 16 columns. The matrix is made up of 24 bytes, which is the sum of the total number of data and error *codewords* is 12 + 12 (see Table 4.7.4).

Table 4.7.4. Data Matrix code symbol attributes (GS1, 2018)

Data matrix size		Data region		Total <i>codewords</i>		Maximum data capacity	
Row	Column	Size	No	Data	Error	Numeric	Alphanumeric
10	10	8x8	1	3	5	6	3
12	12	10x10	1	5	7	10	6
14	14	12x12	1	8	10	16	10
16	16	14x14	1	12	12	24	16

Suppose we want to encode the alphanumeric characters 'ABC'. The value of the *codewords* A, B and C are calculated simply by using "ASCII value + 1". There are three *codewords* to encode (see Table 4.7.4). If we want to encode using numeric values, the *codewords* are calculated as two digits using the "numeric value of digit pairs + 130" (Fig. 4.7.5). By using the Reed-Solomon algorithm (ISO/IEC 16022), the error corrections were added into *codewords*. Afterwards, the *codewords* are translated into binary. Finally, the binary *codewords* are placed in the matrix (matrix building) as symbolic characters based on the algorithm described in Annex F from the ISO/IEC 16022 standard.

Table 4.7.5. Encoding example of ECC200 ASCII based on ISO/IEC 16022 (2006)

Data	Method	Evaluation	Codewords (data)
ABC	ASCII value + 1	(65+1), (66+1), (67+1)	66, 67, 68
123456	Numeric value of digit pairs + 130	(12+130), (34+130), (56+130)	142, 164, 186
23ENC	(Numeric value of digit pairs + 130), (ASCII value + 1)	(23+130), (69+1), (78+1), (67+1)	153, 70, 79, 68

4.7.2.3.2. Procedures

In this study, a maximum DM size was selected according to the maximum encoded data that can be stably read by image processing algorithms after laser treatment (limited to 24 numeric data capacity). Various DM edge lengths were used to determine the minimum pattern size (edge length) that can be stably decoded. The maximum symbol size was limited to 12 mm due to the size of the bananas and their curvature.

The treatments were selected from four levels of a low-power laser. The laser powers used were 1.6 W, 1.8 W, 2.0 W and 2.2 W. Four different sizes of DM code were generated, with edge lengths of 6 mm, 8 mm, 10 mm and 12 mm. Fig. 4.7.4 shows the sizes of the DM symbols given in terms of numbers of rows and columns (10x10 modules, 12x12 modules, 14x14 modules and 16x16 modules). The size of the modules was based on the calculation of a module's area for each DM symbol. All combination treatments were repeated five times.

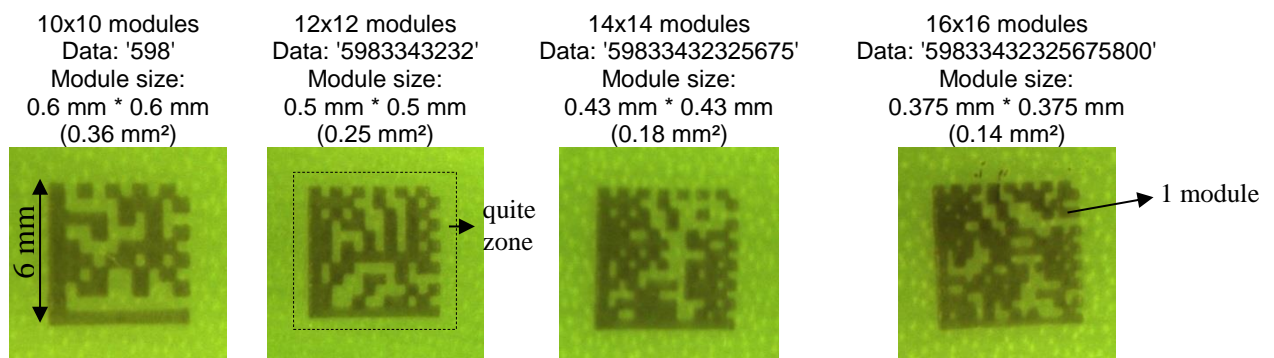


Fig. 4.7.4. Examples of data matrix codes on green bananas with the same edge length (6 mm) and the same laser power immediately after laser marking

Images of the bananas after laser-marking were captured by using a CCD camera (DBK41BU02.H, The Imaging Source Europe GmbH, Bremen, Germany). The readability of the codes was tested with the image processing software Halcon 12 (MVTec Software GmbH, Munich, Germany). The percentage of readability r was calculated as:

$$r = (k*100)/N \quad (4.32)$$

where k denotes the number of decoded codes, and N is the sample size.

5. RESULTS

5.1. Results for optimization of laser positioning

5.1.1. Developed algorithms

5.1.1.1. Algorithms and procedures for poinsettia

Figure 5.1 shows the alignment results between the depth image and the color image. The images are properly aligned; although there are small black regions, they are just invalid depth regions.

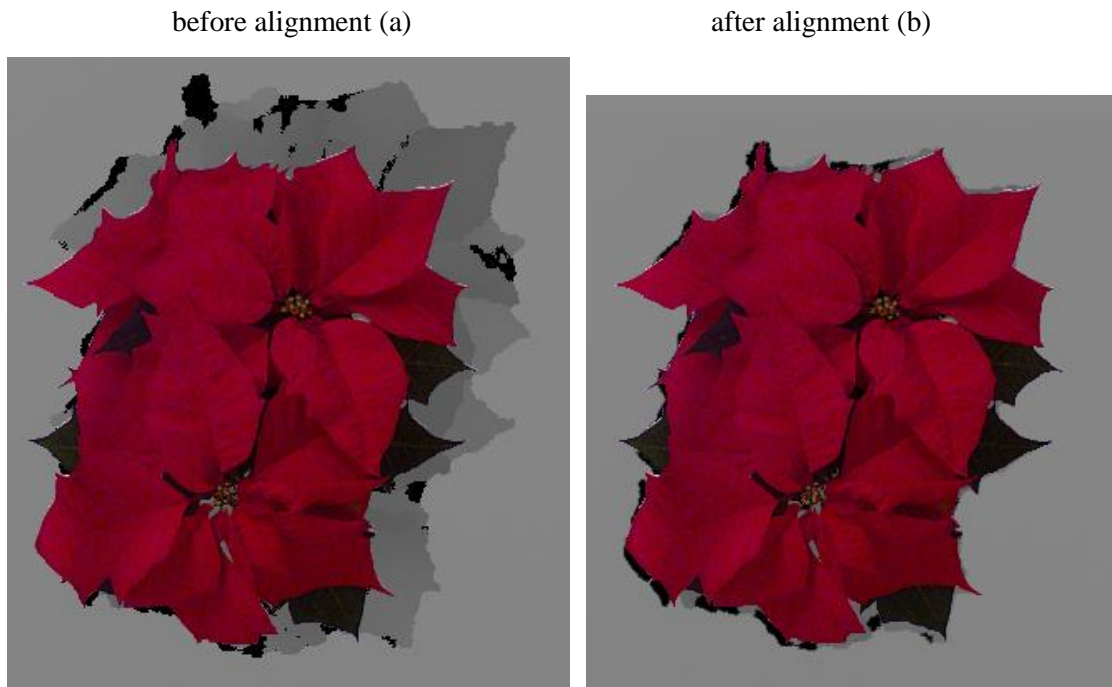


Fig. 5.1. Alignment between depth image and color image

The depth image contains black regions of undefined-depth pixels. The gray value of these pixels is 0 (see Fig. 5.2.c). According to Danciu, et al. (2012), there are two main reasons that the depth image contains the black regions. The first reason is that the objects are too close or too far from the camera, which may cause shadows on the objects. The second reason is that some objects, composed of materials that reflect or refract light, cannot return the correct information.

The black regions that appear on depth images are removed using histogram thresholding. The minimum and maximum gray values of the depth images are based on absolute frequencies of the depth histogram within a region in the input image. The minimum gray value has to be set to more than 0 in order to remove the black regions.

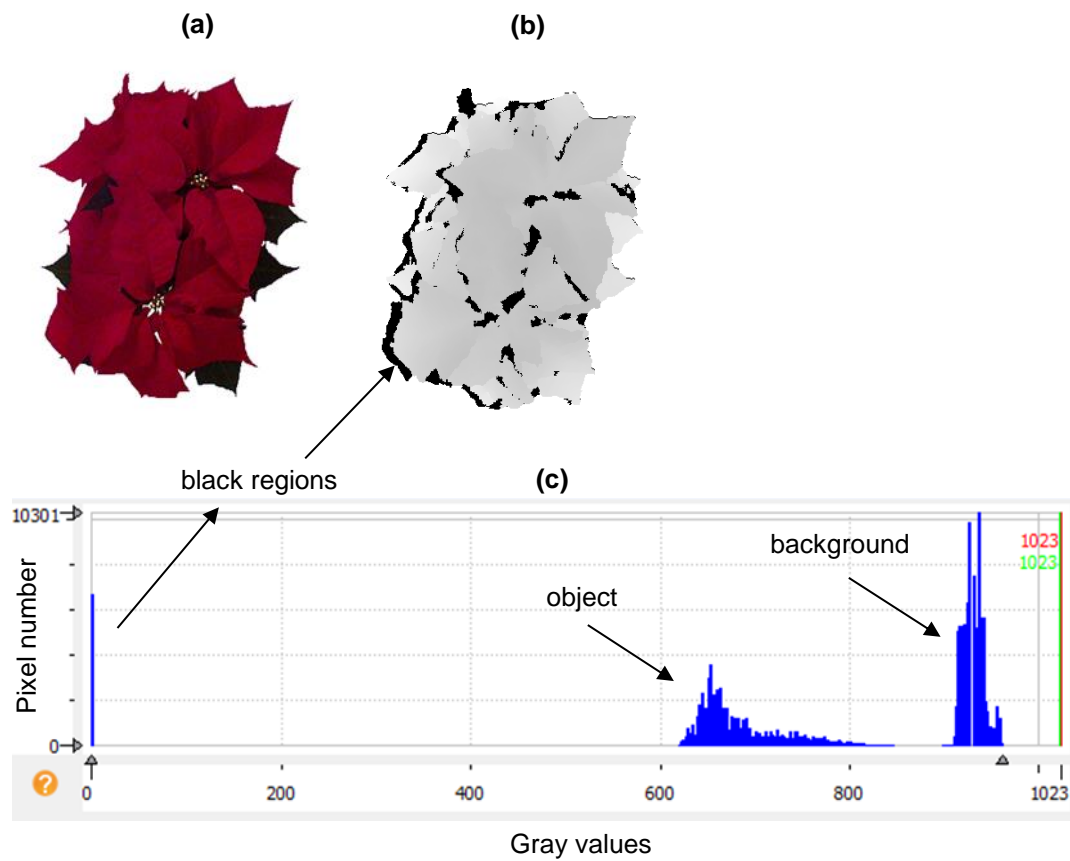


Fig. 5.2. Poinsettia image captured by Kinect camera, (a) RGB image; (b) depth image; (c) depth image histogram

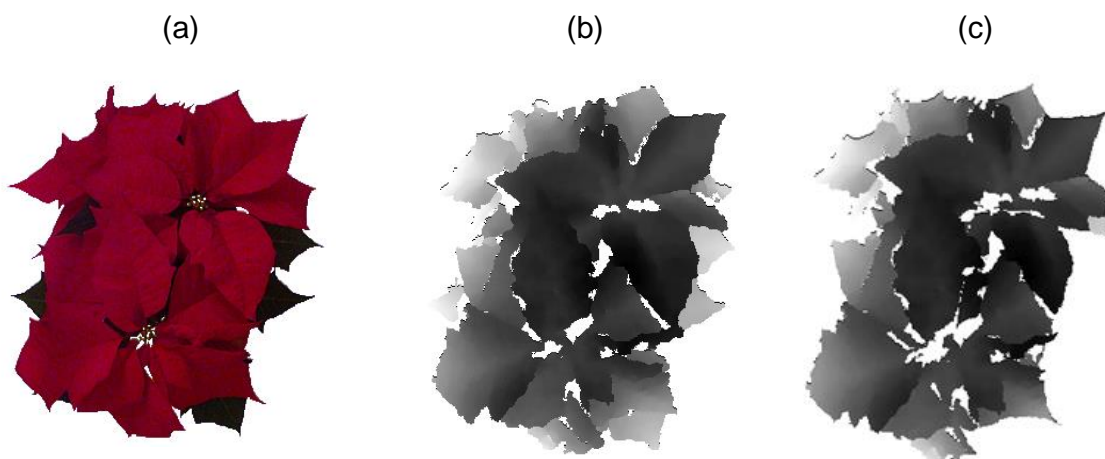


Fig. 5.3. Colored leaves' extraction based on a depth image, (a) Original RGB image, (b) Original depth image, (c) Depth image without green leaves

Fig. 5.3.a shows the green leaves' extraction based on the depth image. For the case of Fig. 5.3.b, the red leaves and the green leaves are identical in the depth image.

According to Fig. 5.4, the best leaf location for laser marking is assessed in two ways. Firstly, all leaves detected have to be equal or more than the shape factor ratio (≥ 0.93). Secondly, the maximum diameter of the selected shape is chosen.

Figure 5.5 shows an example of the algorithm's steps for identifying the main skeleton on poinsettia leaves. Figure 5.5.a is an original input image after segmentation using the Otsu method, and Fig. 5.5.b is the result after applying Canny edge detection. Fig. 5.5 (c) and (d) show hysteresis thresholding and the polygon generated using the Ramer approximation, respectively. Fig. 5.5.e depicts the five longest lines detected on the main leaf skeleton. The length of the lines was calculated as pixel size.

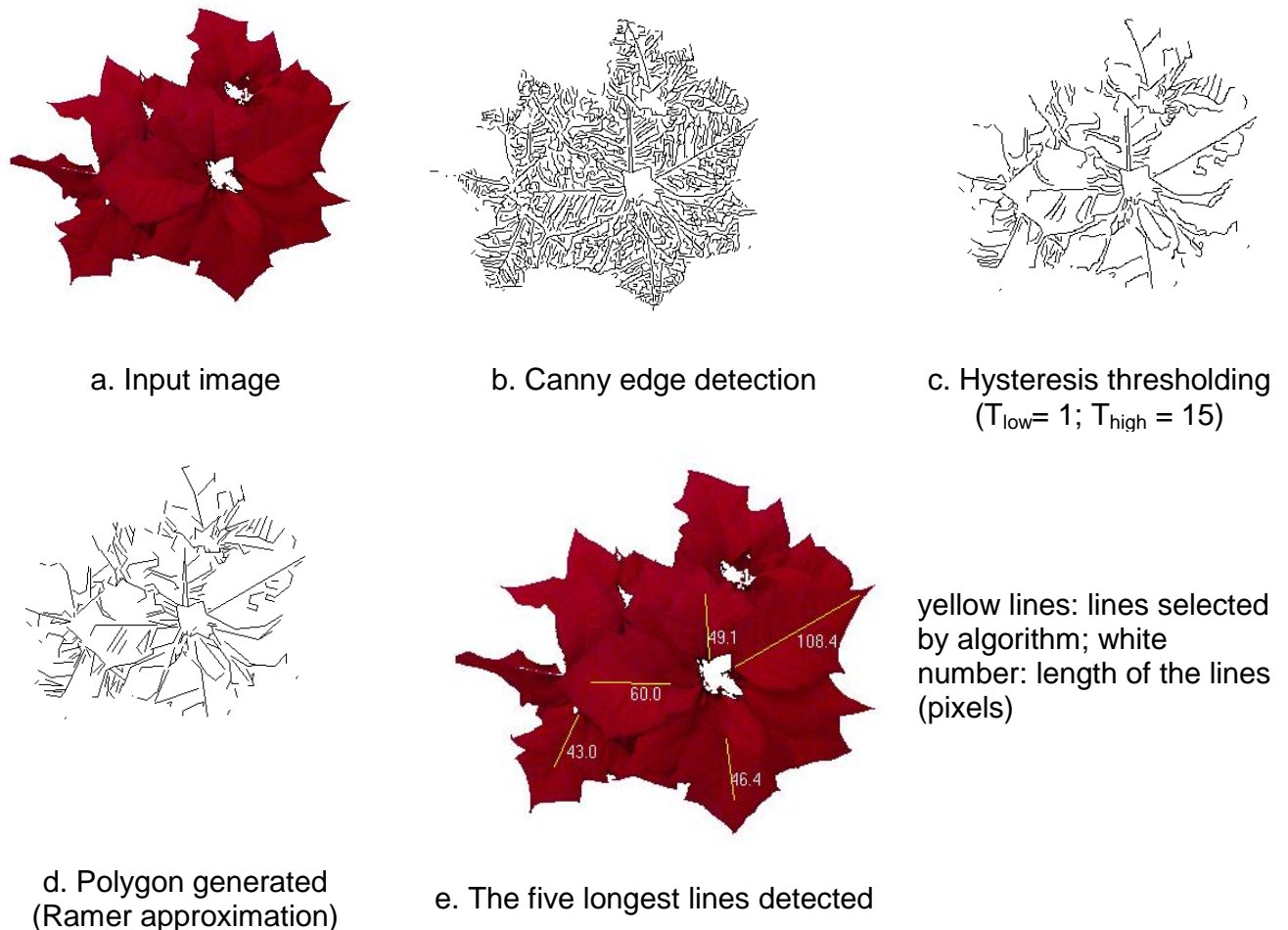


Fig. 5.5. Main leaf skeleton detection steps

The effect of different positions on leaf skeleton detection is shown in Fig. 5.6. The longest five lines are successfully selected from different positions (such as: 0° , 90° ,

180° and 270°). The asterisk symbol represents the starting position of the plant; it changes according to the chosen orientation.

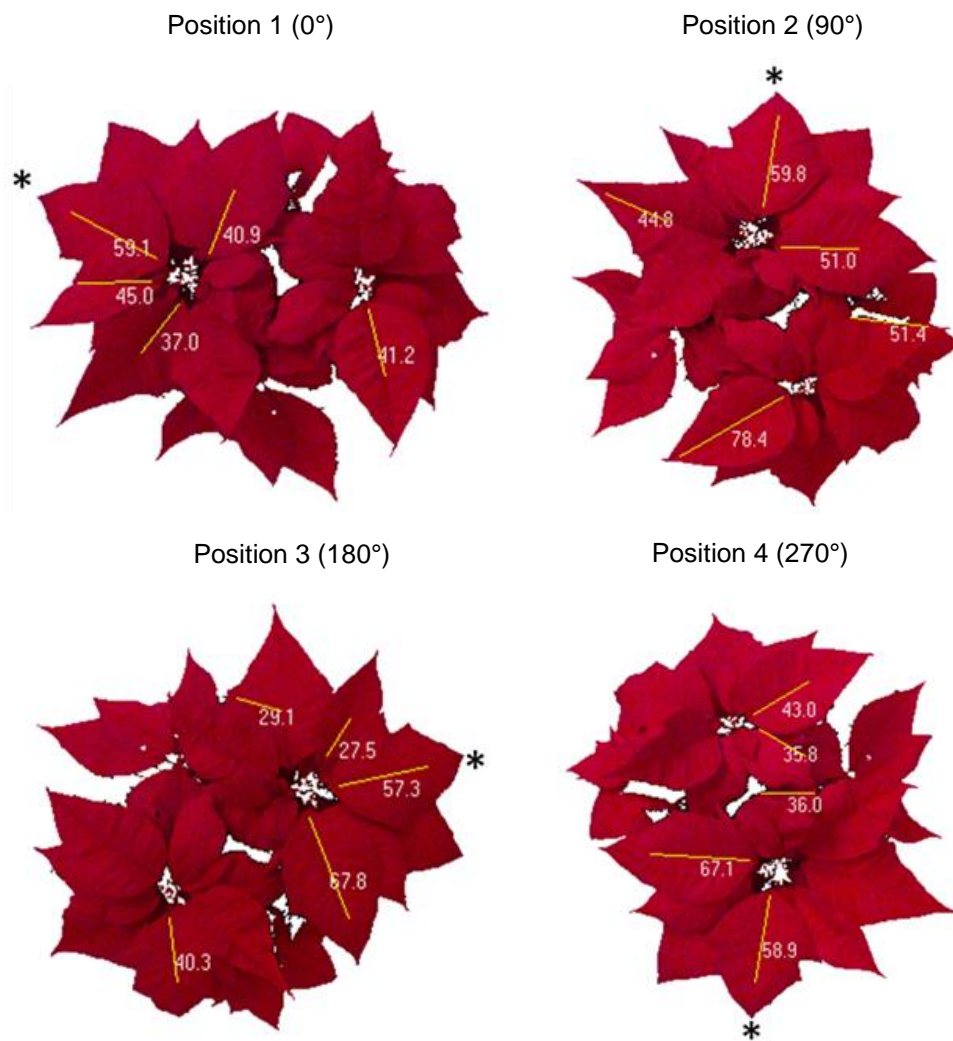


Fig. 5.6. Different position of poinsettia on main leaves' skeleton detection

5.1.1.2. Algorithms and procedure for bananas

Figure 5.7 shows an example of the use of Otsu's thresholding to separate between the background and object of interest. The three different channels ($L^*a^*b^*$) are compared in order to find the best results. According to Fig. 5.7, channel a^* represents the best channel that maximizes the separation between banana and background.

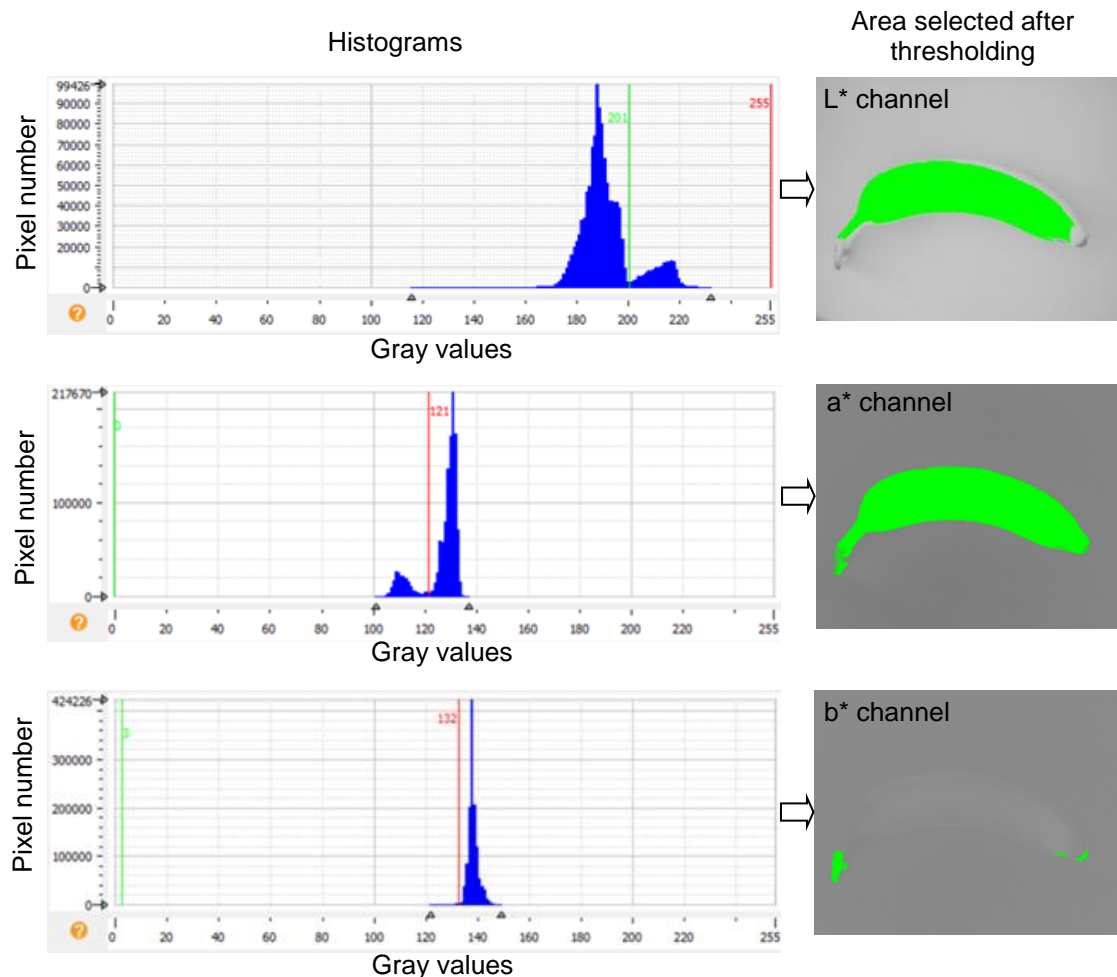


Fig. 5.7. Histogram and banana image after automatic Otsu thresholding

After separating banana images using Otsu's thresholding, binary images are obtained in which foreground parts are numerically displayed with 1 (white) and background is 0 (black). Then, unwanted small objects (noise) are removed. To achieve a whole banana image, the holes in each image are filled. The resulting banana images are shown in Fig. 5.8.

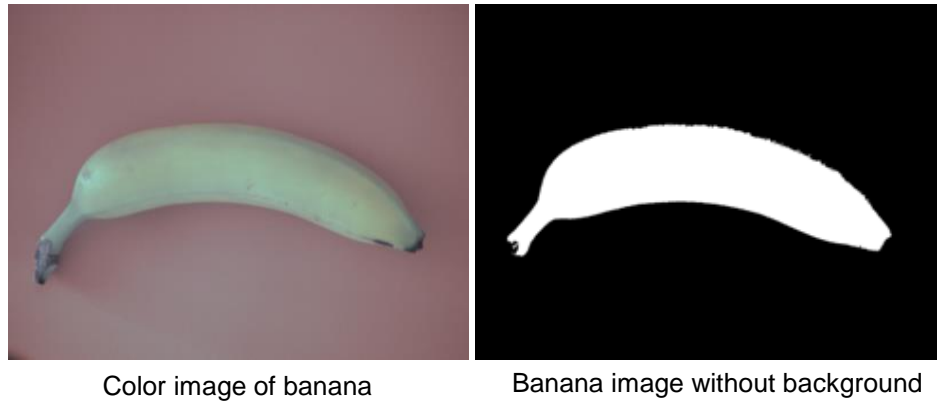


Fig. 5.8. An example of a banana image after background removal

The algorithm steps in Fig. 4.6.14 were applied to banana hands. Figure 5.9 shows the results of the codes' localization on the banana hands. The banana fingers are labelled within the codes on the ventral side. Step 6 in Fig. 5.9 shows three fingers labelled by the algorithms correctly.

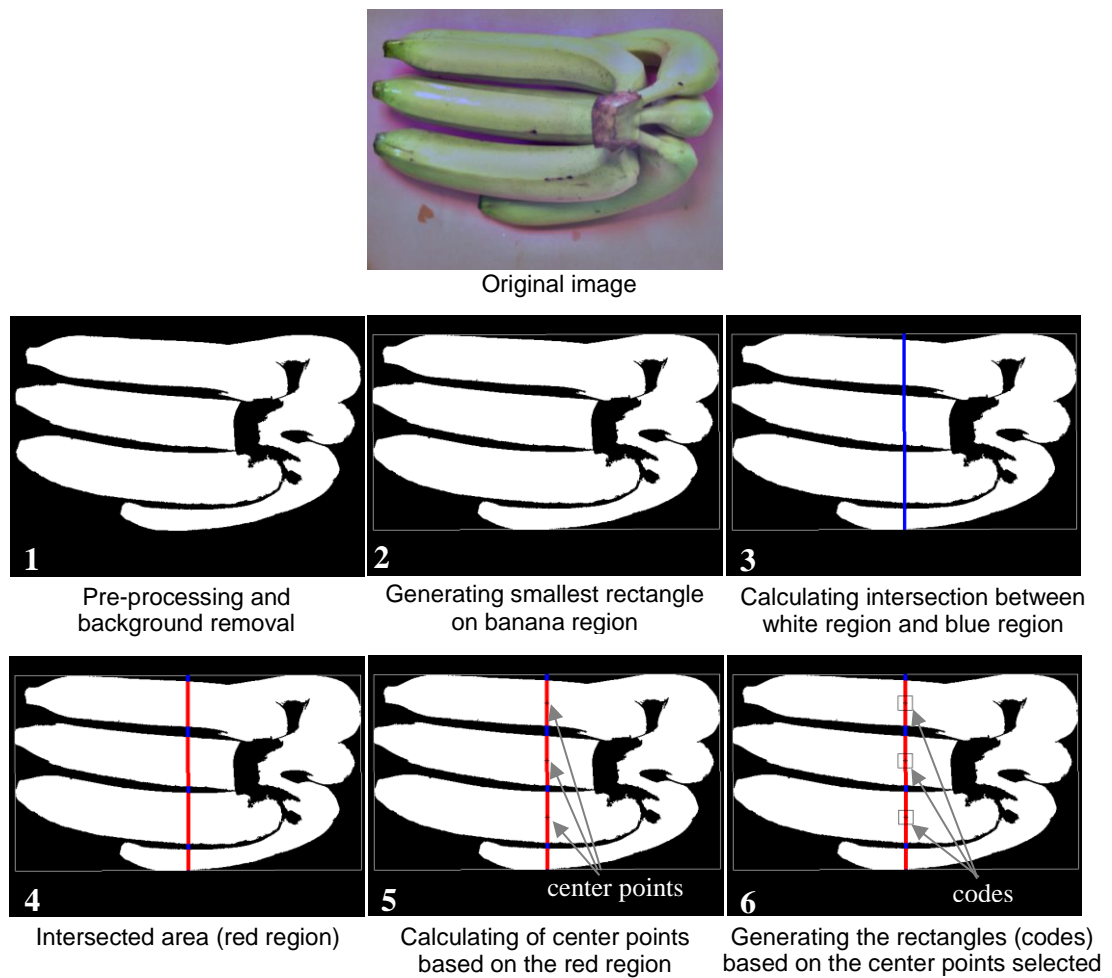


Fig. 5.9. Positioning of codes on banana hands

5.1.2. Evaluation of the developed algorithms

5.1.2.1. Algorithm evaluation for poinsettia

5.1.2.1.1. RGB-Depth algorithms

5.1.2.1.1.1. Color segmentation based on depth images

The method separated different colors of leaves based on a depth image. The segmentation performance of the proposed method is remarkable; only two plants (2.5%) failed to be detected (Table 5.1.2). The experimental results show that the proposed color segmentation based on a depth image can separate green leaves from the image effectively. The results will be used for the next experiment step (sub-section 5.1.2.1.1.2).

Table 5.1.2. Color segmentation based on a depth image of green leaves

	Plant count	Separated	Unseparated
Total	80	78	2
Percent (%)	100	97.50	2.5

N = 80 poinsettia plants

5.1.2.1.1.2. Depth image segmentation based on distance transform-watershed method

The segmentation of the poinsettia leaves was conducted from a top-view image. The experiments were carried out according to watershed segmentation using a distance transform method. The idea is to create a border as far as possible from the center of the overlapping objects. This strategy works very well on rounded objects and is called a distance transform watershed method. It consists of calculating the distance transform of the binary image, inverting it (so the darkest parts of the image become the centers of the objects) and then applying a watershed method to it using the original image as mask. Segmentation of leaf using depth data is robust even with background noise and complex illumination such as shadows. The distance transform-watershed method can efficiently and correctly identify leaves based on their depth. Therefore, accurate segmentation can be obtained for occluded leaves. Overlapping leaves are usually attached close to each other and show small differences in depth.

It can be observed that the classification rate using Kinect v1 was in the range of 47.50% for true positives and 38.75% for false positives (Table 5.1.3). Both true negatives and false negatives yielded an identification rate of 0% and 13.75%, respectively. Moreover, the final classification rate using Kinect v2 was in the range of

92% for true positives and 4% for false positives. True negatives and false negatives yield an identification rate of 0% and 4%, respectively.

Table 5.1.3. Classification rates of poinsettia leaves using Kinect V1 and Kinect V2

	Plant count	True Positive	False Positive	True Negative	False Negative
Kinect v1					
Total	80	38	31	0	11
Percent (%)	100	47.50	38.75	0	13.75
Kinect v2					
Total	80	74	3	0	3
Percent (%)	100	92.50	3.75	0	3.75

True Positive: a correctly identified leaf; False Positive: overlapping leaves detected as a leaf; True Negative: no leaf and no overlapping leaves detected as a leaf; False Negative: a partial leaf is detected.

5.1.2.1.2. Main leaf skeleton algorithms

Table 5.1.4 describes the results in terms of the longest five lines of the main leaf skeleton detected. In the following table, the successful leaf number detected was at least 3.3. Meaning that the algorithm has a correct identification rate of 66%.

Table 5.1.4. Successful detection of the longest five lines of main leaf skeleton

Leaf number	Successful leaf number (mean \pm standard deviation)	Mean success rate (%)
5	3.3 \pm 1.011	66

N = 80 plant samples

In this study, it is assumed that laser marking is performed only on a single leaf. Since Table 5.1.4 illustrates that the number of successful main leaf skeleton detections was 3.3 leaves, the evaluation of a skeleton by the detection of a single leaf becomes possible. The accuracy of developed algorithms based on a confusion matrix is presented in Table 5.1.5. The main skeleton (true positive) is 80% correctly identified. False positives and false negatives have an identification rate of 2.5% and 3.75%, respectively. 13.75% of true negatives are detected.

Table 5.1.5. Classification of the plants from a single poinsettia leaf in the test set

	Plant count	True positive	False positive	True negative	False negative
Total	80	64	2	11	3
Percent (%)	100	80	2.5	13.75	3.75

True positive: main skeleton correctly identified; false positive: branches detected as main skeleton; true negative: no main skeleton and no branches detected as main skeleton; false negative: line detected is too short but it represents a larger leaf.

Examples in Fig. 5.10 illustrate that the developed algorithm successfully detects the longest main skeleton (true positive) in different plant samples.

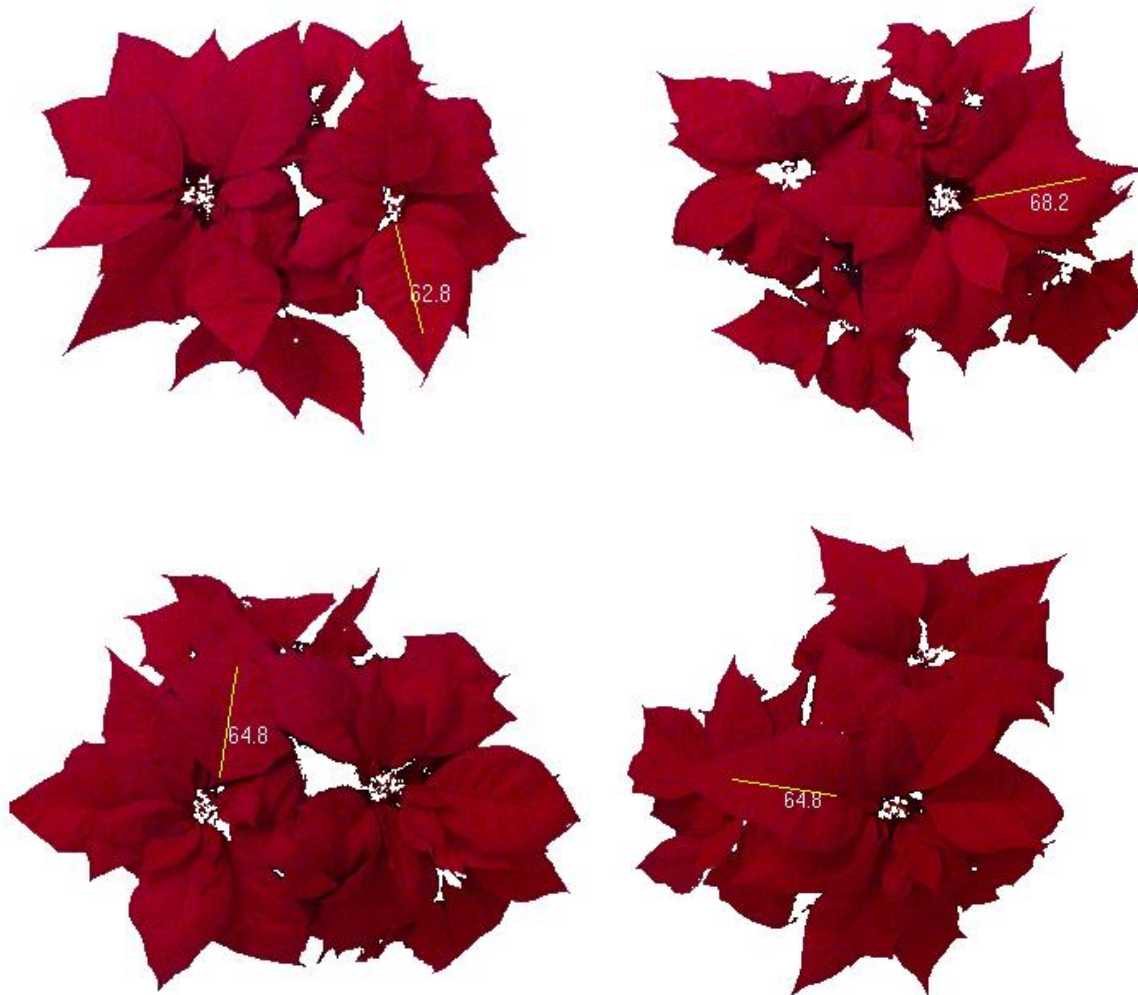


Fig. 5.10. Examples of successful main leaf skeleton detection (true positive)

Figure 5.11 shows false detections of main skeletons of poinsettia leaves by the algorithms. Fig. 5.11.a shows branches detected as the main skeleton (called false

positives), while in Fig. 5.11.b no main skeleton and no branches are detected as the main skeleton by the algorithms (true negative). The third example is the false negative (Fig. 5.11.c), in which the line detected is too short but represents a larger leaf.

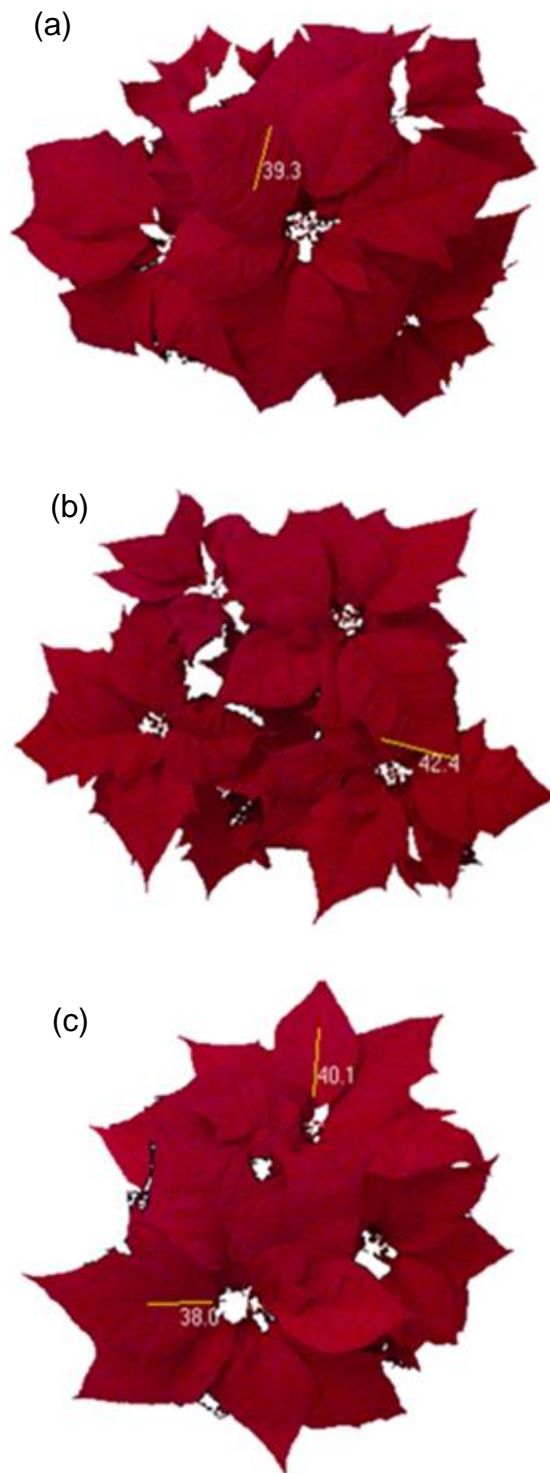


Fig. 5.11. Examples of wrong detection. (a) false positive, (b) true negative, (c) false negative

The detection of main leaf skeletons at various rotations reveals minor differences after evaluation, due to the inconsistency in detecting main leaf skeletons from one position to another position. This shows that the skeleton images become discontinuous. The deviations in leaf detection at various orientations are shown in Table 5.1.6. According to the mean success rate results, the standard deviation obtained is 6.542%. The length of the line is not similar at different positions, which means that the algorithms depend on the orientation. However, the amounts of leaves that are detected indicate conformity with each other, despite the fact that slight variations are visible.

Table 5.1.6. The five longest main leaf skeletons identified at different orientations

Orientation	Successful leaf number (mean \pm standard deviation)	Mean success rate (%)
0°	3.04 \pm 0.95	60.83
90°	2.92 \pm 1.02	58.33
180°	3.37 \pm 1.05	67.50
270°	2.58 \pm 1.10	51.67
Standard deviation		6.542

N = 80 plant samples

5.1.2.2. Algorithm evaluation for bananas

5.1.2.2.1. Algorithm evaluation for banana fingers

Positioning codes on bananas of different shapes is shown in Fig. 5.12. Shape diversity and pedicel of bananas will lead to slight differences in selecting the middle point. The inclination of the rectangular code is slightly non perpendicular to the banana's shape. However, in general the algorithm was 100% successful in placing the rectangular code in the middle of banana fingers with different shapes.

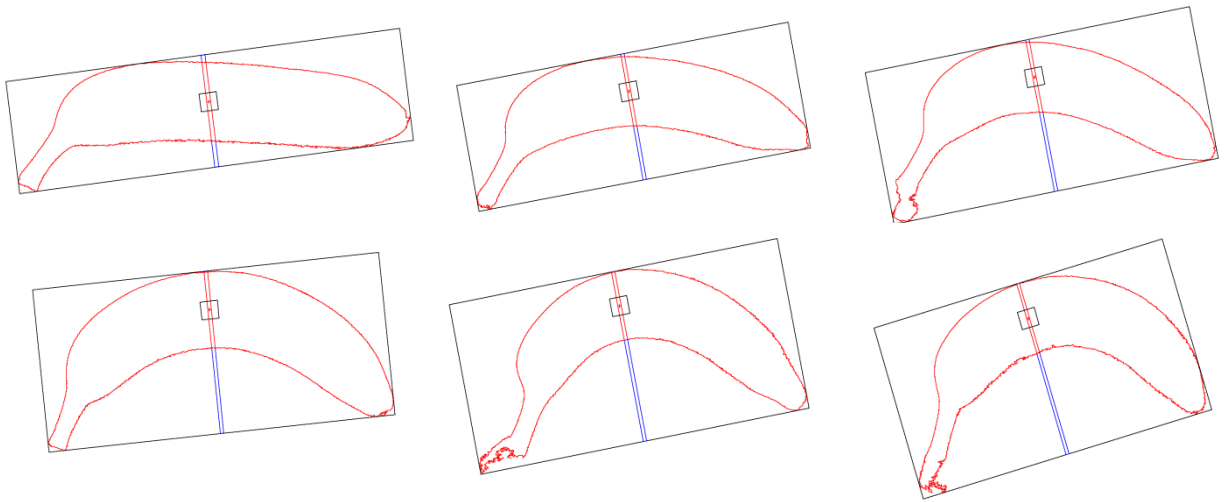


Fig. 5.12. Positioning of the code on bananas with slight curve and curve shape

Fig. 5.13 shows that the algorithm is flexible with any orientation. The method can also be effectively applied to different shapes of horticultural products (Fig. 5.14). Fruits' shapes commonly have an axis-symmetric geometry (i.e. cylindrical and non-cylindrical). Compared with bananas, finding the midpoint using the algorithm is easier for other fruits which have axis-symmetric shapes.

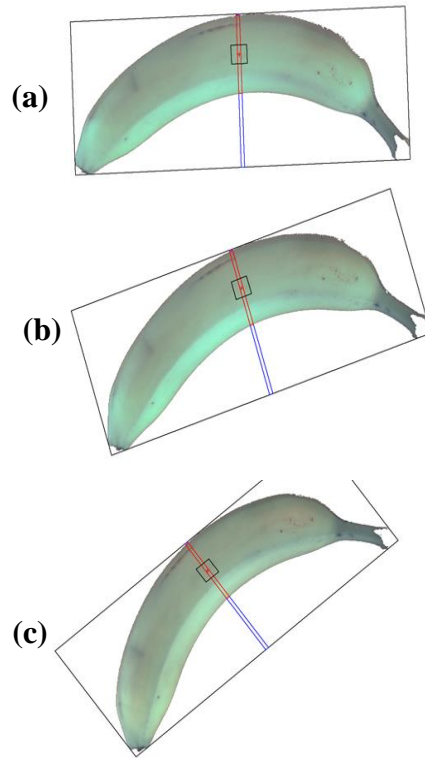


Fig. 5.13. Positioning of a code on a banana with different orientations

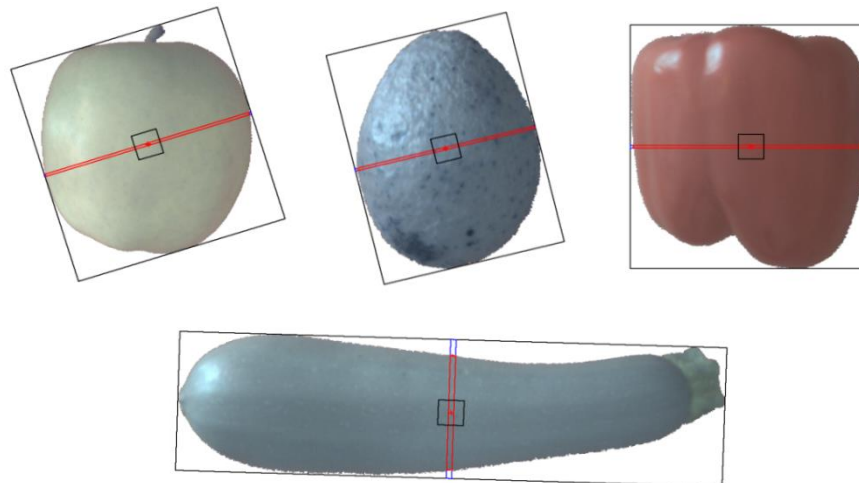


Fig. 5.14. Positioning of a code on fruits and vegetables

5.1.2.2.2. Algorithm evaluation for banana hands

The successful positioning of the codes on ventral and dorsal banana sides are compared in order to obtain the best results (see Table 5.1.7). For ventral banana sides, the system is capable of selecting 92.86% of the banana hands that contain at

least one code (label), with a success rate of 75.71% for banana hands that contains more than one code (labels). The success rate for dorsal banana sides is 67.14% (at least one code selected by the algorithms), while the success rate for selecting more than one code is only 35.71%. Therefore, positioning of the codes on ventral banana sides shows the best results.

Table 5.1.7. Successful rate of localization of codes (labels) on banana hands

	Banana hands counts	Amount		Rate (%)	
		Success	False	Success	False
At least one code:					
- Ventral banana side	70	65	5	92.86	7.14
- Dorsal banana side	70	47	23	67.14	32.86
More than one code:					
- Ventral banana side	70	53	17	75.71	24.29
- Dorsal banana side	70	25	45	35.71	64.29

Some examples in Fig. 5.15 and Fig. 5.16 illustrate the algorithms which successfully locate the codes (labels) on banana hands.

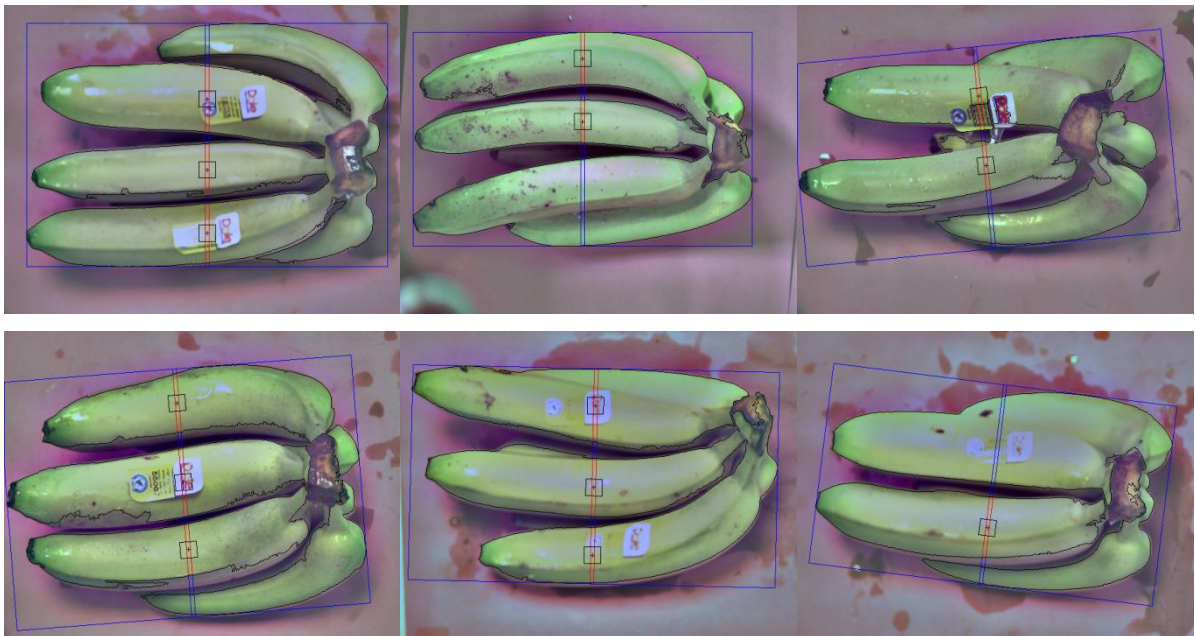


Fig. 5.15. Successful positioning of the 2D codes on banana hands (ventral side)

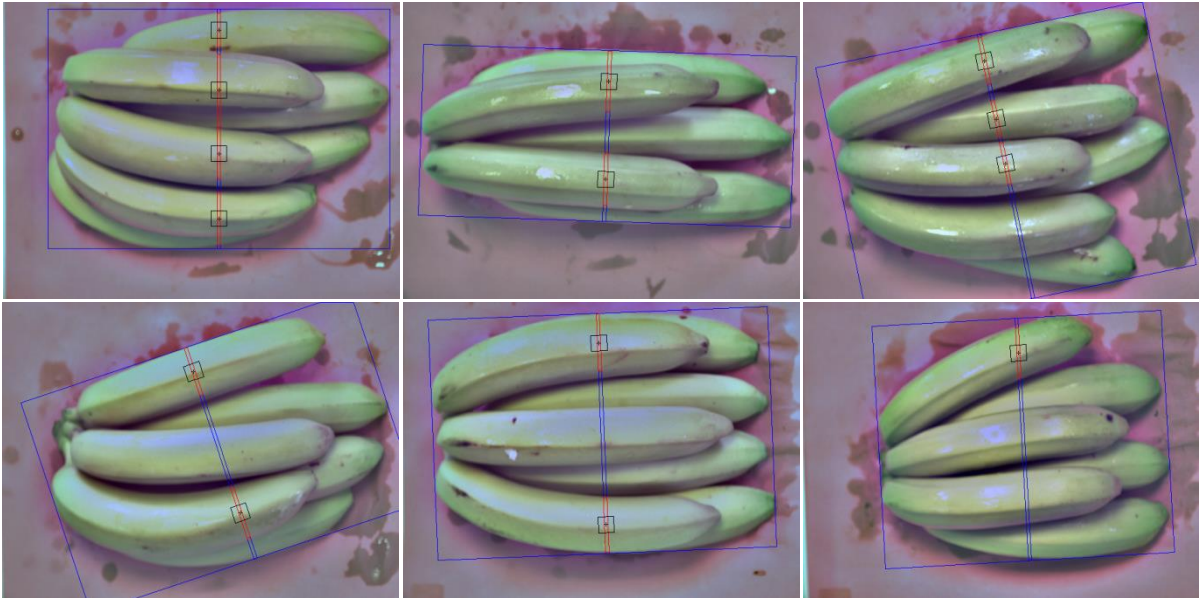


Fig. 5.16. Successful positioning of the 2D codes on banana hands (dorsal side)

Unsuccessfully positioning the codes (labels) on banana hands is shown in Fig. 5.17. Fig. 5.17.a shows incorrect code positioning due to the detection of two fingers as one finger. Since the algorithms always locate the code in the middle point of the intersected line, every banana finger obviously has to be separated. Otherwise, the positioning of the code will remain an error (i.e. the code will be located in the middle of the two or more fingers selected). Although this error rarely happens (1.43%), this matter should be considered in order to increase correct positioning of the code. Another error was shown in Fig. 5.17.b-c, in which the fingers cannot be found by the algorithms. The lighting and the wetness of the bananas could be the reason for this situation. Most of the false detection is caused by these errors (5.71%).



Fig. 5.17. False localization of the 2D codes on banana hands

5.2. Optimization of laser parameters for marking

5.2.1. Evaluation of energy output

The actual beam power is measured as the total energy supplied per unit of time (Watt) with respect to laser power (%), as shown in Fig. 5.18. Figure 5.18 shows a scatter plot of laser power output as a function of laser power (%) with the correlation value of 0.9974. The regression equation is:

$$\text{Laser power output} = (0.0710 * \text{Laser power (\%)}) - 0.0663 \quad (5.1)$$

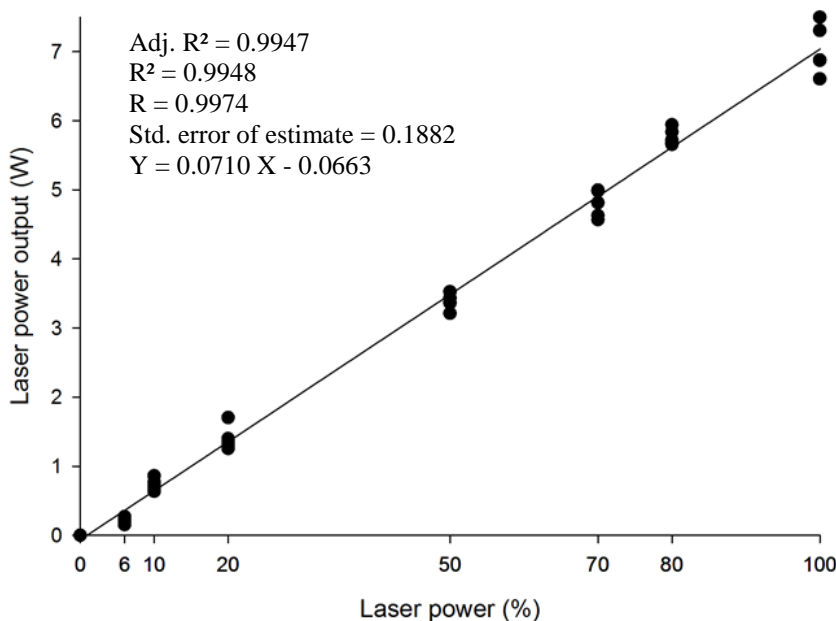


Fig. 5.18. Relationship between percentage of laser power use and actual beam power (5 repetitions)

This regression is useful as it allows one to make predictions of laser output power. Table 5.2.1 shows a comparison between a water calorimeter chamber and a CO₂ laser power meter for calibrating laser power. The following table shows a slight difference between the two methods.

Table 5.2.1. Comparison of using water calorimeter and CO₂ laser power meter

Laser power (%)	water calorimeter (W)	CO ₂ laser power meter (W)*
100	7.03	6.90 ± 0.141
80	5.61	5.68 ± 0.216

* Mean value ± standard deviation (five repetitions)

5.2.2. Laser parameter optimization for poinsettia

The results of the evaluation of laser marking poinsettia leaves, based on a 4-level scale, are shown in Fig. 5.19. The HAZ values of each leaf are calculated as percentages which correspond to the HAZ index (see sub-section 4.7.1.2).



Fig. 5.19. Different levels of heat affected zones (HAZ) 3 days after laser marking on poinsettia leaf, with white numbers showing the calculation of damages on each character; (a) No apparent HAZ; (b) Slight HAZ; (c) Moderate HAZ; (d) Severe HAZ

The result of the HAZ index is presented in Table 5.2.2. The lowest HAZ values are obtained with a low laser power (0.43 W and 0.5 W) while the highest HAZ index was obtained from a high laser power. It is observed that a combination of low power and low energy proved to be the most effective treatment, with a HAZ index of 0. In addition, a HAZ index of 0 will cause no damage to the leaves. Therefore, the analysis of leaves' damage with values of 0 (no apparent HAZ) are considered to be acceptable, as they may be stable during storage. On the other hand, leaves showing damage values of 1, 2 and 3 (slight, moderate and severe HAZ, respectively) are considered to represent unacceptable damages to the marking quality. Nevertheless, some treatments using too-low energy produce incomplete characters, particularly: 0.5

W [0.83 J per character], 0.5 W [0.28 J per character], 0.5 W [0.38 J per character], 0.5 W [0.12 J per character], 0.43 W [1.05 J per character], 0.43 W [0.71 J per character], 0.43 W [0.24 J per character], 0.43 W [0.47 J per character], 0.43 W [0.32 J per character], 0.43 W [0.10 J per character] (see Table. 5.2.2). Fig. 5.20 shows marks with incomplete results or inadequate contrast on poinsettia leaves.

Table 5.2.2. Heat affected zone (HAZ) index of marked poinsettia leaves

No.	Power (W), [resolution (dpi)]	Laser energy (J per character)	HAZ index	No.	Power (W), [resolution (dpi)]	Laser energy (J per character)	HAZ index
1	7.0 [200] v	3.90	3	25	0.71 [600] h	1.08	3
2	7.0 [200] h	1.73	3	26	0.71 [500] h	0.79	2
3	5.2 [200] v	2.92	3	27	0.71 [400] h	0.54	1.2
4	5.2 [200] h	1.29	3	28	0.71 [200] h	0.17	0.4
5	3.5 [200] v	1.93	3	29	0.50 [700] v	2.21	0.4
6	3.5 [200] h	0.85	3	30	0.50 [600] v	1.67	0.2
7	1.7 [200] v	0.95	2	31	0.50 [500] v	1.22	0
8	1.7 [200] h	0.42	2	32	0.50 [400] v	0.83	0*
9	0.93 [700] v	4.08	3	33	0.50 [200] v	0.28	0*
10	0.93 [600] v	3.09	3	34	0.50 [700] h	1.00	0.4
11	0.93 [500] v	2.26	3	35	0.50 [600] h	0.76	0
12	0.93 [400] v	1.54	1.6	36	0.50 [500] h	0.55	0
13	0.93 [200] v	0.51	1	37	0.50 [400] h	0.38	0*
14	0.93 [700] h	1.86	3	38	0.50 [200] h	0.12	0*
15	0.93 [600] h	1.40	2.4	39	0.43 [700] v	1.89	0
16	0.93 [500] h	1.02	2	40	0.43 [600] v	1.43	0*
17	0.93 [400] h	0.69	1	41	0.43 [500] v	1.05	0*
18	0.93 [200] h	0.22	0.2	42	0.43 [400] v	0.71	0*
19	0.71 [700] v	3.14	3	43	0.43 [200] v	0.24	0*
20	0.71 [600] v	2.39	2.2	44	0.43 [700] h	0.86	0
21	0.71 [500] v	1.74	2.2	45	0.43 [600] h	0.65	0*
22	0.71 [400] v	1.19	1.2	46	0.43 [500] h	0.47	0*
23	0.71 [200] v	0.39	0.8	47	0.43 [400] h	0.32	0*
24	0.71 [700] h	1.43	3	48	0.43 [200] h	0.10	0*

HAZ index: [0] no apparent HAZ; [1] slight HAZ; [2] moderate HAZ; [3] severe HAZ; v= vertical scan direction, h= horizontal scan direction. * Incomplete or inadequate contrast marking result

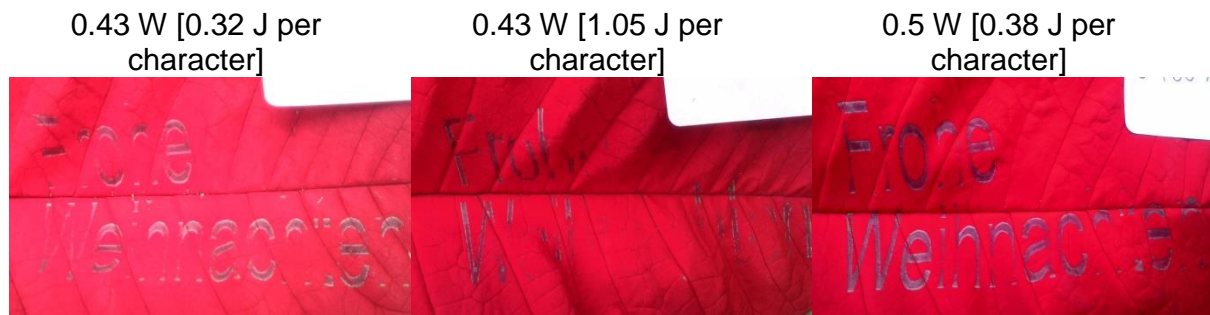


Fig. 5.20. Example of incomplete marking results or inadequate contrast on poinsettia leaves due to too-low laser energy

In general, applying both raster scan directions (i.e. vertical and horizontal) doesn't cause damage to the leaves during the storage period (see Table 5.2.1). However, one scan direction may mark faster than the other depending on the orientation of the raster image. Based on this study (Fig. 5.21), the time ratio based on cycle time between the horizontal direction and vertical direction was 1:2.1 (mean value), respectively.

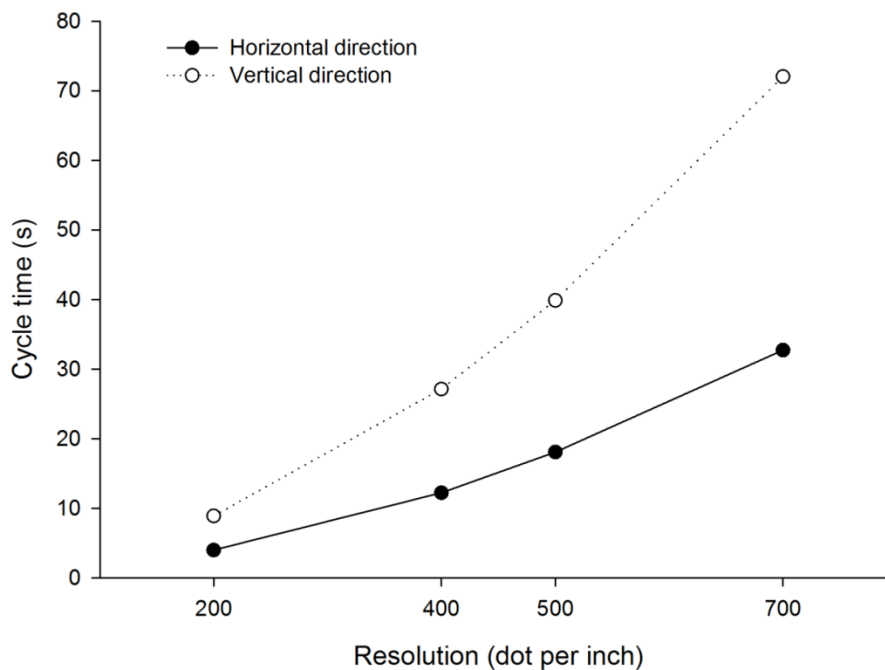


Fig. 5.21. Effect of laser marking resolution and raster scan direction on cycle time

According to Table 5.2.2, it can be seen that laser marking with 0.5 W [1.22 J per character], 0.5 W [0.76 J per character], 0.5 W [0.55 J per character], 0.43 W [1.89 J per character] and 0.43 W [0.86 J per character] respectively prove to have the best marking ability, leading to the lowest HAZ values. Furthermore, based on the energy use during the marking process, 0.5 W [0.55 J per character] was chosen as the best treatment (see Fig. 5.22).



Fig. 5.22. Laser marking on poinsettia leaves using 0.5 W [0.55 J per character]

The mark becomes dark red in color at beginning of storage, and turns to yellowish-white as growth continues until 14 days of storage (see Table 5.2.3). Applying a laser marking with 5.2 W [1.29 J per character] causes severe damage to leaf tissue. At this level the mark became dried-up.

1 Table 5.2.3. Examples of changes to poinsettia leaves on selected samples during
 2 the storage period (five repetitions)

Laser power (W), [Laser energy (J per character)]	Day 1	Day 3	Day 7	Day 14
0.43 [1.89]				
0.5 [0.55]				
0.5 [1.22]				
0.5 [1.67]				
0.71 [1.74]				
0.93 [2.26]				
5.2 [1.29]				

3

5.2.3. Laser parameter optimization for bananas

5.2.3.1. Spectral reflectance of marked bananas

Fig. 5.23 compares the reflectance values of the five different parts in Fig. 4.7.2. According to Fig. 5.23.a, there is no significant difference in the reflectance curves between the unmarked and marked banana surfaces. The curve of unmarked bananas produces different reflectance values compared to marked bananas. Because of this behavior and taking into account the difference between unmarked and marked bananas, the reflection difference is useful to differentiate marked and unmarked parts at low laser power. However, Fig. 5.23.b demonstrates that the distributions of the reflectance differences from 0.8 W to 1.6 W are very low and not useful. On the other hand, the reflectance difference for 2.0 W markings is significant between marked and unmarked parts, however on a very low absolute level.

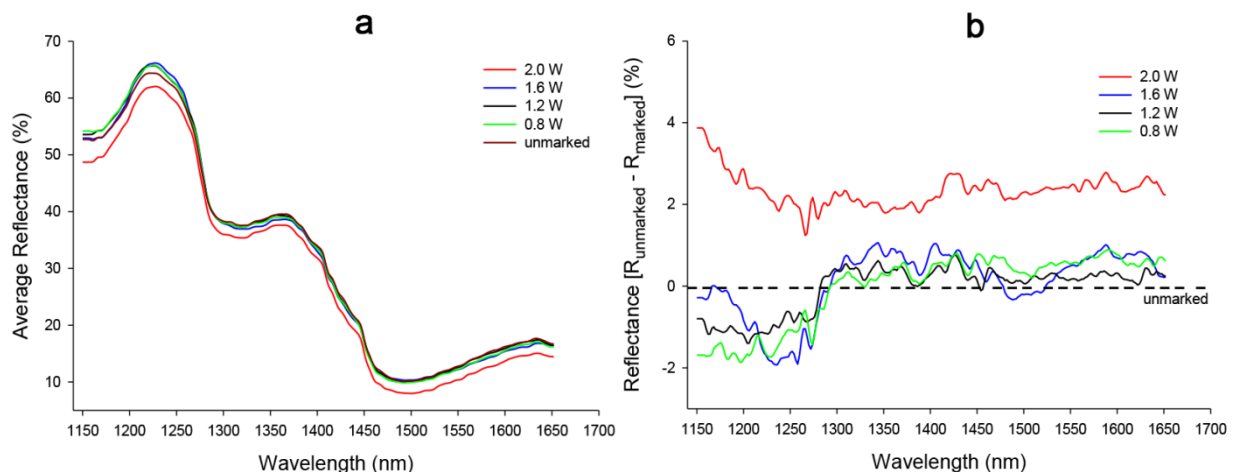


Fig. 5.23. Reflectance spectrum (R) of marked bananas in the infrared waveband (N = 10 bananas): (a) mean reflectance (b) reflectance difference

5.2.3.2. Quality of codes

5.2.3.2.1. Decode

Data matrix codes with a laser power of 1.8 W and 1.6 W with longer marking times (0.094 s per module and 0.072 s per module) can be read constantly, while a laser power of 2.0 W provides better results with a shorter marking time (0.038 s per module). A laser power of 2.2 W with all marking time treatments leads to poor readability (Fig. 5.24).

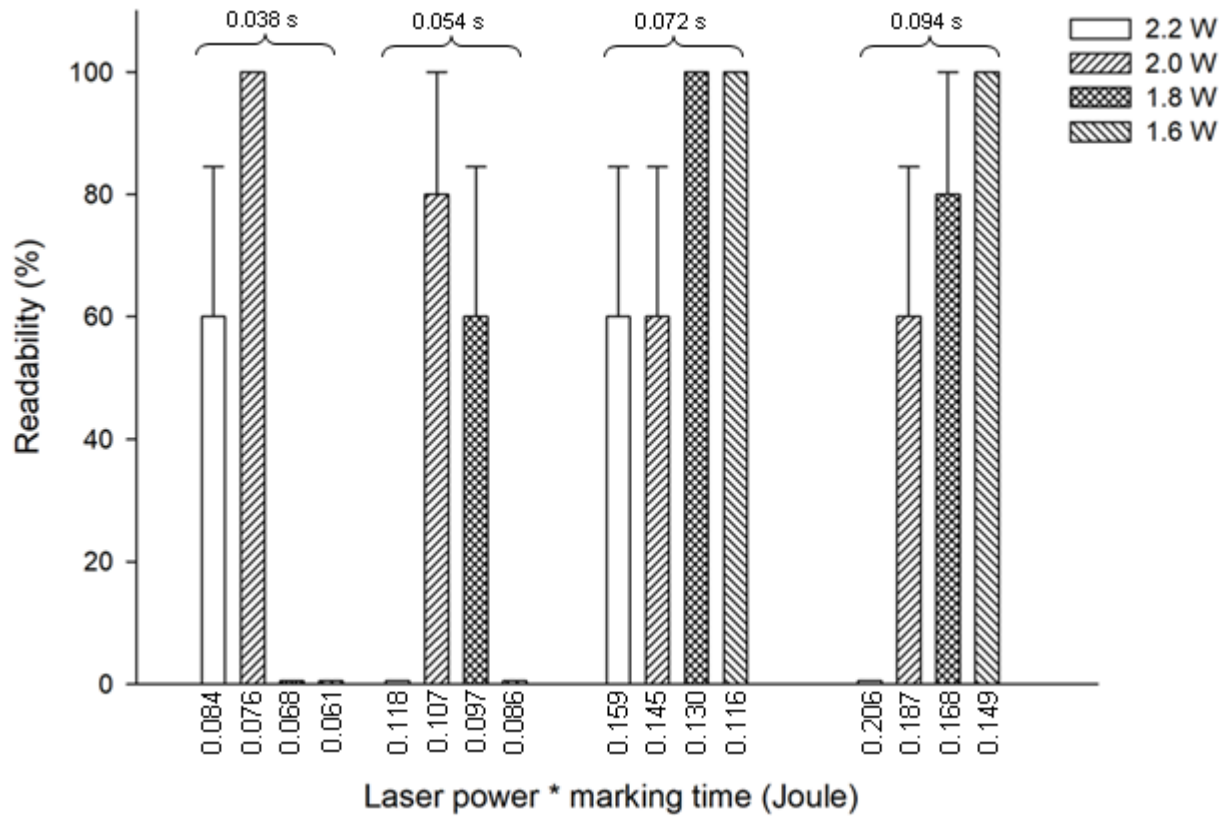


Fig. 5.24. Effects of laser marking and marking time on readability of data matrix code after 9 days of storage. Error bars represent standard error of mean (n= 5).

In terms of energy use, the same laser energy does not guarantee high readability of the code; rather, readability depends on the laser power and marking time. This point is shown by the circle in Fig. 5.25, where similar energy leads to different code qualities.

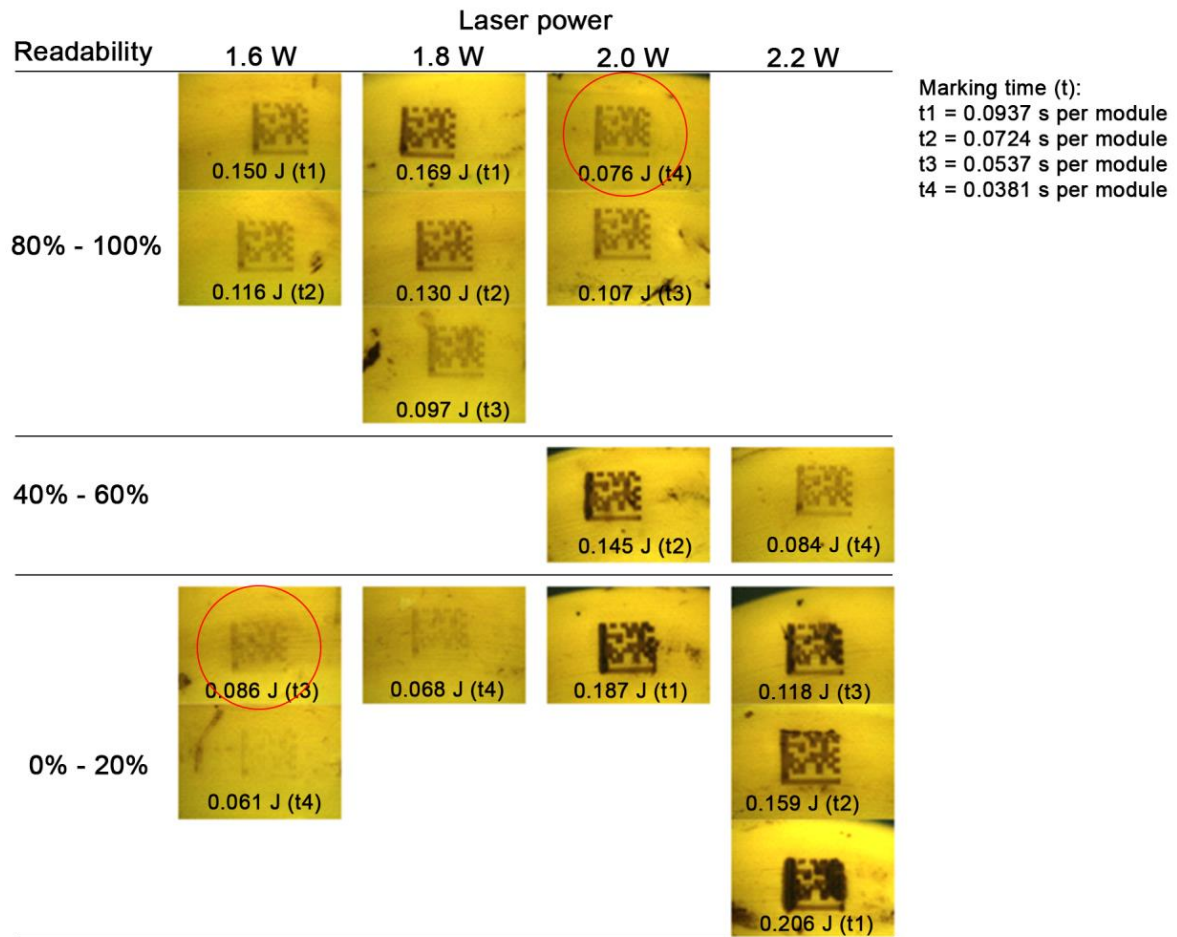


Fig. 5.25. Data matrix codes on bananas after 9 days of storage (data matrix edge length 10 mm, 10x10 modules)

5.2.3.2.2. Contrast values

Figure 5.26 shows an analysis of the effects of both laser power and marking time on contrast values. The optimal combination of laser power and marking time becomes a key factor for producing high contrasts in the codes. As can be seen from this figure, the codes contrast increases when the laser power and marking time are higher. Contrarily, if both parameters decrease, then the code contrast declines. Increasing laser power with a longer marking time causes oxidation under the surface of the bananas and discoloration of the materials, which creates high contrast. A high contrast value does not guarantee a high readability of the code. Conversely, almost all codes cannot be decoded if the contrast value is lower than 25%.

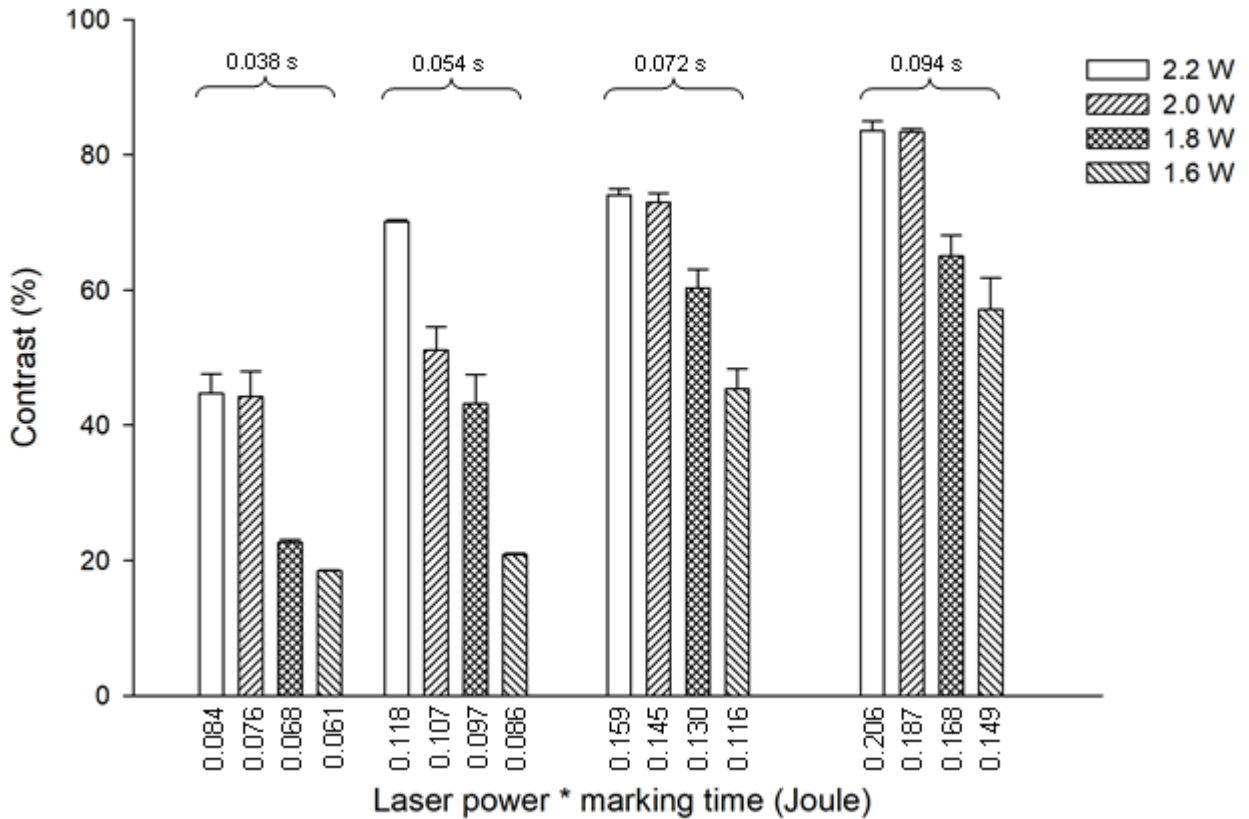


Fig. 5.26. Effects of laser marking and marking time on contrast values of data matrix codes after 9 days of storage. Error bars represent standard error of mean ($n=5$).

5.2.3.2.3. Axial non-uniformity (ANU)

The ANU describes the aspect ratio of the data code, in which the distance between the modules' center positions is the same in the vertical and horizontal direction. If scaled only in one direction (i.e. only in its height or width), the quality of the grade will decrease. If ANU values ≤ 0.06 , then the quality grade is high (ISO/IEC 15415, 2011). Figure 5.27 depicts the effects of laser power and marking on ANU. In general, all treatments show good results ($ANU \leq 0.06$).

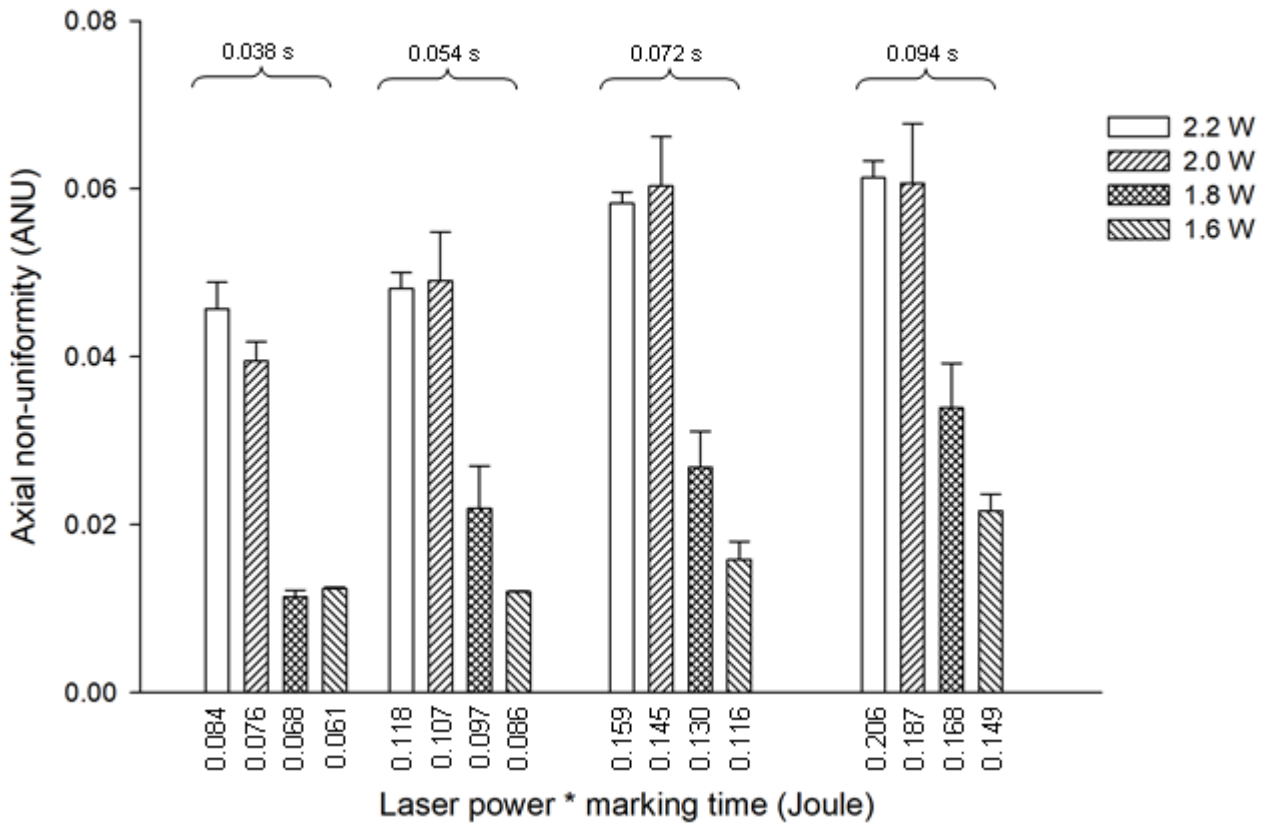


Fig. 5.27. Effects of laser marking and marking time on the axial non-uniformity values of data matrix codes after 9 days of storage. Error bars represent standard error of mean ($n=5$).

5.2.3.2.4. Grid non-uniformity (GNU)

The quality of grid non-uniformity quantifies the deviation of the modules from their ideal grid. If the modules are arranged in a rectangular grid and the value of GNU is ≤ 0.38 , then the quality grade is high (ISO/IEC 15415, 2011). Based on this study (Fig. 4.28), the GNU values of all treatments are less than 0.38. This means that the GNU doesn't change over all treatments. Moreover, there is no statistically significant difference among the treatments for both laser power and marking time on grid non-uniformity values.

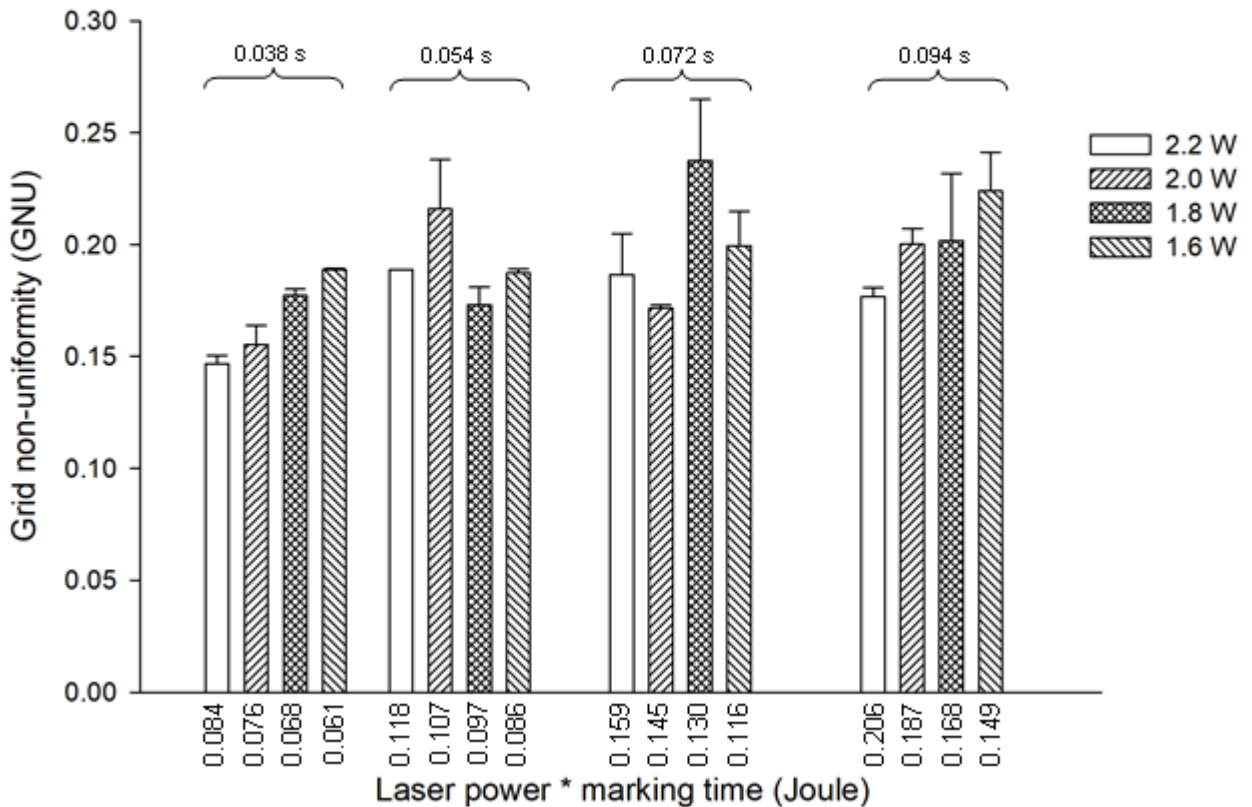


Fig. 5.28. Effects of laser marking and marking time on grid non-uniformity values of data matrix codes after 9 days of storage. Error bars represent standard error of mean (n= 5).

5.2.3.2.5. Unused error correction (UEC)

A code with a high quality grade requires no error correction. This quality grade quantifies the reserves in error correction that is still available after decoding the code. The more defective a code becomes, the more the error correction needs to be applied to be able to decode the data code. Based on Fig. 5.29, data matrix codes with a laser power of 1.8 W and 1.6 W at a marking time of 0.072 s per module show high grade unused error correction (UEC > 0.8). If UEC values are equal or more than 0.62, then the value for the quality grade is high (ISO/IEC 15415, 2011).

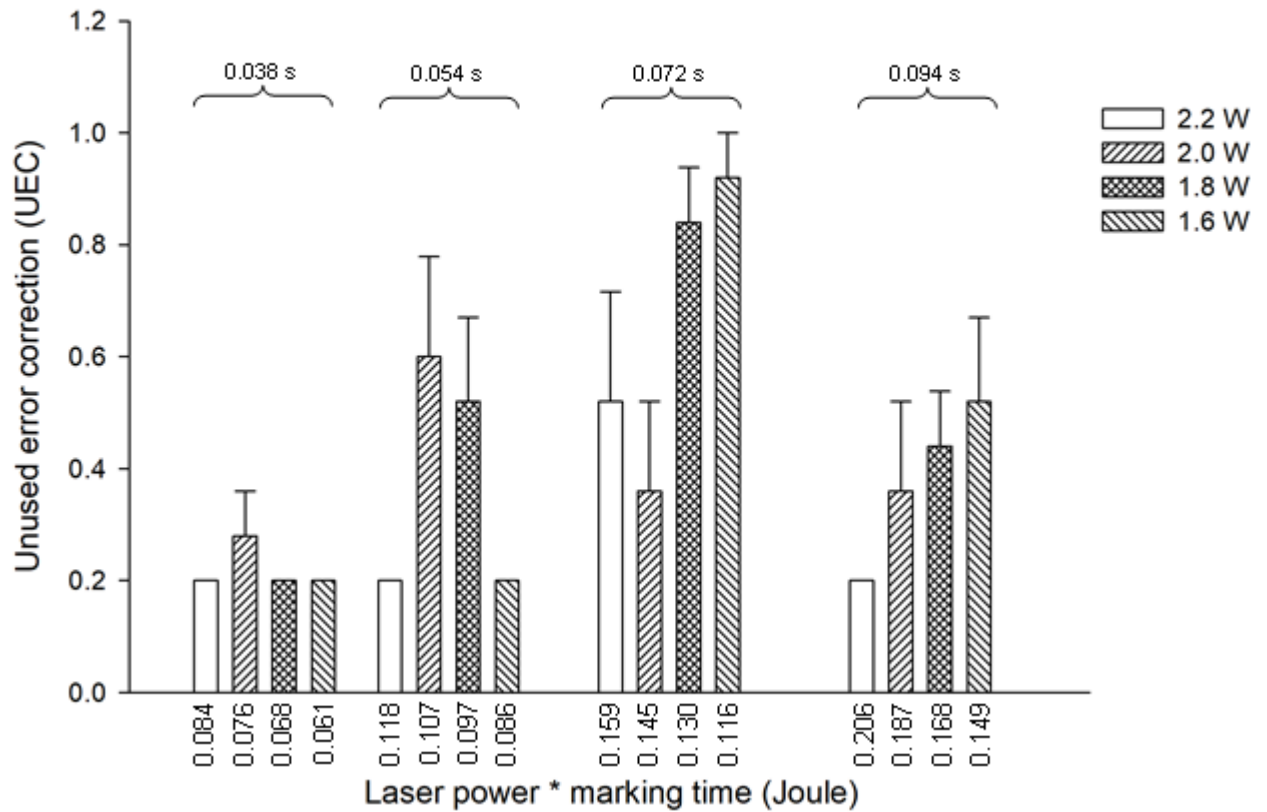


Fig. 5.29. Effects of laser marking and marking time on the unused error correction values of data matrix codes after 9 days of storage. Error bars represent standard error of mean (n= 5).

5.2.3.2.6. Damages to the codes during storage time

Figure 5.30 shows images of bananas marked with different laser powers until 9 days of storage. A laser power of 1.8 W and 1.6 W are appropriate for marking bananas for 9 days of storage. Moreover, laser marking on bananas at these conditions causes insignificant cell damage in the epidermis area. More significant damage appears on markings with high laser power. However, too-low power produces relatively less contrast.

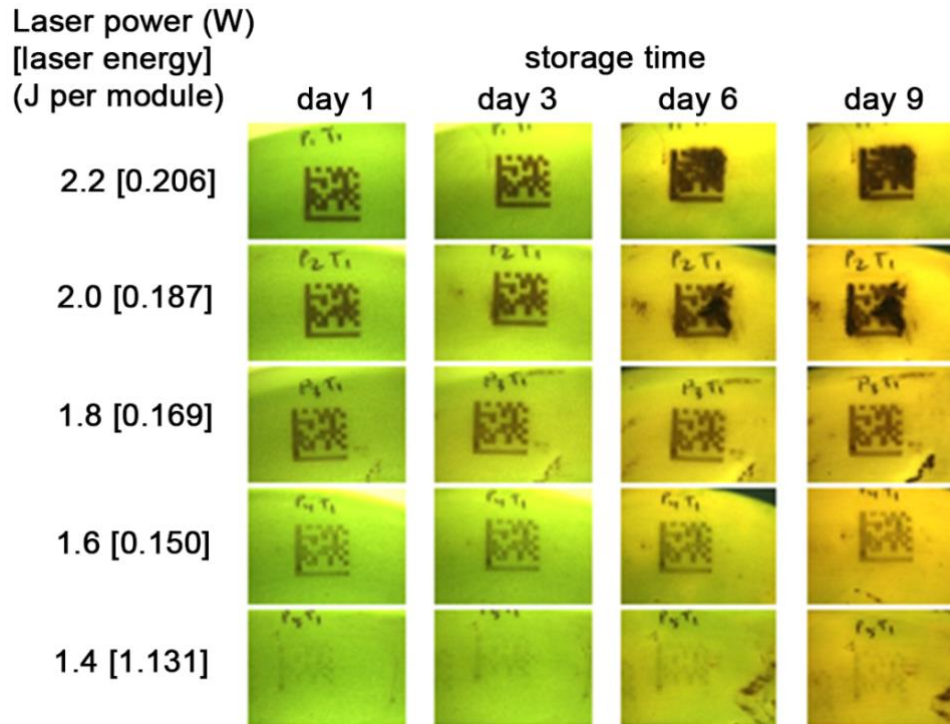


Fig. 5.30. Damage to bananas after laser marking

5.2.3.3. Readability of the codes

Readability results using a laser power of 2.2 W are comparatively low. The readability of the codes with 14x14 modules and 16x16 modules varies from 0% to 20%. Applying 10x10 modules and 12x12 modules increases the readability from 0% to 60% (see Table 5.2.4). A laser power of 2.0 W yields better results compared to a laser power of 2.2 W, due to the fact that increasing the laser power leads to more damage to the codes. High readability, ranging from 80% to 100%, is obtained at a laser power of 1.8 W. A laser power of 1.6 W leads to a wide variation of results (20%-100% of readability). This clarifies that increasing the amount of modules in the code tends to decrease the readability of the code. Moreover, there is a noticeable decrease in code readability if the patterns have smaller sizes.

Table 5.2.4. Effects of DM size, power and edge length on readability after 9 days

Power (W)	Data matrix size (modules x modules)				Color	Readability
	10 x 10	12 x 12	14 x 14	16 x 16		
2.2	s1= 0.281 J	s1= 0.209 J	s1= 0.160 J	s1= 0.122 J		0%
2.0	s1= 0.256 J	s1= 0.190 J	s1= 0.145 J	s1= 0.111 J		20%
1.8	s1= 0.230 J	s1= 0.171 J	s1= 0.131 J	s1= 0.099 J		40%
1.6	s1= 0.205 J	s1= 0.152 J	s1= 0.116 J	s1= 0.088 J		60%
2.2	s2= 0.206 J	s2= 0.153 J	s2= 0.117 J	s2= 0.089 J		80%
2.0	s2= 0.187 J	s2= 0.139 J	s2= 0.106 J	s2= 0.081 J		80%
1.8	s2= 0.168 J	s2= 0.125 J	s2= 0.096 J	s2= 0.073 J		80%
1.6	s2= 0.149 J	s2= 0.111 J	s2= 0.085 J	s2= 0.065 J		100%
2.2	s3= 0.162 J	s3= 0.105 J	s3= 0.081 J	s3= 0.062 J		
2.0	s3= 0.147 J	s3= 0.096 J	s3= 0.074 J	s3= 0.057 J		
1.8	s3= 0.132 J	s3= 0.086 J	s3= 0.066 J	s3= 0.051 J		
1.6	s3= 0.118 J	s3= 0.077 J	s3= 0.059 J	s3= 0.045 J		
2.2	s4= 0.104 J	s4= 0.068 J	s4= 0.051 J	s4= 0.040 J		
2.0	s4= 0.095 J	s4= 0.062 J	s4= 0.046 J	s4= 0.036 J		
1.8	s4= 0.085 J	s4= 0.055 J	s4= 0.042 J	s4= 0.033 J		
1.6	s4= 0.076 J	s4= 0.049 J	s4= 0.037 J	s4= 0.029 J		

Edge length (s): s1= 12 mm; s2= 10 mm; s3= 8 mm; s4= 6 mm; N = 5

Fig. 5.31 shows the graphical output of the sigmoid regression analysis of different module sizes. The figure shows the sigmoid regression of readability (%) as a function of module size (mm²) with the correlation value of 0.96. The sigmoid regression equation is:

$$Y = \frac{99.35}{1 + e^{-\left(\frac{x-0.149}{0.19}\right)}} \quad (5.2.1)$$

This information is necessary for re-identification when considering the minimum size of the module. The probability of readability of bananas' codes is about 48.5% with small modules (0.14 mm²), while bigger modules (1.44 mm²) show 99.2% readability. Hence, good readability (82.4%) is achieved with data matrix codes with module sizes of more than 0.45 mm², while all codes smaller than 0.36 mm² are decoded less than 75% of the time.

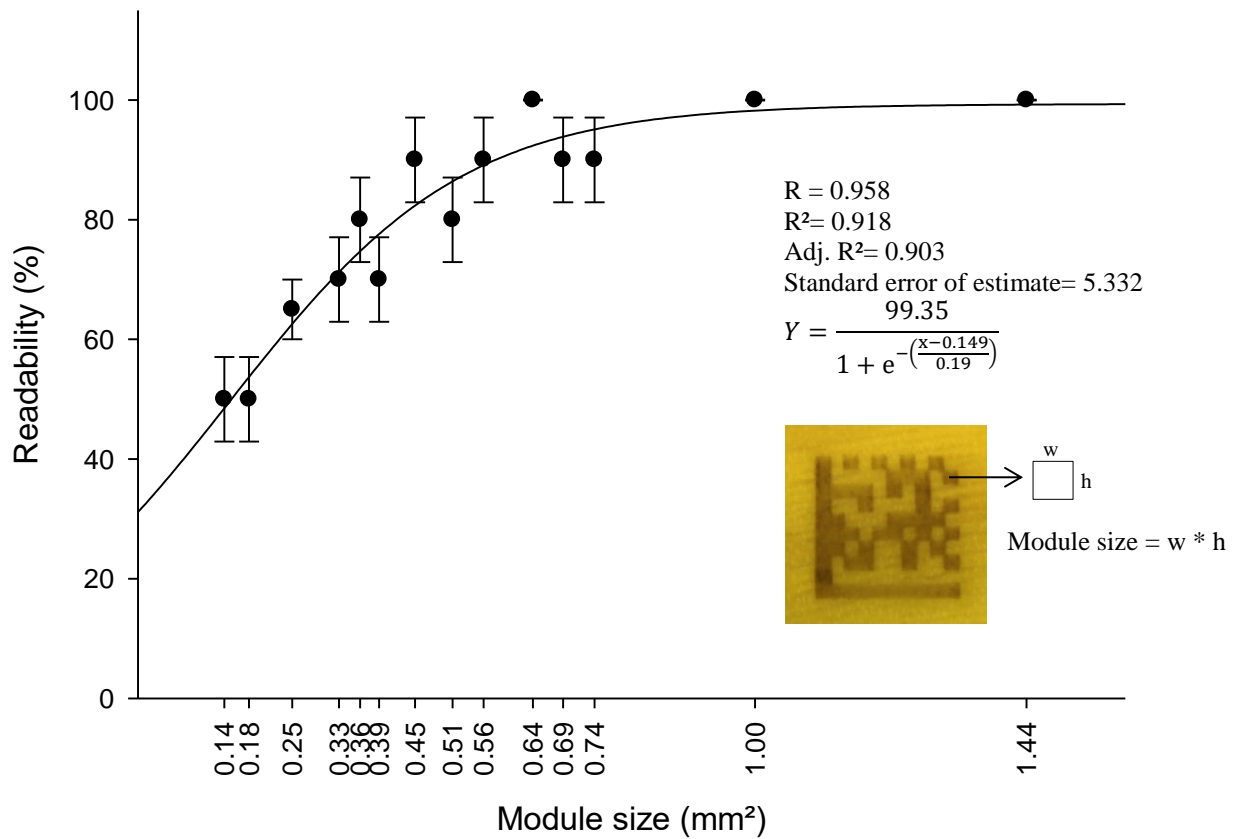


Fig. 5.31. Probability of readability of the laser marked codes on bananas based on the module size. The graph represents mean \pm standard errors, and uses a sigmoidal regression equation

The image processing algorithm provides the ability to classify the contours of the code into foreground and background modules. Figure 5.32 visualizes the binary modules detected by the algorithms. These modules are the final binary *codewords* which are placed in the matrix as symbolic characters, according to the algorithm described in Annex F of ISO/IEC 16022 standards. Figure 5.33 shows the changes in the modules detected by image processing algorithms during the storage time. The figure shows an example of module damage detected on a DM size (16x16 modules) in which the 17-character text string “59833432325675800” is encoded in the code. At the beginning of the storage, the modules can be clearly detected with enough contrast; the code is also readable. However, after a week of storage the code becomes unreadable as the damage to the modules increases.

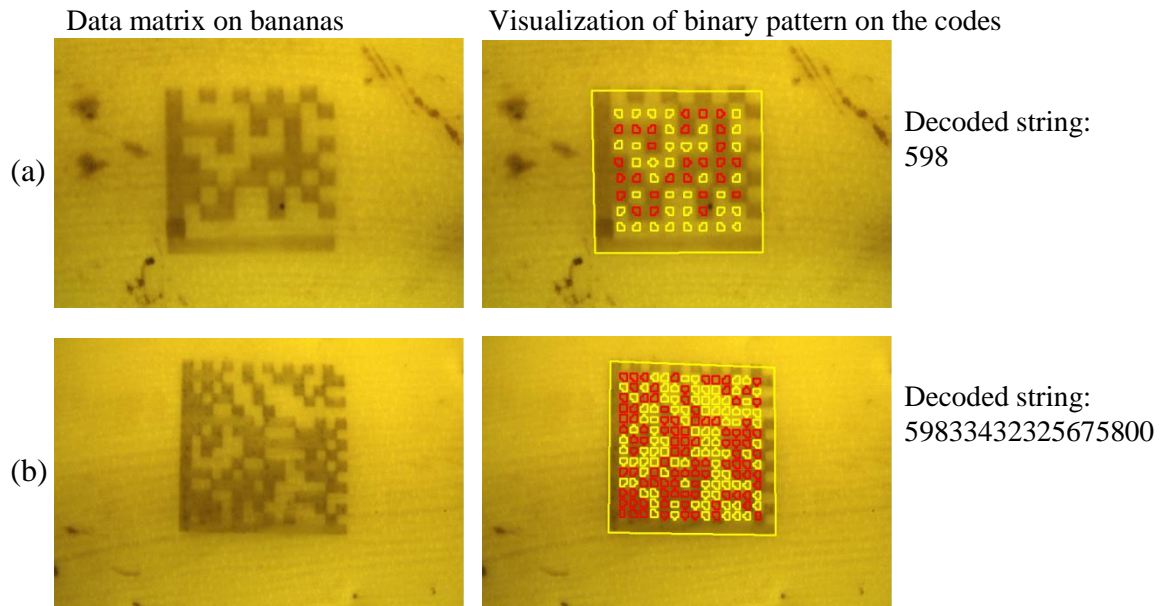


Fig. 5.32. Examples of successful encoding of data matrix code on banana after laser marking with a laser power of 1.8 W. (a) Data matrix size 10x10; (b) Data matrix size 16x16 modules. Red and yellow represent binary 1 and binary 0, respectively.

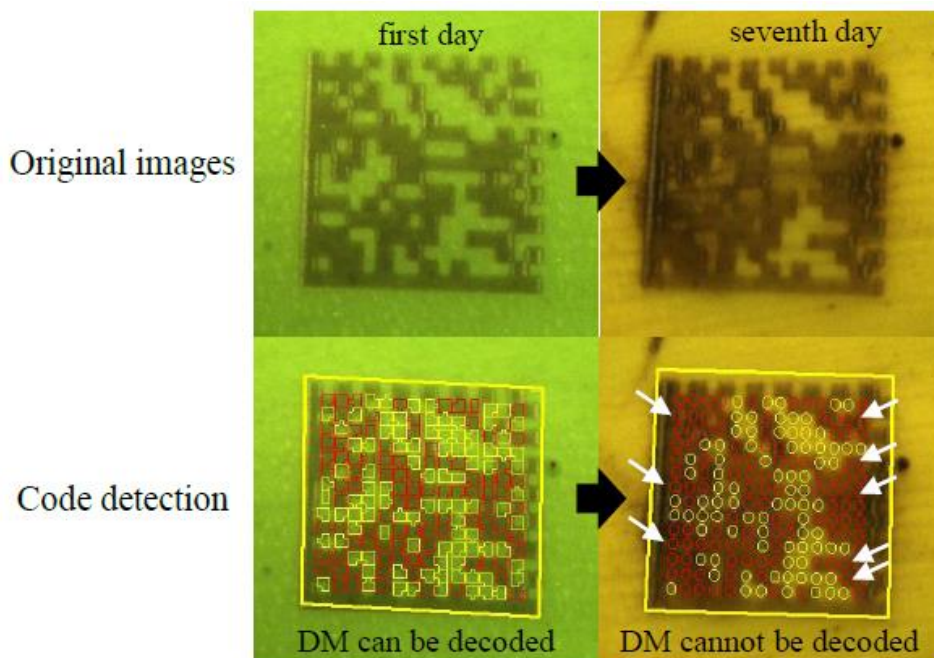


Fig. 5.33. Module damage detection on bananas over the storage time with a laser power of 2 W (white arrows represent error detection of modules)

6. DISCUSSION

6.1. Discussion of the results relating to the positioning problems

6.1.1 Procedures for poinsettia

6.1.1.1. Color segmentation based depth image

The segmentation algorithms were used on color and depth images obtained from the Kinect sensor. The color segmentation algorithm based on depth image achieved satisfactory results (see Table 5.1.2). Some studies have proposed the use of depth imaging techniques for phenotyping plants. Chéné, et al. (2012) presented that depth imaging from Kinect V1 could identify rosebush leaves with an accuracy of 68%. These algorithms detect an object to be segmented when a stable number of connected components are reached. Azzari, et al. (2013) studied depth images with the manual measurements of plant structure and size of two plants growing in grassland. The results show that the depth images agreed well with the manual horizontal and vertical measurements of plant size. Moreover, Wang and Li (2014) estimated onion diameter from depth images with a greater average accuracy and robustness (root mean square error = 2 mm) than color images (root mean square error = 3.4 mm). Additionally, the predicted volume of onions had an accuracy of 96.3%. Our experimental results proposed leaf segmentation that accurately extracted leaves based on depth image (97.5%), allowing us to suggest this approach as a feasible solution. In addition, the low cost makes this camera a promising tool for phenotyping specific plants in a greenhouse.

6.1.1.2. Depth image segmentation based on a distance transform-watershed method

The segmentation of poinsettia leaves is complex since more than two-thirds of the surface underneath the leaf is invisible as well as due to occlusion. Furthermore, sometimes only part of a leaf is detected (false negative) due to the difficulty in measuring accurate depth information of leaves in an irregular image gradient (i.e. leaf angle distribution). Changes in intensity value on the leaf surface produce an interrupted depth that consequences in over-segmentation of leaves (Xia, et al., 2015). In this situation, the leaf is detected as several small pieces of partial leaves. It is also challenging to model leaf shapes using geometric or statistical models, particularly parametric models and active shape models (Manh, et al. 2001; Xia, et al. 2013). Additionally, measurement of small objects might not be recognized by the Kinect V1, due to the physical limitations and resolution of the camera.

The exactness of depth measurement can be enhanced by using the Kinect V2. In this study, the Kinect V2 showed high accuracy (92.5%). Xia, et al. (2015) presented 3D segmentation of individual plant leaves from occlusions in complicated natural scenes using Kinect V1; the segmentation rate for overlapping leaves was 86.67%. In their study, mean shift clustering was applied to extract plant leaves in depth images. Compared with Kinect V1, the Kinect V2 has improved hardware, according to coefficients published on the official website. Andujar, et al. (2016) investigated using depth cameras (Kinect V2) for estimating weed volume estimation. Maize plants were identified with a correlation of 77% with maize biomass. According to Yang, et al. (2015), the Kinect V2 has good accuracy (less than 2 mm) if the object is positioned perpendicularly towards Kinect within 0.5-3 m. Therefore, this method could be effective for separating heavy overlapping plant leaves showing significant differences in depth. The Kinect V2 shows acceptable performance with a great potential for application in many fields in agriculture. Leaf segmentation was tested on poinsettia plants and could also be applied to other plant species. More experiments should be carried out in order to improve the efficiency of segmentation.

6.1.1.3. Main leaf skeleton

Segmentation using the main leaf skeleton has the potential for development. The detection of a single main leaf skeleton yielded high results (80%). This result is due to the fact that the main skeleton is approximately linear. Another reason is that the light intensity of the pixels in the main skeleton is greater than in other leaf pixels. False positives occurred when the light intensity of the pixels in the branch skeleton was higher than in the main skeleton, due to the fact that the leaves' surfaces were not smooth. A true negative was detected when three characteristics (i.e. linear main skeleton, high main skeleton intensity and smooth leaves) were not fulfilled. In these cases, the edges of the leaves were selected. A false negative occurred in cases of image degradation, where the main skeleton image became discontinuous.

The images seemed to show differences in illuminance due to their variable orientations. Some of the main skeletons were not clear, and therefore the leaves could not be recognized. Different luminance affects the light intensity of the pixels on the main skeleton. However, the system was still able to correctly identify individual leaves. For further study, we assume that poinsettia images will become clearer and

that this system will be able to recognize more main leaf skeletons after the improvement of the image-capturing techniques.

The performances of the proposed algorithms are compared to six existing references (Du, et al. 2013; Kirka, et al. 2009; Teng, et al. 2011; Wang, et al. 2013; and Zhang, et al. 2016) as shown in Table 6.2.1. Du, et al. (2013) proposed algorithms for a single leaf with no occlusion. The algorithms described a method of determining the characteristics of plant leaves according to the main fractal dimensions and venation of fractal dimensions. The experimental results showed that the effectiveness of the fractal dimension feature method reached 87.14%. Kirka, et al. (2009) labels pixels as soil or vegetation based on a combination of the greenness and intensity. However, the leaves are considered only one target and are not separated by a segmentation system. Teng, et al. (2011) studied 3D reconstructions of leaves in order to segment leaves. In this study, a camera was moved a slightly to take 3D images of each leaf. However, occluded leaves are difficult to separate. Wang, et al. (2013) described leaf segmentation of a leaf with a complex background. They use the Otsu and Canny operators to segment the target leaf. However, this method can only analyze one leaf image. Zhang, et al. (2016) developed a segmentation algorithm based on similar tangential directions, relative moments, and number of pixels as directions to calculate the leaf distribution. The rate of successful extraction from horticultural crop images reached 76.92%.

Table 6.2.1. Comparison between our study and existing references

References	Methods	Occluded leaves	Leaf number	Individual leaf identification
Du, et al. 2013	Fractal dimension feature	no	1	yes
Kirka, et al. (2009)	Gap fraction model	yes	Numerous	no
Teng, et al. (2011)	Three-dimensional	no	Several	yes
Wang, et al. (2013)	Otsu-Canny	no	1	yes
Zhang, et al. (2016)	Skeleton	yes	Numerous	yes
Our study	Skeleton	yes	Numerous	yes

The detection of poinsettia leaves is challenging due to leaves' different orientations, partial occlusion, and the presence of other leaves with similar colors. However, the algorithm detects skeletons according to the skeletons' characteristics. Therefore, if touching boundaries do not possess skeleton-like characteristics, this algorithm can eradicate the interference caused by occluding leaves. This system is able to identify leaves with a similar color, a similar depth, and complex overlapping leaves.

Furthermore, the proposed algorithms always chooses the longest main leaf skeleton, meaning that errors due to the tilt angle of the leaves can be reduced. At a higher tilt angle, defined as the angle between the normal vector and the vertical axis, the plant's 2D surface is represented by fewer pixels and thus measurement of area becomes less reliable (Apelt, et al. 2015). Chen, et al. (2009) stated that it is possible to mark an egg shell using a two dimensional CO₂ laser. They investigated the correlation between the focus and the drilled holes on the eggshell's surface. CO₂ laser beam is delivered by varying the f-theta focusing lens relative to the curved surface. This is achieved by using a different number of laser pulses to mark different regions of the surface. However, they establish only labels on the parts of eggshells with minor surface curvature. If all leaves are tilted and have complex freeform surfaces, a three dimensional laser marking system should be performed (Wang, et al. 2017b). Three dimensional laser marking system provides synchronized movement of the laser beam to focus in three mutually perpendicular axes. Shape, orientation and position of the processed surface need to be identified in advance in 3D laser marking systems in order to handle curved, tilted and even freeform surfaces (Diaci, et al. 2011).

6.1.2. Procedures for bananas

6.1.2.1. Evaluation for banana fingers

The a* channel represents a green-red axis that maximizes the separation between the fruit and background colors. Studies have used L*a*b* color space to separate the object from its background when testing horticultural products. L*a*b* is found to be the best color space for plant and soil segmentation of lettuce (García-Mateos, et al. (2015). Similar results are supported by other researchers (Shih and Liu, 2005; Hernandez-Hernandez, et al. 2016). Locating the rectangle in the central section of a banana is due to its larger diameter. Although different shapes of banana will influence the selection of a midpoint, the technique is overall successful in placing

a code (label) in the center of a banana (see Fig. 5.1.1). The advantage of this method is that it can adapt to different orientations of bananas (Fig. 5.1.2). This technique can also be adapted to other fruits and vegetables (Fig. 5.1.3).

6.1.2.2. Evaluation of banana hands

The results show that a small number of the banana hands cannot be labeled properly (7.14%, see Table. 5.1.1). There are some factors that affected the performance of the algorithms:

Firstly, the algorithms place the code falsely in between banana fingers due to the algorithm's failure to separate each finger. Two or more fingers are sometimes detected as one finger due to variable lighting. The changing of illumination due to the wetness of banana hands added substantial difficulty to the image segmentation process. Wetting a surface leads to a variety of changes in color and in luminance distribution, and saturation is generally lower for dry surfaces than for wet ones (Sawayama, et al. 2017). Moreover, due to their biological nature, horticultural products have high variability in sizes, forms, textures and colors (Blasco, et al. 2007; Du and Sun, 2004), which makes it challenging to establish a universal system of illumination that will be effective for all products (e.g. banana hands) and all kinds of situations. Such problems arise in horticultural products that are more or less spherical in shape, which results in a darkening of the edges of the object, while the central part looks brighter. This makes them more difficult to analyse (Unay and Gosselin, 2007; Aleixos, et al. 2002). Although regular color camera is capable of assessing banana hands' parameters with high speed, the use of the color camera fails to exploit the full shape of fruits due to lighting conditions (Zhou, et al. 2012). This was also confirmed by Polder, et al. (2002) who classified tomatoes according to five ripeness stages by using an RGB camera, in which 51% of the pixels were misclassified.

Secondly, occlusion between upper-row fingers and bottom-row fingers may cause errors in the selection of the midpoints. Overlapping banana fingers possess similar colors and luminance, and the overlapping boundaries are usually unclear. If each finger can be separated during segmentation, the algorithms can eliminate the interference due to overlapping. Hatou, et al. (1998) studied a segmentation technique for overlapping fruits using a thinning algorithm. However, the algorithm only applied to overlapping circle-shaped fruits. Song, et al. (2012) suggested a recognition and

positioning method for occluded apples based on a convex hull method. The convex hull of an object boundary was used to extract the smooth and real contours, as well as the center and radiuses of the extracted contours. The experimental results showed that the average positioning error of the method was 4.28%.

Fruits or vegetables, which are sold loose or in multiples of the same type, must be labelled individually with the Fairtrade certification. According to Fairtrade certification mark guidelines (2011), bananas need to carry at least one adhesive label applied to banana hands. In this study, the algorithms were able to mark one or more label on banana hands and demonstrate the effectiveness of the proposed algorithm. Additionally, marking on the ventral side of banana hands, which has a high accuracy, is recommended over marking on the dorsal side.

6.2. Discussion of the results relating to the optimization of laser parameters

6.2.1. Application for poinsettia

6.2.1.1. Laser-poinsettia leaves interactions

During the marking process, the temperature rise on the mark area and the quality of the mark are influenced by thermal conductivity. This can damage the surrounding leaf area, producing a heat affected zone (HAZ). Therefore, it is very important to minimize the size of the HAZ by selecting the optimal laser parameters. In the experiment performed, low output power and low energy proved to be an optimal treatment. The red bracts of poinsettia are susceptible to bract brushing and abrasion; however, changes of the mark into a yellowish-white color don't cause mechanical injury, which can lead to leaf distortion. Otherwise, this leaf distortion could expand, as a result of fungus infection, to damage the entire bract.

High contrast laser marking between undisturbed leaf tissue (red bracts) and the affected tissue could occur due to the laser energy being absorbed by bracts' latex. Latex is a regularly milky plant exudate which is found in cells called laticifers. Latex contains a great variety of defense chemicals and also defense proteins in high concentrations (Konno, 2011). Coagulation of latex is able to seal wounds, preventing infections and further fluid loss (Dussourd and Elsner, 1987; Dussourd, 1995). According to Fineran (1982), the laticifers of poinsettia leaf are present in the spongy mesophyll and between the spongy and palisade layers. From this study, it can be speculated that leaf tissue is discolored when exposed to focused laser energy through thermal disruption of the mesophilic layer. Generally, the laticifers function as as depositories for the intracellular excretion of terpenoids, resins, tannins, alkaloids and others (Esau, 1967). Laser energy could be also absorbed by resins. Resin is also a sap exuded from injury. In some species it is a white color similar to latex, but in other species it is transparent. Resin is kept in canalicular inter-cellular spaces called resin ducts and is not kept inside cells (Konno, 2011). According to Kinoyari, et al. (1991), Sakai, et al. (1994) and Hieltjes, et al. (2002), the use of resin composition for laser marking allows for the achievement of highly visible white marking and easily adjustable transparency of the marked product. These reasons will be interesting background for further study.

6.2.1.2. Technical aspects

WinMark pro software (Synrad Inc., USA) enables selection of the resolution and the type of raster scan. These treatments together with velocity and laser power are the primary factors that determine the speed and quality of the mark (Synrad, 2006). Choosing the right raster scan direction is necessary in determining the smaller number of scanning lines. Thus the cycle time can be reduced and the laser energy can be effectively used. A higher resolution represents a higher number of dots per square inch. Increasing the resolution increases the quality of the text. On the other hand, this will require a longer contact time and more energy, resulting in a greater engraving effect. When using high resolution, a lower laser power should be applied in order to avoid damage to the leaf.

6.2.2. Application for bananas

6.2.2.1. Spectral reflectance of marked bananas

The reflectance spectra in the near-infrared waveband between unmarked and marked bananas are almost identical, except when using a laser power of 2 W. However, the infrared reflections of the 2 W marks are low and the differences between marked and unmarked areas are insignificant. Considering these results, it would be not appropriate to use near-infrared detection systems to assess DM codes on marked bananas. Nonetheless, it indicates very clearly that CCD cameras are recommended for use in the visible waveband to assess laser markings on bananas. Moreover, the difference in reflection between marked and unmarked bananas in the visible waveband is noticeable. Especially at higher laser powers, the banana skin develops more contrast and becomes browner. Based on the results, the reflectance values of marked bananas are lower than those of unmarked bananas (see Fig. 5.2.1). These results are in line with Ariana, et al. (2006) and Lu, (2003). Ariana, et al. (2006) stated that reflectance of bruised tissue of cucumber fruit is generally lower than normal tissue. According to Lu (2003), bruised tissue on Red Delicious apples also had a lower reflectance than normal tissue.

In term of mechanical injury, particularly bruises, Ariana, et al. (2006) stated that within two hours after bruising, bruises on a cucumber became darker than normal tissue in an image. The spectral differences between the bruised and normal tissue declined over time. The bruised areas were no longer visible on the image after six days. According to Miller (1992), this characteristic might be affected by the wound healing of the cucumbers in response to mechanical stress. However, in terms of laser

marking, minimal changes or damage during storage was observed when a low laser energy was used. The surface appearance of apples was unchanged at seven days after treatment at a lower laser power (Marx, et al. 2013). Based on Etxeberria, et al. (2009), fruits to which an individual pinhole was applied after laser marking retained their morphological structure during storage. However, sub-epidermal cells became darker due to metabolic activity and development of protective deposits. A similar effect was also observed on stored tomato and avocado, where a typical protective layer was deposited below the pinhole (Etxeberria, et al., 2006).

6.3.2.2. Quality of the codes

Marking at low laser power for a short time tends to yield relatively low readability due to a low contrast. However, applying low laser power for a longer time yields better readability. This behavior was also described by Sood, et al. (2008), namely that higher exposure time at a low laser energy level ($0.000752 \text{ W dot}^{-1}$) produces darker labels without significantly increasing peel disruption on tangerines. By contrast, using high laser power and a longer time may potentially harm bananas' outer cell layers and lead to unsuccessful readability of the codes. Once the laser beam has irradiated the outer cells, photons penetrate into the epidermis layer and convert into thermal energy. Thus, the heat is distributed within the epidermis cells. According to Blanaru, et al. (2003), the heat distribution is influenced by thermal properties, conductivity, heat capacity, convective coefficients, and emissivity of the plant material.

Laser power and marking time are positively correlated with contrast values. Consequently, an optimal combination of laser power and marking time leads to higher contrast values. The more laser energy absorbed by the banana the higher the contrast values. The portion of the energy absorbed deforms the banana peel sufficiently to produce a noticeable mark. Jones, et al. (2001) reported that various contrast levels in leaf surface labelling may be adjusted to the level at which the mesophilic layer is sufficiently etched under the epidermal layer by the laser.

Axial non-uniformity (ANU) and grid non-uniformity (GNU) values achieved a high grade, based on ISO/IEC 15415: 2011. The high quality grades of both ANU and GNU are due to the very well designed technical setup (see Fig. 4.2.1 and Fig. 4.2.2). This is in accordance with well-known quality criteria of GS1 (2018): (1) the decoder or camera axis should be perpendicular to the object surface; (2) there should be no

vibration, acceleration or deceleration during marking; (3) there should be no variable distances between the marking head and material surface; and (4) there should be no difference in the transport speed while marking the DM element. Unused error correction (UEC) values are influenced by small local deformations on marked areas over time. According to Fig. 5.29, a laser power of 1.8 W and 1.6 W with a marking time of 0.072 s per module shows the best result for laser marking bananas. These parameter values are recommended for commercial use.

The presence of darker color areas in the DM modules and distortions in the finder pattern of the codes (see Fig. 5.30) indicate damage to the banana peel. The damage could be explained by a physiological mechanism due to wound reactions like natural healing, browning or the repair response of outer epidermis cells over time. Laser marking on the banana led to the breaking of epidermis cells and consequently the darkening of areas around the affected location. Marx, et al. (2013) stated that tissue damage after laser marking can be explained by three different phenomena: (1) browning happens due to oxidation processes in the marked area; (2) color changes are caused by local tissues' water being completely vaporized at a high laser intensity; and (3) tissue of a marked area becomes burnt, which leads to deep engraving. Etxeberria, et al. (2006) reported that a light brownish color of the laser-marked area is likely because of the natural color of dry cellulose, resulting from loss of water in the etched area. The process of natural healing occurred in pinhole depressions by accumulating cutin and wax deposits in and around the depression after the laser marking of tomatoes and avocados. Buron-Moles, et al. (2014) explained that the increased abundance of proteins after wounding of "Golden Delicious" apples is due to "response to stress."

6.3.2.3. Readability of the codes

Most of the codes generated with high laser power may damage outer cell layers of the bananas and lead to unsuccessful readability of the codes. However, labeling at a low laser power (1.6 W) tends to produce relatively low readability due to decreased contrast (Table 5.2.4). The results show that a laser power of 1.8 W is suitable for labeling of bananas after 9 days of storage (80-100% of readability). Laser labeling on bananas leads to insignificant cell damage in the epidermis area. According to Drouillard and Kanner (1999), the depth of the mark should not exceed

the thickness of one skin cell, in order to prevent thermal degradation and the breakdown of underlying tissue.

The exact size of the DM code depends on the exact encoded data. Numbers or characters are encoded in terms of bits, represented by dark or light modules of an identical size. The larger the amount of bits required, the larger the DM code will be, but the density of modules in the code will increase. The readability of the code is indirectly affected by the DM code size, because an increasing amount of encoded data raises the density of modules in the code. For this reason the modules become smaller. Therefore, small module size stimulates damage on a banana during storage, since damage already arises on the cuticular barrier from the beginning of storage after applying high laser power. Consequently, the decision whether a region belongs to the foreground (object) or the background is not reliable (see Fig. 5.2.33). Tarjan, et al. (2014) stated that the readability of a QR code is influenced by the size of the modules. In this case, a small module size increases the possibility of detecting modules incorrectly. Normally, this indicates that the code has a low unused error correction grade (UEC less than 0.62).

Laser marking of bananas allows up to 24 numerical characters to be encoded into a symbol with dimensions of 6 x 6 mm². This gives an indication of the very compact nature of the DM codes, which makes them suitable for small part marking. Regarding the DM size, a greater data capacity can be implemented in a smaller pattern size. However, in several cases a preliminary test should be applied in order to define the minimum requirements for the readability of the code.

6.3. Possible application relating to the results

6.3.1. Application for poinsettia and bananas

The methods discussed here could be utilized for quality control via a computer vision inspection of the horticultural products prior to and after laser marking, in order to increase cost effectiveness and efficiency in manufacturing processes. For example, the pre-laser operations could aid in automatically transfer the plants onto a conveyor, by accurately determine the position and orientation of the object to be marked by the laser and optimizing placement of the codes, characters, or design onto the products (Fig. 6.3.1). The post-laser marking operations could evaluate the marking quality of the codes, characters, or figures to produce an optimal marked result. The code qualities are visually evaluated according to ISO/IEC 15415:2011

standards. The characters' qualities could be evaluated by using optical character recognition (OCR) quality testing based on ISO/IEC 30116:2016 standards. Another possibility is that the development of image processing could be used to automatically assess damage to laser marking products. Furthermore, integrated laser systems and vision machines (called laser eye's systems) for marking horticultural products have potential for development. Until now these applications have been largely unavailable.



Fig. 6.3.1. (a) The character mark is placed on the upper and bottom part of the main skeleton of a poinsettia leaf; (b) Positioning of 2D barcodes on banana hands

Developed algorithms that use an RGB-D camera could also be utilized for plant phenotyping in the greenhouse. The algorithms could be used to monitor the growing condition of the plants as well as the shape and architecture of the plants. The plant architecture provides information necessary to understand physiological processes governing plant functioning.

Furthermore, since it is possible to apply laser marking to poinsettia leaves without harm or stress to the product's surface, laser marking on horticultural leaves could be developed as antimicrobial treatments. This potential as an antimicrobial treatment needs more studies for further information. For bananas, the application of laser marking 2D codes on bananas could be a great space-saver for companies trying to incorporate a lot of data in their barcodes with limited room for labels.

6.3.2. Application for other products (for example: petunia stems)

The laser eye's system could also be developed for other products, such as: apples, eggplant, mangos, coconut, oranges, tangerines, grapefruits, apples, pears,

plums, nectarines, pears, kiwi, avocados, potatoes, peppers, cucumbers, tomatoes, and so on. It is also possible to mark 2D codes on ornamental stems, such as petunia stems. The maximum 2D code dimension that could be positioned on petunia stems is 3 x 3 mm² (Fig. 6.3.2). A smaller code size could be used as well; however, preliminary tests should be applied to determine the minimum requirements of the readability of the code. In the preliminary research, petunia stems were marked with different laser parameters (data not shown). The surface curvature and roughness as well as color changes of the upper layer of epidermis affect both the readability of the code marking pattern and contrast value.



Fig. 6.3.2. Laser marking on petunia stem (2D code dimension is 3 x 3 mm²)

6.4 Future work

The findings of this thesis have presented some potential topics for further research:

- a. Further study is suggested to use a three-dimensional (3D) camera for positioning the code on banana hands.
- b. In practical approaches, the RGB-D method and the main skeleton method could be combined to create optimum results for complex overlapping plant leaves.
- c. Some parameters, such as variety, product color, moisture content, maturity, surface curvature, and roughness could be incorporated in order to acquire more predictable results of optimal laser marking to achieve a desired effect on a particular product's characteristics.

7. CONCLUSIONS

7.1. Optimization of laser positioning for poinsettia leaves

An image processing system for marking plant leaves has been presented. The distance transform-watershed segmentation and the main leaf skeleton segmentation have been adopted to extract poinsettia leaves' images and to find the optimal laser position. The distance transform-watershed segmentation using Kinect V2 achieves a satisfactory result of 92.5%. This method has shown reliability when operated with overlapping leaves. The distance transform-watershed segmentation effectively segments overlapped plant leaves that show significant differences in depth. Compared to the main leaf skeleton segmentation, different luminance and orientations may affect the light intensity of the pixels on the skeleton; however, the method is still able to correctly identify the individual leaf. The detection of the main leaf skeleton (true positive) yields a high result (80%).

7.2. Optimization of laser positioning for bananas

The proposed algorithms are successful in placing 2D code in the center of fruit images, which are selected for optimal laser marking positioning. Additionally, the algorithms are effective when applied to differently shaped fruits. Positioning the 2D codes on the ventral banana side is recommended for some factors, such as variable lighting conditions and the overlapping of banana fingers can affect the ability to correctly detect codes. However, the proposed method, which marks at least one 2D code on a banana hand, obtains very satisfactory results (92.86%).

7.3. Optimization of laser parameters for marking poinsettia leaves

Laser marking can be applied to poinsettia leaves without damaging the product's surface. Laser marking of 0.5 W [0.55 J per character] shows the lowest energy use that produces a high contrast with no apparent heat affected zone detected. Some parameters such as laser power and laser marking resolution are essential factors in increasing the quality of the text, contact time, and laser energy. Laser marking poinsettia leaves changes the leaves to dark red at the beginning of storage, becoming yellowish-white in color until 14 days of storage. The color changes are an additional benefit that increases contrast between leaf color and texts.

7.4. Optimization of laser parameter for marking bananas

Laser marking of 2D codes can be implemented on bananas. The laser power and the marking time are suggested as useful parameters to ensure the best readability of DM codes on bananas. It is recommended to use a low laser power (i.e. 1.8 W and 1.6 W) and a longer marking time (i.e. 0.072 s per module) for optimal marking, because the obtained readability of the DM codes on bananas after nine days of storage is high (80%-100%) and reaches a high grade of unused error correction. The readability of DM codes on bananas depends on the laser power, the DM size and the edge length. Applying the low laser power obtains a high readability, which allows up to 24 alphanumeric characters to be encoded into a 2D code with dimensions of 6 x 6 mm².

REFERENCES

- Aksoy, E., Abramov, A., Wörgötter, F., Scharr, H., Fischbach, A. and Dellen, B. (2015). Modeling leaf growth of rosette plants using infrared stereo image sequences. *Computers and Electronics in Agriculture*, 110, 78-90.
- Alec Chang, C., Lo, C. and Hsieh, K. (1997). Neural networks and Fourier descriptors for part positioning using bar code features in material handling systems. *Computers and Industrial Engineering*, 32, 467-476.
- Aleixos, N., Blasco, J., Navarron, F. and Molto, E. (2002). Multispectral inspection of citrus in real-time using machine vision and digital signal processors. *Computers and Electronics in Agriculture*, 33, 121-137.
- Allotta, B., Giorgetti, F., Nincheri, M. and Pugi, L. (2016). *Modelling and control of a galvanometer for the application to a laser engraving system*. Paper presented at the IECON 2016 - 42nd Annual Conference of the IEEE Industrial Electronics Society, 24-27 October, Florence (Italy): Institute of Electrical and Electronics Engineers (IEEE).
- Amara, E., Haid, F. and Noukaz, A. (2015). Experimental investigations on fiber laser color marking of steels. *Applied Surface Science*, 351, 1-12.
- Amin, A. and Khan, A. (2013). One-shot classification of 2-D leaf shapes using distributed hierarchical graph neuron (DHGN) scheme with k-NN classifier. *Procedia Computer Science*, 24, 84-96.
- Andujar, D., Ribeiro, A., Fernandez-Quintanilla, C. and Dorado, J. (2016). Using depth cameras to extract structural parameters to assess the growth state and yield of cauliflower crops. *Computers and Electronics in Agriculture*, 122, 67-73.
- Andujar, D., Dorado, J., Fernandez-Quintanilla, C. and Riberio, A. (2016). An approach to the use of depth cameras for weed volume estimation. *Sensors*, 16, 1-11.
- Apelt, F., Breuer, D., Nikoloski, Z., Stitt, M. and Kragler, F. (2015). Phytotyping^{4D}: a light-filed imaging system for non-invasive and accurate monitoring of spatio-temporal plant growth. *The Plant Journal*, 82, 693-706.
- Arefi, A., Motlagh, A., Mollazade, K. and Teimourlou, R. (2011). Recognition and localization of ripen tomato based on machine vision. *Australian Journal of Crop Science*, 5, 1144-1149.
- Ariana, D., Lu, R. and Guyer, D. (2006). Near-infrared hyperspectral reflectance imaging for detection of bruises on pickling cucumbers. *Computers and Electronics in Agriculture*, 53, 60-70.
- Armenta, S. and de la Guardia, M. (2016). Analytical Approaches for the Evaluation of Food Protected Designation of Origin. *Advances in Food Traceability Techniques and Technologies*, 275-301.

- Aung, M. and Chang, Y. (2014). Traceability in food supply chain: safety and quality perspectives. *Food Control*, 172-184.
- Audouard, E., Lopez, J., Ancelot, B., Gaudfrin, K., Kling, R. and Mottay, E. (2017). Optimization of surface engraving quality with ultrafast lasers. *Journal of Laser Applications*, 29, 022210.
- Azzari, G., Goulden, M. and Rusu, R. (2013). Rapid characterization of vegetation structure with a Microsoft kinect sensor. *Sensors*, 13, 2384-2398.
- Ba, F. (1998). Technical study on laser marking of slide calipers. *Proceedings of SPIE*, 3550, 336-341.
- Bain, J. (1957). Morphological, anatomical and physiological changes in the developing fruit of the Valencia orange, *Citrus sinensis* (L.) Osbeck. *Australian Journal of Botany*, 6, 1-24.
- Bansal, R., Lee, W. and Satish, S. (2013). Green citrus detection using fast fourier transform (FFT) leakage. *Precision Agriculture*, 14, 59-70.
- Barcikowski, S., Koch, G. and Odermatt, J. (2006). Characterisation and modification of the heat affected zone during laser material processing of wood and wood composites. *Holz als Roh- und Werkstoff*, 64, 94-103.
- Beck, R., Jaworski, P., Weston, N. and Hand, D. (2016). *Parallel robot platform for freeform laser manufacturing*. Paper presented at the 9th International Conference on Photonic Technologies LANE, 19-22 September, Fürth (Germany): Bayerisches Laserzentrum GmbH.
- Bernhausen, J., Joochim, C. and Roth, H. (2011). Mobile robot self-localization and 3D map building using a 3D PMD-camera for tele-robotic applications. *IFAC Proceedings Volumes*, 44, 6851-6856.
- Bertolini, M., Bevilacqua, M. and Massini, R. (2006). FMECA approach to product traceability in the food industry. *Food Control*, 17, 137-145.
- Blanaru, C., Cernat, R., Chitu L. and Dumitras, D. (2003). Marking of materials by CO₂ laser beam scanning. *Laser Processing of Advanced Materials and Laser Microtechnologies*, 157-163.
- Blasco, J., Aleixos, N. and Molto, E. (2007). Computer vision detection of peel defects in citrus by means of a region oriented segmentation algorithm. *Journal of Food Engineering*, 81, 535-543.
- Borgefors, G. (1984). Distance transformations in arbitrary dimensions. *Computer Vision, Graphics, and Image Processing*, 27, 321-345.
- Brihmat-Hamadi, F., Amara, E., Lavisse, L., Jouvard, J., Cicala, E. and Kellou, H. (2017). Surface laser marking optimization using an experimental design approach. *Applied Physics A*, 123 (4).
- Buchfink, G. (2007). The laser as a tool. Vogel Buchverlag, Würzburg.

- Budzan, S. and Kasprzyk, J. (2016). Fusion of 3D laser scanner and depth images for obstacle recognition in mobile applications. *Optics and Lasers in Engineering*, 77, 230-240.
- Bulanon, D., Burks, T. and Alchanatis, V. (2008). Study on temporal variation in citrus using thermal imaging for citrus fruit detection. *Biosystems Engineering*, 101, 161-171.
- Bulanon, D.M., Burks, T.F. and Alchanatis, V. (2009). Image fusion of visible and thermal images for fruit detection. *Biosystems Engineering*, 103, 12-22.
- Buron-Moles, G., Torres, R., Amoako-Andoh, F., Viñas, I., Teixidó, N., Usall, J., Keulemans, W. and Davey, M. (2014). Analysis of changes in protein abundance after wounding in 'Golden Delicious' apples. *Postharvest Biology and Technology*, 87, 51-60.
- Canessa, A., Chessa, M., Gibaldi, A., Sabatini, S. and Solari, F. (2013). Calibrated depth and color cameras for accurate 3D interaction in a stereoscopic augmented reality environment. *Journal of Visual Communication and Image Representation*, 25, 227-237.
- Canny, J. (1986). A computational approach to edge detection. *IEEE Transactions on Pattern Analysis and Machine Intelligence*, PAMI-8(6), 679-698.
- Carpene, E., Höche, D. and Schaaf, P. (2010). Fundamental of Laser-Material Interactions. *Laser Processing of Materials*, 21-47.
- Cerutti, G., Tougne, L., Vacavant, A. and Coquin, D. (2013). A parametric active polygon for leaf segmentation and shape estimation. *Advance in Visual Computing*, 6938, 202-213.
- Chaki, J., Parekh, R. and Bhattacharya, S. (2015). Plant leaf recognition using texture and shape features with neural classifiers. *Pattern Recognition Letters*, 58, 61-68.
- Chaves, M., Piancastelli, A., de Araujo, A. and Pinotti, M. (2017). Effects of low-power light therapy on wound healing: LASER x LED. *Anais Brasileiros de Dermatologia*, 89, 616-23.
- Chen, M., Chen, Y., Hsiao, W., Wu, S., Hu, C. and Gu, Z. (2008). A scribing laser marking system using DSP controller. *Optics and Lasers in Engineering*, 46, 410-418.
- Chen, M., Hsiao, W., Huang, W., Hu, C. and Chen, Y. (2009). Laser coding on the eggshell using pulsed-laser marking system. *Journal of Materials Processing Technology*, 209, 737-744.
- Chen, C., Marziliano, P. and Kot, A. (2012). 2D finite rate of innovation reconstruction method for step edge and polygon signals in the presence of noise. *IEEE Transactions on Signal Processing*, 60, 2851–2859.

- Chéné, Y., Rousseau, D., Lucidarme, P., Bertheloot, J., Caffier, V., Morel, P., Belin, É. and Chapeau-Blondeau, F. (2012). On the use of depth camera for 3D phenotyping of entire plants. *Computers and Electronics in Agriculture*, 82, 122-127.
- Cherniavsky, O. (1999). Data encoding with Data Matrix. Available at http://www.qualitydigest.com/mar99/html/body_datamat.html [Accessed 2 Dec 2017].
- Chitu, L., Cernat, R., Bucatica, I., Puiu, A. and Dumitras, D. (2003). Improved technologies for marking of different materials. *Laser Physics*, 13, 1108-1111.
- Chopin, J., Laga, H. and Miklavcic, S. (2016). A hybrid approach for improving image segmentation: application to phenotyping of wheat leaves. *Plos One*, 11, 1-18.
- Cselle, M. (2011). *Fundamentals of Light Sources and Lasers*. New York, NY: John Wiley & Sons, 293.
- Chung-Wang, D., Yang, Y., Jian-qiang, Z., Hong-kai, Z. and Fei, L. (2013). Detection of thrips defect on green-peel citrus using hyperspectral imaging technology combining PCA and B-spline lighting correction method. *Journal of Integrative Agriculture*, 1-9.
- Commision Regulation (EU) No 510. (2013). Available at <https://eur-lex.europa.eu/legal-content/EN/TXT/?uri=celex%3A32013R0510> [Accessed 2 Dec 2017].
- Danciu, G., Banu, S. and Caliman, A. (2012). *Shadow removal in depth images morphology-based for Kinect cameras*. Paper presented at the 16th International Conferences on System Theory, Control and Computing (ICSTCC), 12-14 October, Sinaia (Romania): Institute of Electrical and Electronics Engineers (IEEE).
- Danielsson, P. (1980). Euclidean Distance Mapping. *Computer Graphics and Image Processing*, 14, 227-248.
- Danyluk, M., Interiano, L., Friedrich, L., Schneider, K. and Etxeberria, E. (2010). Natural-light labeling of tomatoes does not facilitate growth or penetration of *Salmonella* into the fruit. *Journal of Food Protection*, 73, 2276-2280.
- Danyluk, M., Friedrich, L., Sood, P. and Etxeberria, E. (2013). Growth or penetration of *Salmonella* into citrus fruit is not facilitated by natural-light labels. *Food Control*, 34, 398-403.
- Dawood, M. and Salman, S. (2013). Low level diode laser accelerates wound healing. *Lasers in Medical Science*, 28, 941-945.
- de Mezzo, B., Fiorio, C. and Rabatel, G. (2003). *Weed leaves recognition in complex natural scenes by model-guided edge pairing*. Paper presented at the 4th European Conference on Precision Agriculture, 15-19 June, Berlin (Germany): Wageningen Academic Publishers.

- Deprez, P, Melian, C., Breaban, F. and Coutouly, J. (2012). Glass marking with CO₂ laser: Experimental study of the interaction laser-material. *Journal of Surface Engineered Materials and Advanced Technology*, 2, 32-39.
- Dhankar, P. and Sahu, N. (2013). A review and research of edge detection technique for image segmentation. *International Journal of Computer Science and Mobile Computing*, 2, 86-92.
- Diaci, J., Bracun, D., Gorkic, A. and Mozina, J. (2011). Rapid and flexible laser marking and engraving of tilted and curved surfaces. *Optics and Lasers in Engineering*, 49, 195-199.
- Diaz, G. (2017). Contour recognition of complex leaf shapes. *PLoS ONE*, 12, 189427.
- Dongyun, W. and Xinpiao, Y. (2014). An Embedded Laser Marking Controller Based on ARM and FPGA Processors. *The Scientific World Journal*, 7.
- Drouillard, G. and Rowland, R. (1997). Method of laser marking of produce. U.S. Patent 5,660,747.
- Drouillard G. and Kanner R. (1999). Produce marking system. U.S. Patent 5,897,797.
- Du, C. and Sun, D. (2004). Recent development in the applications of image processing techniques for food quality evaluation. *Trends in Food Science and Technology*, 15, 230-249.
- Dussourd, D. and Eisner, T. (1987). Vein-cutting behavior: insect counter ploy to the latex defense of plants. *Science*, 237, 898-901.
- Dussourd, D. (1995). Entrapment of aphids and whiteflies in lettuce latex. *Annals of the Entomological Society of America*, 88, 163-172.
- Du, J., Wang, X. and Zhang, G. (2007). Leaf shape based plant species recognition. *Applied Mathematics and Computation*, 185, 883-893.
- Du, J., Zhai, C. and Wang, Q. (2013). Recognition of plant leaf image based on fractal dimension features. *Neurocomputing* 116, 150-156.
- Esau, K. (1967). *Plant Anatomy*, Wiley, New York.
- Etxeberria, E., Miller, W. and Achor, D. (2006a). Anatomical and morphological characteristics of laser etching depressions for fruit labeling. *HortTechnology*, 16, 527-532.
- Etxeberria, E., Miller, W. and Achor, D. (2006b). Characteristics of laser etching depressions on Florida fruits and vegetables. *Proceedings of the Florida State Horticultural Society*, 119, 353-357.
- Etxeberria, E., Narciso, C., Sood, P., Gonzalez, P. and Narcis, J. (2009). The anatomy of a laser label. *Proceeding of the Florida State Horticultural Society*, 122, 347-349.

- Etxeberria, E. and Gonzalez, P. (2014). The use of laser light to enhance penetration of antimicrobials into citrus leaves. *Proceeding of the Florida State Horticultural Society*, 127, 75-77.
- Etxeberria, E., Gonzalez, P., Borges, A. and Brodersen, C. (2016). The use of laser light to enhance the uptake of foliar applied substances into citrus (*Citrus sinensis*) leaves. *Applications in Plant Sciences*, 4, 1500106.
- Fawcett, T. (2006). An introduction to ROC analysis. *Pattern Recognition Letters*, 27, 861-874.
- Fairtrade certification mark. (2012). Fairtrade certification mark guide. Fairtrade Labelling Organizations International e.V. Available at https://www.masteroast.co.uk/uploads/3/1/5/5/31550939/producer_impact_may_2012_3.pdf [Accessed 4 July 2017].
- Farkas, J., Hoopman, J. and Kenkel, J. (2013). Five parameters you must understand to master control of your laser/light-based devices. *Aesthetic Surgery Journal*, 33, 1059-1064.
- Farivar, S., Malekshahabi, T. and Shiari, R. (2014). Biological effects of low level laser therapy. *Journal of Lasers in Medical Sciences*, 5, 58-62.
- Fineran, B. (1982). Distribution and organization of non-articulated laticifers in mature tissues of Poinsettia (*Euphorbia pulcherrima* Willd.). *Annals of Botany*, 50, 207-220.
- Freeman, H. and Shapira, R. (1975). Determining the minimum-area enclosing rectangle for an arbitrary closed curve. *Communications of the ACM*, 18, 409-413.
- García-Mateos, G., Hernández-Hernández, J., Escarabajal-Henarejos, D., Jaen-Terrones, S. and Molina-Martínez, J. (2015). Study and comparison of color models for automatic image analysis in irrigation management applications. *Agricultural Water Management*, 151, 158-166.
- Ge, Z., Wu, W., Yu, Y. and Zhang, R. (2013). Design of mechanical arm for laser weeding robot. *Applied Mechanics and Materials*, 347, 834-838.
- Golnabi, H. (1999). Image evaluation for the synchronised laser scanning systems. *Optics and Laser Technology*, 31, 225-232.
- Gonzalez, R. and Woods, R. (2006). Digital Image Processing, 3rd Ed., Prentice-Hall, Inc., Upper Saddle River, NJ, USA.
- Grand-Brochier, M., Vacavant, A., Cerutti, G., Kurtz, C., Weber, J. and Tougne, L. (2015). Tree leaves extraction in natural images: comparative study of preprocessing tools and segmentation methods. *IEEE Transactions on Image Processing*, 24, 1549-1560.

- Griepentrog, H., Norremark, M. and Soriano, J. (2006). *Close-to-crop thermal weed control using a CO₂ laser*. Paper presented at the CIGR World Congress Agricultural Engineering for a Better World, 3-7 September, Bonn (Germany): VDI-Verl.
- GS1. (2018). Overview and technical introduction of the use of GS1 DataMatrix. Available at http://www.gs1.org/docs/barcodes/GS1_DataMatrix_Guideline.pdf [Accessed 20 Mai 2018].
- Guo, J. and Xu, L. (2017). Automatic segmentation for plant leaves via multiview stereo reconstruction. *Mathematical Problems in Engineering*, 2017, 1-11.
- Haferkamp, H., Jaschke, P., Stein, J. and Goede, M. (2002). Decoding of invisible laser markings using infrared technology. *Infrared Physics and Technology*, 43, 171-174.
- Han, A. and Gubencu, D. (2008). Analysis of the laser marking technologies. *Nonconventional Technologies Review*, 4, 17-22.
- Hannan, M., Burks, T. and Bulanon, D. (2010). A machine vision algorithm combining adaptive segmentation and shape analysis for orange fruit detection. *Agricultural Engineering International: The CIGR EJournal*, 1281, 1-17.
- Hatou, K., Takayama, A., Morimoto, T. and Hashimoto, Y. (1998). A segmentation technique fruits using a thinning algorithm. *IFAC Control Applications and Ergonomics in Agriculture*, 31, 81-86.
- Hayakawa, H. (2000). A laser method for marking bar codes on glass substrates. *Proceedings of SPIE*, 4088, 363-366.
- Heck, R., Gutierrez Ibarra, J. and Sheffler, J. (2007). Method and apparatus for non-invasive laser based labeling of plant products. U.S. Patent 0252006.
- Henry, P., Krainin, M., Herbst, E., Ren, X. and Fox, D. (2010). RGB-D mapping: using depth cameras for dense 3D modeling of indoor environments. *Experimental Robotics*, 79, 477-491.
- Hernández-Hernández, J., García-Mateos, G., González-Esquivá, J., Escarabajal-Henarejos, D., Ruiz-Canales, A. and Molina-Martínez, J. (2016). Optimal color space selection method for plant/soil segmentation in agriculture. *Computers and Electronics in Agriculture*, 122, 124-132.
- Hieltjes, W., Breda, Lohmeijer, J., Hoogerheide, Merex, F. and Zoom B. (2002). Composition for laser marking. US Patent 6,482,879 B2.
- Hoult, A. (2017). System and method of laser marking produce. US Patent 0239754 A1.
- Hossen, M., Arefin, M. and Karim, R. (2017). *Developing a framework for fruits detection from images*. Paper presented at the International Conference on Electrical, Computer and Communication Engineering (ECCE), 16-18 February,

- Cox's Bazar (Bangladesh): Institute of Electrical and Electronics Engineers (IEEE).
- Huang, Q., Chen, W., Huang, X. and Zhu, Y. (2018). Data Matrix Code Location Based on Finder Pattern Detection and Bar Code Border Fitting. *Hindawi Publishing Corporation Mathematical Problems in Engineering*, 2012, 1-12.
- Illecas-Montes, R., Melguizo-Rodriguez, L., Manzano-Moreno, F., Garcia-Martines, O., Ruiz, C. and Ramos-Torrecillas, J. (2017). Cultured human fibroblast biostimulation using a 940 nm diode laser. *Materials*, 10, 793.
- Ion, J. (2005). *Laser Processing of Engineering Materials*. Elsevier, Oxford, UK.
- ISO/IEC 16022. (2006). International Organization for Standardization. Information Technology-Automatic Identification and Data Capture Techniques–Data Matrix Bar Code Symbology Specification. Available at <https://www.iso.org/obp/ui/#iso:std:iso-iec:16022:ed-2:v1:en> [Accessed 20 Mai 2018].
- ISO/IEC 15415. (2011). Information technology-Automatic identification and data capture techniques-Bar code symbol print quality test specification-Two-dimensional symbols. Available at <https://www.iso.org/standard/54716.html> [Accessed 12 Mai 2017].
- Jangsombatsiri, W. and Porter, J. (2007). Laser direct-part marking of data matrix symbols on carbon steel substrates, *Journal of Manufacturing Science and Engineering*, 129, 583-591.
- Ji, W., Zhao, D., Cheng, F., Xu, B., Zhang, Y. and Wang, J. (2012). Automatic recognition vision system guided for apple harvesting robot. *Computers and Electrical Engineering*, 38, 1186-1195.
- Jiang, W., Xie, X., Wei, X., Hu, W., Ren, L. and Zou, Z. (2017). High contrast patterning on glass substrates by 1064 nm pulsed laser irradiation. *Optical Materials Express*, 7, 1565.
- Jones, R., Pierson, Vaughn, E., Beach, O., Harrel, R. and Gainesville. (2001). Laser marking of plant material. U.S. Patent 6,172,328 B1.
- Kaminski, D. (2011). How to choose the best laser for your marking application. Available at <https://www.laserfocusworld.com/articles/2011/04/laser-marking-how-to-choose-the-best-laser-for-your-marking-application.html> [Accessed January 2018].
- Kan, H., Jin, L. and Zhou, F. (2017). Classification of medicinal plant leaf image based on multi-feature extraction. *Pattern Recognition and Image Analysis*, 27, 581-587.
- Kapon, B. (2010). *Botany for gardeners* 3rd Edition. Timbers Press, Portland London.
- Kasman, S. (2013). Impact of parameters on the process response: A Taguchi orthogonal analysis for laser engraving. *Measurement*, 46, 2577-2584.

- Kazmi, W., Foix, S., Alenyà, G. and Andersen, H. (2014). Indoor and outdoor depth imaging of leaves with time-of-flight and stereo vision sensors: Analysis and comparison. *ISPRS Journal Photogrammetry and Remote Sensing*, 88, 128-146.
- Kinoyari, T., Hirabayashi, S., Kidokoro, N., Takimoto, F. and Kawanishi. (1991). Laser-marking method and resin composition for laser marking. US Patent 5,063,137.
- Kirka, K., Andersen, H., Thomsen, A., Jorgensen, J. and Jorgensen, R. (2009). Estimation of leaf area index in cereal crops using red-green images. *Biosystems Engineering*, 104, 308-317.
- Konno, K. (2011). Plant latex and other exudates as plant defense systems: Roles of various defense chemicals and proteins contained therein. *Phytochemistry*, 72, 1510-1530.
- Kubovsky, I. and Kacik, F. (2014). Colour and chemical changes of the lime wood surface due to CO₂ laser thermal modification. *Applied Surface Science*, 321, 261-267.
- Lakshmi, B. and Mohan, V. (2017). Plant leaf detection method using a midpoint circle algorithm for shape-based feature extraction. *Journal of Modern applied Statistical Methods*, 16, 461-480.
- Langner, H., Detlef, E., Michael, H. and Andreas, K. (2006). The thermal effect of laser radiation on plants. *Landtechnik*, 5, 252-253.
- Larese, M., Namías, R., Craviotto, R., Arango, M., Gallo, C. and Granitto, P. (2014). Automatic classification of legumes using leaf vein image features. *Pattern Recognition*, 47, 158-168.
- Lazov, L. and Angelov, N. (2012). Influence of some technological parameters on the contrast of laser marking on the fly. *Laser Physics*, 22, 1755–1758.
- Lazov, L. Deneva, H. and Narica P. (2015). Laser marking methods. *Proceeding of the 10th International Scientific and Practical Conference Latvia*, 108-115.
- Lee, W. and Slaughter, D. (2004). Recognition of partially occluded plant leaves using a modified watershed algorithm. *Transaction of ASAE*, 47, 1269-1280.
- Lee, C. and Chen, S. (2006), Classification of leaf images. *International Journal of Imaging Systems and Technology*, 16, 15-23.
- Lehmann, W. (2017). Laser + Camera = Innovation. *Laser Technik Journal*, 14, 46-48.
- Li, J. and Tang, L. (2017). Developing a low-cost 3D plant morphological traits characterization system. *Computers and Electronics in Agriculture*, 143, 1-13.
- Li, C. and Lu, C. (2017). Laser direct-part marking of data matrix barcodes on the surface of metal alloy material. *Key Engineering materials*, 744, 244-248.

- Li, J., Lu, C., Wang, A., Ma, Z., Fang, X. and Tao, L. (2016a). Experimental investigation and mathematical modeling of laser marking two-dimensional barcodes on surfaces of aluminum alloy. *Journal of Manufacturing Processes*, 21, 141-152.
- Li, X., He, W., Wang, J., Guo, G., Zhang, T. and Yue, T. (2016b). Laser direct marking applied to rasterizing miniature data matrix code on aluminum alloy. *Optics and Laser Technology*, 77, 31-39.
- Linker, R., Cohen, O. and Naor, A. (2012). Determination of the number of green apples in RGB images recorded orchards. *Computers and Electronics in Agriculture*, 81, 45-57.
- Longobardi, R. (2007). Process and device for the marking of fruits through laser with, before the marking, a cleaning/drying step and, after the marking, a sealing of the marked area. European Patent EP1747838.
- Lu, R. (2003). Detection of bruises on apples using near infrared hyperspectral imaging. *Transactions of the ASAE*, 46, 523-530.
- Maiman, T. (1960). Stimulated optical radiation in ruby. *Nature*, 187, 493-494.
- Manh, A., Rabatel, G., Assemat, L. and Aldon, M. (2001). Automation and emerging technologies: Weed leaf image segmentation by deformable templates. *Journal of Agricultural Engineering Research*, 80, 139-146.
- Markov, V., Lebedeva, L. and Kanatnikov, N. (2015). Results of research on causes of the defects of laser marking articles. *IOP Conference Series: Materials Science and Engineering*, 91, 012027.
- Marx, C., Peres, P., Cesar, J., Hustedt, M., Barcikowski, S., Haferkamp, H. and Rath, T. (2012). Investigations on the absorption of the application of laser radiation for weed control. *Landtechnik*, 67, 95-101.
- Marx, C., Hustedt, M., Hoja, H., Winkelmann, T. and Rath, T. (2013). Investigations on laser marking of plants and fruits. *Biosystems Engineering*, 116, 436-446.
- Marx, C. (2014). Untersuchungen zum Einsatz von Lasertechnologie in der Pflanzenproduktion. Dissertation, University of Hannover.
- Matsunaga, T., Ogawa, D., Taguchi-Shiobara, F., Ishimoto, M., Matsunaga, S. and Habu, Y. (2017). Direct quantitative evaluation of disease symptoms on living plant leaves growing under natural light. *Breeding Science*, 67, 316-319.
- Mencarelli, F. and Mejia, D. (2004). Technical guide on post-harvest of banana (*Musa paradisiaca* var. sapientum) use of refrigeration and ethylene generator equipment. FAO, Rome, Italy.
- Meyer, G., Mehta, T., Kocher, M., Mortensen, D. and Samal, A. (1998). Textural imaging and discriminant analysis for distinguishing weeds for spot spraying. *Transactions of the ASAE*, 41, 1189-1197.

- Microsoft. (2010). Kinect. Available at <http://www.xbox.com/en-US/xbox-360/kinect> [Accessed 9 June 2016].
- Microscan (2018). Barcode scanning. Available at <http://www.microscan.com/en-us> [Accessed 15 April 2018].
- Miller, A. (1992). Physiology, biochemistry and detection of bruising (mechanical stress) of fruits and vegetables. *Postharvest News Info*, 3, 53-58.
- Munisami, T., Ramsurn, M., Kishnah, S. and Pudaruth, S. (2015). Plant leaf recognition using shape features and colour histogram with K-nearest neighbour classifier. *Procedia Computer Science*, 58, 740-747.
- MVTec Software GmbH. (2014). HALCON/HDevelop 12.0 Reference Manual, München, Germany.
- NASA. (2002). Application of Data of Data Matrix Identification Symbols to Aerospace Parts Using Direct Part Marking Methods/Techniques, NASA Press, Washington D.C.
- Ng, T. and Yeo, S. (2001). Aesthetic laser marking assessment using luminance ratios. *Optics and Lasers in Engineering*, 35, 177-186.
- Noble, S. and Brown, R. (2008). Spectral band selection and testing of edge-subtraction leaf segmentation. *Canadian Biosystems Engineering*, 50, 21-28.
- O'Reilly, J., Mosher, R. and Goffe, W. (1979). Scanned Laser Marking of Metallic and Organic Films. *Photographic Science and Engineering*, 23(5), 314-318.
- Ohta, Y., Kanade, T. and Sakai, T. (1980). Colour information for region segmentation. *Computer Graphics and Image Processing*, 13, 222-241.
- Okamoto, H. and Lee, W.S. (2009). Green citrus detection using hyperspectral imaging. *Computers and Electronics in Agriculture*, 66, 201-208.
- Opara, L.U. (2003). Traceability in agriculture and food supply chain: a review of basic concepts, technological implications, and future prospects. *Food, Agriculture and Environment*, 1, 101-106.
- Otsu, N. (1979). A Threshold Selection Method from Gray-Level Histogram. *IEEE Transactions on Systems, Man, and Cybernetics*, 9, 62-66.
- Owen, S. and Switkin, D. (2015). ZXing (Zebra Crossing). Available at <https://github.com/zxing/zxing> [Accessed 23 October 2017].
- Parker, B. (2004). Method and apparatus for marking an egg with an advertisement and a freshness data, US Patent WO2,004,064,530.
- Parreño-Marchante, A., Alvarez-Melcon, A., Trebar, M. and Filippin, P. (2014). Advanced traceability system in aquaculture supply chain. *Journal of Food Engineering*, 122, 99-109.

- Pastrana, J. and Rath, T. (2013). Novel image processing approach for solving the overlapping problem in agriculture. *Biosystems Engineering*, 115, 106-115.
- Paulus, S., Behmann, J., Mahlein, A., Plümer, L. and Kuhlmann, H. (2014). Low-cost 3D systems: suitable tools for plant phenotyping. *Sensors*, 14, 3001-3018.
- Payne, A., Walsh, K., Subedi, P. and Jarvis, D. (2014). Estimating mango crop yield using image analysis using fruit at 'stone hardening' stage and night time imaging. *Computers and Electronics in Agriculture*, 100, 160-167.
- Peres, B., Barlet, N., Loiseau, G. and Montet, D. (2007). Review of the current methods of analytical traceability allowing determination of the origin of foodstuffs. *Food Control*, 18, 228-235.
- Persson, M. and Astrand, B. (2008). Classification of crops and weeds extracted by active shape models. *Biosystems Engineering*, 100, 484-497.
- Philipp, I. and Rath, T. (2002). Improving plant discrimination in image processing by use of different colour space transformations. *Computers and Electronics in Agriculture*, 35, 1-15.
- Plebe, A. and Grasso, G. (2001). Localization of spherical fruits for robotic harvesting. *Machine Vision and Applications*, 13, 70-79.
- Polder, G., van der Heijden, G. and Young, I. (2002). Spectral image analysis for measuring ripeness of tomatoes. *Transactions of the ASAE*, 45, 1155-1161.
- Preuksakarn, C., Boudon, F., Ferraro, P., Durand, J., Nikinmaa, E. and Godin, C. (2010). Reconstructing plant architecture from 3D laser scanner data. 6th *International Workshop on Functional–Structural Plant Models*, 16-18.
- Qi, J., Wang, K., Liang, M., Zhu, Y. and Fang, M. (1998). Laser marking of stainless steel with a Q-switched Nd:YAG Laser. *SPIE*, 3550, 311-315.
- Qi, J., Wang, K. and Zhu, Y. (2003). A study on the laser marking process of stainless steel. *Journal of Materials Processing Technology*, 139, 273-276.
- Qi, L., Zhang, Y., Wang, S., Tang, Z., Yang H. and Zhang, X. (2015). Laser cutting of irregular shape object based on stereo vision laser galvanometric scanning system. *Optics and Lasers in Engineering*, 68, 180-187.
- Qiu, H., Lu, C. and Xiao, R. (2011). Processing parameters influence in direct part marking barcodes on aluminum alloy. *Chinese Journal of Lasers*, 38, 1-5.
- Ramer, U. (1972). An iterative procedure for the polygonal approximation of plane curves. *Computer Graphics and Image Processing*, 1, 244-256.
- Rath, T. (1997). Methoden zur computerbild-analytischen Pflanzenidentifikation am Beispiel dendrologischer Bestimmungen. Institut für Technik in Gartenbau und Landwirtschaft der Universität Hannover, Germany.

- Regattieri, A., Gamberi, M. and Manzini, R. (2007). Traceability of food products: general framework and experimental evidence. *Journal of Food Engineering*, 81, 347-356.
- Reed, I. and Solomon, G. (1960). Polynomial codes over certain finite fields. *Journal of the Society for Industrial and Applied Mathematics*, 8, 300-304.
- Rinkalkumar, R., Jadav, K. and Somani, A. (2014). Review on 1D and 2D barcode with QR code basic structure and characteristics. *International Journal for Scientific Research and Development*, 1, 2418-2421.
- Robert, E. and Erik, O. (1997). Machinery's handbook. Industrial Press Inc., New York.
- Roerdink, J. and Meijster, A. (2000). The watershed transform: definitions, algorithms and parallelization strategies, *Fundamenta Informaticae* 41, 187-228.
- Ruiz-Garcia, L. and Lunadei, L. (2011). The role of RFID in agriculture: applications, limitations and challenges. *Computers and Electronics in Agriculture*, 79, 42-50.
- Saifi, M. and Paek, U. (1973). Scribing glass with pulsed and Q-switched CO₂ laser. *American Ceramic Society Bulletin*, 52, 838-841.
- Sakai, K., Kitamura, T., Kato, H. and Utsunomiya. (1994). Resin compositions for laser marking. US Patent 5,373,039.
- Sanz-Cortiella, R., Llorens-Calveras, J., Arnó-Satorra, J., Ribes-Dasi, M., Masip-Vilalta, J., Camp, F., Gràcia-Aguilá, F., Solanelles-Batlle, F., Planas-DeMartí, S. and Pallejà-Cabré, T. (2011). Innovative lidar 3D dynamic measurement system to estimate fruit-tree leaf area. *Sensors*, 11, 5769-5791.
- Satti, V., Satya, A. and Sharma, S. (2013). An automatic leaf recognition system for plant identification using machine vision technology. *International Journal of Engineering Science and Technology*, 5, 874-879.
- Sawayama, M., Adelson, E. and Nishida, S. (2017). Visual wetness perception based on image color statistics. *Journal of Vision*, 17, 1-24.
- Scanlab. (2017). Laser marking. Available at <http://www.scanlab.de/> [Accessed November 2017].
- Scarfe, A., Flemmer, R., Bakker, H. and Flemmer, C. (2009). *Development of an autonomous kiwifruit picking robot*. Paper presented at the 4th International Conference on Autonomous Robots and Agents, 10-12 February, Wellington (New Zealand): Institute of Electrical and Electronics Engineers (IEEE).
- Scholten, H., Verdouw, C., Beulens, A. and van der Vorst, J. (2016). Defining and analyzing traceability system in food supply chains. *Advances in Food Traceability Techniques and Technologies*, 9-33.
- Shah, R. and Lee, W. (2015). An approach to a laser weeding system for elimination of in-row weeds. *Precision Agriculture*, 15, 307-312.

- Shih, P. and Liu, C. (2005). Comparative assessment of content-based face image retrieval in different color spaces. *Audio and Video-Based Biometric Person Authentication*, 3546, 1039-1048.
- Sobotova, L. and Demec, P. (2014). Laser marking systems as an optimization method at marking of machines and workpieces. *Transactions of the Universities of Kosice*, 2, 83-88.
- Sobotova, L. and Demec, P. (2015). Laser marking of metal materials. *Modern Machinery Science Journal*, 808-812.
- Søgaard, H. (2005). Weed classification by active shape models. *Biosystems Engineering*, 91, 271-281.
- Song, H., He, D. and Pan, J. (2012). Recognition and localization methods of occluded apples based on convex hull theory. *Transactions of the Chinese Society of Agricultural Engineering*, 28, 174-180.
- Sood, P., Ference, C., Narciso, J. and Etxeberria, E. (2008). Effects of laser labeling on the quality of tangerines during storage. *Proceedings of the annual meeting of the Florida State Horticultural Society*, 297-300.
- Sood, P., Ference, C., Narciso, J. and Etxeberria, E. (2009). Laser marking: a novel technology to label Florida grapefruit. *Horttechnology*, 19, 504-510.
- Stajanko, D., Lakota, M. and Hocevar. (2004). Estimation of number and diameter of apple fruits in an orchard during the growing season by thermal imaging. *Computers and Electronics in Agriculture*, 42, 31-42.
- Sun, M., Kumar, S., Bradski, G. and Savarese, S. (2013). Object detection, shape recovery, and 3D modelling by depth-encoded Hough voting. *Computer Vision and Image Understanding*, 117, 1190-1202.
- Synrad. (2006). WinMarkpro® Laser marking software user guide. Mukilteo, USA.
- Tanigaki, K., Fujiura, T., Akase, A. and Imagawa, J. (2008). Cherry-harvesting robot. *Computers and Electronics in Agriculture*, 63, 65-72
- Tarjan, L., Senk, I., Tegeltija, S., Stankovski, S. and Ostojic, G. (2014). A readability analysis for QR code application in a traceability system. *Computers and Electronics in Agriculture*, 109, 1-11.
- Teng, C., Kuo, Y. and Chen, Y. (2011). Leaf segmentation, classification, and three-dimensional recovery from a few images with close viewpoints. *Optical Engineering*, 50, 937-946.
- Trienekens, J., Vorst, J.V.D. and Verdouw, C. (2014). Global food supply chains. *Encyclopedia of Agriculture and Food Systems*, 2nd edition, Academic Press, Wageningen University.
- Ueda, M., Saitoh, Y., Hachisuka, H., Ishigaki, H., Gokoh, Y. and Mantani, H. (1990). Studies on CO laser marking. *Optics and Laser in Engineering*, 12, 245-249.

- Unay, D. and Gosselin, B. (2007). Stem and calyx recognition “Jonagold” apples by pattern recognition. *Journal of Food Engineering*, 78, 597-605.
- Van Roy, J., Keresztes, C., Wouters, N., Ketelaere De, and Saeys, W. (2017). Measuring colour of vine tomatoes using hyperspectral imaging. *Postharvest Biology and Technology*, 129, 79-89.
- van Rijswijk, W. and Frewer, L. (2008). Consumer perceptions of food quality and safety and their relation to traceability. *British Food Journal*, 110, 1034-1046.
- Verbeke, W., Frewer, L., Scholderer, J. and De Brabander, H. (2007). Why consumers behave as they do with respect to food safety and risk information. *Analytica Chimica Acta*, 586, 2-7.
- Wang, J., Qi, K. and Zhu, Y. (2003). A study on the laser marking process of stainless steel. *Journal of Materials Processing Technology*, 139, 273-276.
- Wang, X., Huang, D., Du, J., Xu, H. and Heutte, L. (2008). Classification of plant leaf images with complicated background. *Applied Mathematics and Computation*, 205, 916-926.
- Wang, J., He, J., Han, Y., Ouyang, C. and Li, D. (2013). An adaptive thresholding algorithm of field leaf image. *Computers and Electronics in Agriculture*, 96, 23-39.
- Wang, J. and Tan, Y. (2013). Efficient euclidean distance transform algorithm of binary images in arbitrary dimensions. *Pattern Recognition*, 46, 230-242.
- Wang, W. and Li, C. (2014). Size estimation of sweet onions using consumer-grade RGB-depth sensor. *Journal of Food Engineering*, 142, 153-162.
- Wang, X. Feng, B., Bai, X., Liu, W. and Latecki, L. (2014). Bag of contour fragments for robust shape classification. *Pattern recognition*, 47, 2116-2125.
- Wang, D., Yu, Q. and Zhang, Y. (2015). Research on Laser Marking Speed Optimization by Using Genetic Algorithm, *Plos One*, 10, 2015.
- Wang, Z., Wang, K., Yang, F., Pan, S. and Han, Y. (2017a). Image segmentation of overlapping leaves based on Chan-Vese model and Sobel operator, *Information Processing in Agriculture*, 1-18.
- Wang, X., Duan, J., Jiang, M., Ke, S., Wu. and Zeng, X. (2017b). Study of laser precision ablating texture patterns on large-scale freeform surface. *The International Journal of Advanced Manufacturing Technology*, 92, 4571-4581.
- Wangui, E., Ikua, B.W. and Nyakoe, G.N. (2012). A study on influence of beam orientation in engraving using CO2 laser. *Journal of Sustainable Research in Engineering*, 1, 42-48.
- Weiss, U. and Biber, P. (2011). Plant detection and mapping for agricultural robots using a 3D lidar sensor. *Robotics and Autonomous Systems*, 59, 265-273.

- Wöltjen, C., Haferkamp, H., Rath, T. and Herzog, D. (2008). Plant growth depression by selective irradiation of the meristem with CO₂ and diode lasers. *Biosystems Engineering*, 101, 316-324.
- Xia, C., Lee, J., Li, Y., Song, Y., Chung, B. and Chon, T. (2013). Plant leaf detection using modified active shape models. *Biosystems Engineering*, 116, 23-35.
- Xia, C., Wang, L., Chung, B. and Lee, J. (2015). In situ 3D segmentation of individual plant leaves using a RGB-D camera for agricultural automation. *Sensors*, 15, 20463-20479.
- Xiang, R., Ying, Y., Jiang, H. and Peng, Y. (2010). 3-D location of tomato based on binocular stereo vision for tomato harvesting robot. *Proceedings of SPIE -The International Society for Optical Engineering*, 7658, 106-112.
- Xie, Z., Xu, Y., Ji, C., Guo, X. and Zhu, S. (2012). Estimation method of apple growing attitude based on computer vision. *Transactions of the Chinese Society of Agricultural Engineering*, 42, 154-157.
- Xiong, Ya., Ge, Y., Liang, Y. and Blackmore, S. (2017). Development of a prototype robot and fast path-planning algorithm for static laser weeding. *Computers and Electronics in Agriculture*, 142, 494-503.
- Xuele, W., Jie, H., Dongjie, Z., Honghong, G., Chuanjun, L. and Bin, Z. (2016). Kinematics and statics analysis of a novel 4-DOF parallel mechanism for laser weeding robot. *INMATEH-Agricultural Engineering*, 50, 29-38.
- Yamamoto, K., Guo, W., Yoshioka, Y. and Ninomiya, S. (2014). On plant detection of intact tomato fruits using image analysis and machine learning methods. *Sensors*, 14, 12191-12206
- Yan, D., Wintz, J., Mourrain, B., Wang, W., Boudon, F. and Godin, C. (2009). *Efficient and robust reconstruction of botanical branching structure from laser scanned points*. Paper presented at the 11th IEEE International Conference on Computer-Aided Design and Computer Graphics (CAD/Graphics), 19-21 August, Huangshan (China): Institute of Electrical and Electronics Engineers (IEEE).
- Yang, L., Zhang, L., Dong, H., Alelaiwi, A. and Saddik, A. (2015). Evaluating and Improving the Depth Accuracy of Kinect for Windows v2. *IEEE Sensors Journal* 15, 4275-4285.
- Yuk, H., Warren, B. and Schneider, K. (2007). Infiltration and survival of *Salmonella* spp. on tomato surfaces labeled using a low-energy carbon dioxide laser device. *HortTechnology*, 17, 67-71.
- Zawbaa H., Abbass M., Hazman M. and Hassenian A. (2014). Automatic Fruit Image Recognition System Based on Shape and Color Features. *Communications in Computer and Information Science*, 278-290.

- Zhao, Y., Gong, L., Huang, Y. and Liu, C. (2016). A review of key techniques of vision-based control for harvesting robot. *Computers and Electronics in Agriculture*, 127, 311–323
- Zhang, L., Weckler, P., Wang, N., Xiao, D. and Chai, X. (2016). Individual leaf identification from horticultural crop images based on the leaf skeleton. *Computers and Electronics in Agriculture*, 127, 184-196.
- Zhou, R., Damerow, L., Sun, Y. and Blanke, M. (2012). Using color features of cv. 'Gala' apple fruits in an orchard in image processing to predict yield. *Precision Agriculture*, 13, 568-580.
- Zigelboim, M.S. (2015). Method and apparatus for marking coconuts and similar food products. US Patent 0030731 A1.
- ZXing. (2016). Multi-format 1D/2D Barcode Image Processing Library. Available at <http://code.google.com/p/zxing/S> [Accessed October 2017].

LIST OF FIGURES

Fig. 2.1.1. The absorption of materials vs wavelengths (Kaminski, 2011)	6
Fig. 2.2.2. Illustration of the penetration depth on tissue of various common wavelengths (Farkas, et al. 2013)	15
Fig. 2.2.3. Absorption spectra of fresh and dried leaves (<i>A. retroflexus</i>) depend on the laser wavelength (Marx, et al. 2012)	16
Fig. 2.2.4. Data matrix structure	20
Fig. 4.1.1. Capturing poinsettia plant using Kinect camera from top view, (a) RGB image; (b) Depth image	26
Fig. 4.1.2. Poinsettia plants after laser marking in greenhouse	26
Fig. 4.1.3. Example of banana hands image using CCD camera (top view)	27
Fig. 4.2.1. Laser marking setup on poinsettia plants: CO ₂ laser, laser scanner, manual lifting table and computer-based control	30
Fig. 4.2.2. Laser marking setup on bananas: CO ₂ laser, laser scanner and focus system, lifting machine and computer-based control	30
Fig. 4.2.3. Water calorimeter systems	31
Fig. 4.2.4. The use of a CO ₂ laser power meter (Mahoney, USA)	31
Fig. 4.2.5. Lighting setup	32
Fig. 4.3.1. Kinect V1 (left) and Kinect V2 (right)	34
Fig. 4.4.1. Image acquisition application for Kinect V1 camera	34
Fig. 4.4.2. Image acquisition application for Kinect V2 camera	35
Fig. 4.6.1. Separation of green leaves the depth image of poinsettia leaves	38
Fig. 4.6.2. Illustration of Euclidean distance transform	41
Fig. 4.6.3. Illustration of watershed segmentation, local minima of gray level yield catchment basins, and local maxima define the watershed lines	41
Fig. 4.6.4. Illustration of shape factor ratio (SF) of two different types of poinsettia leaves. (A) major radius of ellipse; (B) minor radius of ellipse; (C) maximum diameter of leaf region	43
Fig. 4.6.5. Confusion matrix (Fawcet, 2006)	43
Fig. 4.6.6. Main skeleton and branches of poinsettia leaf	44
Fig. 4.6.7. Overview of leaf identification system	49
Fig. 4.6.8. Kernels used in Sobel operator	45
Fig. 4.6.9. Illustration of the non-maximum suppression	46

Fig. 4.6.10. Simplifying a curve using Ramer approximation. (1-6) A curve (blue line) together with the initial approximation (black line) is shown. First step: As the maximum distance d_1 between the curve and its approximation (marked red) is larger than threshold (t), the line is subdivided. Second step: The lower line is subdivided again ($d_2 > t$). The final Ramer approximation is illustrated at number (6)	48
Fig. 4.6.11. The process of removing the background of single banana fruit	51
Fig. 4.6.12. CIE-Lab color space structure	52
Fig. 4.6.13. Steps for positioning a code on banana	55
Fig. 4.6.14. Ventral side and dorsal side of banana hands	57
Fig. 4.7.1. Laser-marked poinsettia leaf and illustration of raster marking method	59
Fig. 4.7.2. Laser-marked areas on a banana created at different laser powers	60
Fig. 4.7.3. Image analysis steps to evaluate data matrix codes using the Halcon software	61
Fig. 4.7.4. Examples of data matrix codes on green bananas with the same edge length (6 mm) and the same laser power immediately after laser marking ..	63
Fig. 5.1. Alignment between depth image and color image	65
Fig. 5.2. Poinsettia image captured by Kinect camera, (a) RGB image; (b) depth image; (c) depth image histogram	66
Fig. 5.3. Colored leaves' extraction based on a depth image, (a) Original RGB image, (b) Original depth image, (c) Depth image without green leaves	66
Fig. 5.4. Leaves' image segmentation using distance transform and watershed algorithm	67
Fig. 5.5. Main leaf skeleton detection steps	68
Fig. 5.6. Different position of poinsettia on main leaves' skeleton detection	69
Fig. 5.7. Histogram and banana image after automatic Otsu thresholding	70
Fig. 5.8. An example of a banana image after background removal	71
Fig. 5.9. Positioning of codes on banana hands	71
Fig. 5.10. Examples of successful main leaf skeleton detection (true positive)	74
Fig. 5.11. Examples of wrong detection. (a) false positive, (b) true negative, (c) false negative	75
Fig. 5.12. Positioning of the code on bananas with slight curve and curve shape	77
Fig. 5.13. Positioning of a code on a banana with different orientations	78
Fig. 5.14. Positioning of a code on fruits and vegetables	78
Fig. 5.15. Successful positioning of the 2D codes on banana hands (ventral side)	79

Fig. 5.16. Successful positioning of the 2D codes on banana hands (dorsal side) 80

Fig. 5.17. False localization of the 2D codes on banana hands 80

Fig. 5.18. Relationship between percentage of laser power use and actual beam power (5 repetitions) 81

Fig. 5.19. Different levels of heat affected zones (HAZ) 3 days after laser marking on poinsettia leaf, with white numbers showing the calculation of damages on each character; (a) No apparent HAZ; (b) Slight HAZ; (c) Moderate HAZ; (d) Severe HAZ..... 82

Fig. 5.20. Example of incomplete marking results or inadequate contrast on poinsettia leaves due to too-low laser energy 84

Fig. 5.21. Effect of laser marking resolution and raster scan direction on cycle time..... 84

Fig. 5.22. Laser marking on poinsettia leaves using 0.5 W [0.55 J per character] 85

Fig. 5.23. Reflectance spectrum (R) of marked bananas in the infrared waveband (N = 10 bananas): (a) mean reflectance (b) reflectance difference 87

Fig. 5.24. Effects of laser marking and marking time on readability of data matrix code after 9 days of storage (Cavendish bananas with five repetitions) 88

Fig. 5.25. Data matrix codes on bananas after 9 days of storage (data matrix edge length 10 mm, 10x10 modules)..... 89

Fig. 5.26. Effects of laser marking and marking time on contrast values of data matrix codes after 9 days of storage (Cavendish bananas with five repetitions)..... 90

Fig. 5.27. Effects of laser marking and marking time on the axial non-uniformity values of data matrix codes after 9 days of storage (Cavendish bananas with five repetitions)..... 91

Fig. 5.28. Effects of laser marking and marking time on grid non-uniformity values of data matrix codes after 9 days of storage (Cavendish bananas with five repetitions)..... 92

Fig. 5.29. Effects of laser marking and marking time on the unused error correction values of data matrix codes after 9 days of storage (Cavendish bananas with five repetitions)..... 93

Fig. 5.30. Damage to bananas after laser marking..... 94

Fig. 5.31. Probability of readability of the laser marked codes on bananas based on the module size. The graph represents mean \pm standard errors, and uses a sigmoidal regression equation..... 96

Fig. 5.32. Examples of successful encoding of data matrix code on banana after laser marking with a laser power of 1.8 W. (a) Data matrix size 10x10; (b) Data matrix size 16x16 modules. Red and yellow represent binary 1 and binary 0, respectively. 97

Fig. 5.33. Module damage detection on bananas over the storage time with a laser power of 2 W (white arrows represent error detection of modules) 97

Fig. 6.3.1. (a) The character mark is placed on the upper and bottom part of the main skeleton of a poinsettia leaf; (b) Positioning of 2D barcodes on banana hands 109

Fig. 6.3.2. Laser marking on petunia stem (2D code dimension is 3 x 3 mm²) 110

LIST OF TABLES

Table 2.1.2. Various examples of laser marking on horticultural products.....	7
Table 2.2.1. Examples features used in leaves detection.....	10
Table 2.2.2. Different cameras used in plants detection.....	10
Table 2.2.3. Some examples of multiple features used in fruits detection	12
Table 2.2.4. Some applications of thermal cameras for fruits detection	13
Table 2.2.5. Some applications of hyperspectral cameras for fruits	13
Table 4.1.1. Number of plant tested	25
Table 4.1.2. Banana ripening stages based on a five-day schedule.....	28
Table 4.2.1 Specifications of the CO ₂ laser	29
Table 4.2.2. Specifications of SH series marking head	29
Table 4.2.3. Specifications of Kinect V1 and Kinect V2	35
Table 4.4.1 Halcon operators used (Halcon MV/Tec, 2014).....	36
Table 4.7.1. Different laser output power, resolution, and raster scan direction applied to poinsettia leaves	58
Table 4.7.2. Laser energy applied to the bananas depending on the laser power (p) and the marking time (t).....	60
Table 4.7.3. Data matrix code print quality (ISO/IEC 15415, 2011)	61
Table 4.7.4. Data Matrix code symbol attributes (GS1, 2018)	62
Table 4.7.5. Encoding example of ECC200 ASCII based on ISO/IEC 16022 (2006)	63
Table 5.1.2. Color segmentation based on a depth image of green leaves	72
Table 5.1.3. Classification rates of poinsettia leaves using Kinect V1 and Kinect V2	73
Table 5.1.4. Successful detection of the longest five lines of main leaf skeleton	73
Table 5.1.5. Classification of the plants from a single poinsettia leaf in the test set	74
Table 5.1.6. The five longest main leaf skeletons identified at different orientations	76
Table 5.1.7. Successful rate of localization of codes (labels) on banana hands	79
Table 5.2.1. Comparison of using water calorimeter and CO ₂ laser power meter	81
Table 5.2.2. Heat affected zone (HAZ) index of marked poinsettia leaves	83
Table 5.2.3. Examples of changes to poinsettia leaves on selected samples during the storage period (five repetitions)	86
Table 5.2.4. Effects of DM size, power and edge length on readability after 9 days.....	95
Table 6.2.1. Comparison between our study and existing references	100

PUBLICATIONS

Scientific Papers:

Nasution I.S., Rath T. (2017). Optimal laser marking of 2D data matrix codes on Cavendish bananas. *Res. Agr. Eng.*, 63: 172-179.

Doi: 10.17221/26/2016-RAE (Peer Reviewer)

Hülsmann, S., Nasution, I., Rath, T., and Bettin, A. (2017). *Methoden zur 3D-Pflanzenvermessung mit Kinect v2 Kamera im Unterglasanbau*, DGG-Proceedings, 7(11):1-5.

Doi: 10.5288/dgg-pr-sh-2017 (Peer Reviewer)

Nasution, I.S., Rath, T. (2015). Studies of laser marking on Cavendish banana, *DGG-Proceeding*, 5(18): 1-5.

Doi: 10.5288/dgg-pr-05-18-in-2015. (Peer Reviewer)

Conference Presentations:

Nasution, I.S. (2018). Introducing laser marking of fruits and vegetables for future labeling. International DAAD Alumni Summer School, "Sustainable Food Production and Food Security in Developing Countries-Quality Management and Resource Use Efficiency along Agri-Value Chains", in Hannover, 13-19 March 2018.

Nasution, I.S. and Rath, T. (2017). Separation overlapping poinsettia leaves for laser marking. 51. Gartenbauwissenschaftliche Jahrestagung, in Osnabrueck 1-4 March 2017, ISSN 1613-088X, p. 49.

Hülsmann, S., Nasution, I.S., Rath, T. and Bettin, A. (2017). Methoden zur 3D-Pflanzenvermessung mit Kinect V.2 im Unterglasanbau. 51. Gartenbauwissenschaftliche Jahrestagung, in Osnabrueck 1-4 March 2017, ISSN 1613-088X, p. 48.

Nasution, I.S. and Rath, T. (2016). Development and comparison of methods for analyzing overlapping poinsettia leaves for laser marking. Poster presentation at *Kontaktstudientage Hochschule Osnabrueck* in Osnabrueck on 11th-12th of November 2016.

S. Hülsmann, I.S. Nasution, T. Rath, A. Bettin. (2016). *3D-Pflanzenvermessung zur Optimierung der Energieeffizienz von Gewächshauskulturen*. *Kontaktstudientage Hochschule Osnabrueck* in Osnabrueck on 11th-12th of November 2016.

Stephan H., I.S. Nasution, D. Wilms, T. Rath und A. Bettin. (2016). *Pflanzenvermessung mit Kinect-Kameras*, KTBL-Beratertagung, Regenstauf-Germany, 22.09.2016.

- Hülsmann, S., Nasution, I.S., and Bettin, A. (2016). *Erfassung von Pflanzen-Höheninformationen*, Poster presentation for Senate Hamburg, Hamburg-Germany, 27.06.2016.
- Nasution, I.S., and Rath, T. (2015). Studies of laser marking on Cavendish banana. The German Society for Horticultural Science (DGG), the Federal Association of Graduates/Engineers in Horticulture and Landscape Architecture (BHGL) and the BMBF- AgroClustEr WeGa conference on 24th-28th of Februari 2015. *BHGL Tagungsband* 31, ISSN 1613-088X, p. 130.
- Nasution, I.S., and Rath, T. (2015). Investigation of laser marking on fruits and ornamental plants, International WeGa Symposium "Horticultural Production - Safety and Predictability" in Freising-Weihenstephan (Germany) on 24th-28th of Februari 2015. *BHGL Tagungsband* 31, ISSN 1613-088X, p. 14.
- Rath, T., Marx, C., and Nasution, I.S. (2014). *Markierung gartenbaulicher produkte mit laserstrahlung*, *Kontaktstudententage Hochschule OsnabruECK* in OsnabruECK on 7th-8th of November 2014.

CURRICULUM VITAE

Personal data

Name : Indera Sakti Nasution
Date of birth : 04.07.1980
Place of birth : Padangsidempuan, Indonesia
Marital status : Married



Education

2012-2018 : Dr. rer. hort. at Faculty of Natural Sciences, Leibniz
Universität Hannover, Germany
2006-2008 : M.Sc. Tropical and International Agriculture, Georg-August
University of Göttingen, Germany
1998-2004 : B.Sc. Agricultural Engineering, Syiah Kuala University, Aceh,
Indonesia
1995-1998 : Senior High School, SMUN 3 Padangsidempuan, Indonesia
1992-1995 : Junior High School, SMPN 1 Padangsidempuan, Indonesia

Awards

2012-2016 : PhD scholarship under Directorate General of Higher Education of
the Republic of Indonesia (DGHE)
2006-2008 : DAAD scholarship for M.Sc. studies

Work experience

2015-2016 : Scientific assistance at the University of Applied Science
Osnabrück, Germany, responsible for the following activities:
supporting experimental set up in the field of workshop and
evaluation, supporting data analysis of Hamburg project
2005-Now : Lecturer and Researcher at Agricultural Engineering Department,
Faculty of Agriculture, Syiah Kuala University, Banda Aceh-
Indonesia